# Trajectory Analysis and Comparison of a Linear Aerospike Nozzle to a Conventional Bell Nozzle for SSTO Flight

A Thesis Presented for the
Master of Science
Degree
The University of Tennessee, Knoxville

Elizabeth Lara Lash
May 2015

Copyright © 2015 by Elizabeth Lara Lash
All rights reserved.

# ACKNOWLEDGEMENTS

I would like to thank Dr. Trevor Moeller for his faith and persistence in pushing me to work and learn from this project. Without his encouragement, I would never have gained a better understanding of launch vehicles and their components nor how to accurately model and analyze their trajectories. I would also like to thank Dr. Monty Smith and Dr. Steve Brooks for serving on my committee.

I would like to thank NASA Kennedy Space Center for the use of OTIS and the support they provided. I am also thankful to Mr. Paul Gloyer of Gloyer-Taylor Laboratories for providing the opportunity to work on this project and for his constant guidance and direction.

I would also like to acknowledge the help and support of my family; to my Mom and Dad, brother, and the continued love and support of my extended family and numerous friends: thank you.

This work was funded by Gloyer-Taylor Laboratories, LLC through a NASA STTR under subcontract number GTL-NAS-107-UTSI-A, and the NASA Tennessee Space Grant College and Fellowship Program under contract number 21603-S12.

# ABSTRACT

Single-stage to orbit (SSTO) rocket technology offers the potential to substantially reduce launch costs, but has yet to be considered practical for conventional launch vehicles. However, new research in composite propellant tank technology opens the field for renewed evaluation. One technology that increases the efficiency and feasibility of SSTO flight is an altitude compensating rocket engine nozzle, as opposed to a conventional constant area, bell nozzle design. By implementing an altitude compensation nozzle, such as a linear, aerospike nozzle for in-atmosphere flight, the propellant mass fraction (PMF) may be reduced by as much as seven percent compared to a conventional rocket engine. In this thesis, Optimal Trajectories by Implicit Simulation (OTIS) is used to model SSTO flight trajectories by comparing a high performance, aerospike nozzle configuration to a conventional bell nozzle; this includes thrust, specific impulse ($I_{sp}$), and nozzle configuration combinations to show that nozzle variability increases the efficiency of SSTO flight through a reduction in PMF. Results suggest that having a limited nozzle configuration, where the nozzle is not allowed to expand to infinity, further increases the engine efficiency by lowering the PMF by 0.1-0.2 %. Thus, the limited nozzle design performs as well as the linear aerospike, and presents itself as an alternative if the aerospike is too complex, even if the added benefit is within the uncertainty of the simulation results. Additional modeling is required to confirm this, but it is evident that altitude compensating nozzles perform better than the conventional bell nozzles used in these simulations.

# TABLE OF CONTENTS

**CHAPTER I INTRODUCTION AND GENERAL INFORMATON ..... 1**
1.1 Introduction to Aerospike Nozzle ..... 1
1.1.1 Design and Purpose ..... 1
1.1.2 Comparison to Bell and Cone Nozzle Designs ..... 2
1.2 Thesis Objective ..... 4
1.2.1 Thesis Significance ..... 5
1.3 Thesis Organization ..... 5
**CHAPTER II LITERATURE REVIEW ..... 6**
2.1 Single-Stage to Orbit Flight ..... 6
2.1.1 Georgia Tech *Hyperion* ..... 6
2.1.2 NASA GTX ..... 8
2.2 Linear Aerospike Nozzles ..... 10
2.2.1 NASA/Lockheed Martin Linear Aerospike SR-71 Experiment (LASRE) ..... 11
2.2.2 Aerospike Study since LASRE/X-33 ..... 13
2.3 Current Work ..... 15
2.3.1 SKYLON Spaceplane ..... 15
2.3.2 Firefly ..... 15
**CHAPTER III MATERIALS AND METHODS ..... 16**
3.1 Theory ..... 16
3.1.1 Compressible Gas Dynamics ..... 16
3.1.1.1 Nozzle Theory ..... 16
3.1.1.2 Nozzle Designs ..... 19
3.1.2 Launch Vehicle Mechanics ..... 25
3.1.2.1 Basic Equations ..... 25
3.1.2.2 Engine/Rocket Performance Parameters ..... 27
3.1.3 Calculating Effective Nozzle Exit Area of an Aerospike ..... 28
3.2 Optimal Trajectories by Implicit Simulation (OTIS) ..... 29
3.2.1 Implementation & Design ..... 30
3.2.2 Bell Nozzle ..... 32
3.2.3 Aerospike Nozzle ..... 32
3.3 Trajectory Modeling Process ..... 32

**CHAPTER IV RESULTS AND DISCUSSION ..... 34**
4.1 Trajectory Analysis and Comparison ..... 34
4.1.1 Optimizing Trajectory Profiles ..... 34
4.1.2 Cases 1 & 2 ..... 44
4.1.3 Cases 3, 4, 5 ..... 44
4.1.4 Cases 6, 7, 8 ..... 44
4.2 Performance Analysis ..... 45
**CHAPTER V CONCLUSIONS AND RECOMMENDATIONS ..... 48**
5.1 Which Nozzle Performs Better? ..... 48
5.2 Recommendations ..... 49
**LIST OF REFERENCES ..... 50**
**APPENDICES ..... 55**
**APPENDIX A ..... 56**
**APPENDIX B ..... 67**
**VITA ..... 92**

# LIST OF TABLES

Table 1: All Trajectory Case Configurations ..... 35
Table 2: Trajectory Case Configurations with Propellant Performance Parameters ..... 43
Table 3: Trajectory Performance Parameters ..... 43

# LIST OF FIGURES

Figure 1: Aerospike Nozzle, Exhaust Plume Diagram at High (overexpanded), Optimized (perfectly expanded), and Low (underexpanded) Ambient Pressures ..... 2
Figure 2: Bell Nozzle, Exhaust Plume Diagram at High (overexpanded), Optimized (perfectly expanded), and Low (underexpanded) Ambient Pressures ..... 3
Figure 3: Conical Nozzle, Exhaust Plume Diagram at High (overexpanded), Optimized (perfectly expanded), and Low (underexpanded) Ambient Pressures ..... 4
Figure 4: *Hyperion* Configuration ..... 7
Figure 5: *Hyperion* Artist Rendering of RBCC Ascent ..... 7
Figure 6: NASA GTX Vehicle Concept ..... 9
Figure 7: GTX Propulsion Pod ..... 9
Figure 8: GTX Flight Demonstrator (dimensions in feet) ..... 10
Figure 9: Rocketdyne Linear Aerospike Nozzle Concept ..... 11
Figure 10: Lockheed Martin Linear Aerospike Hot Fire Test as Part of the LASRE Program ..... 12
Figure 11: California State University Aerospike Engine Test Stand. ..... 14
Figure 12: California State University Curved vs. Linear Aerospike Thruster Design ..... 14
Figure 13: Rocket Engine Basic Design ..... 17
Figure 14: Cone, Bell, and Aerospike Basic Configurations ..... 19
Figure 15: Cross-section of Conical Plug Spike Nozzle, Exhaust Plume Diagram at High (overexpanded), Optimized (perfectly expanded), and Low (underexpanded) Ambient Pressures ..... 20
Figure 16: Truncated, Conical Spike ..... 21
Figure 17: Cross-Section of Conical, Truncated Plug Spike Nozzle, Exhaust Plume Diagram at High (overexpanded), Optimized (perfectly expanded), and Low (underexpanded) Ambient Pressures ..... 21
Figure 18: Truncated, Linear Aerospike ..... 22
Figure 19: Linear Aerospike Nozzle Design under Altitude Conditions ..... 22
Figure 20: Cross-Section of Various Altitude Compensating Nozzle Designs ..... 24
Figure 21: Extendable Exit Cone Altitude Compensation Nozzle ..... 24
Figure 22: Launch Vehicle Trajectory Diagram ..... 26
Figure 24: Aerodynamic Force Direction Diagram ..... 30
Figure 25: Case 6 Velocity Profile, Prior to Optimization. ..... 37
Figure 26: Case 6 Velocity Profile, After Optimization. ..... 38
Figure 27. Case 6 Altitude Profile, Prior to Optimization. ..... 39
Figure 28. Case 6 Altitude Profile, After Optimization. ..... 39
Figure 29: Case 6 Drag, Weight, and Thrust Profile for Initial Takeoff Time ..... 41
Figure 30: Case 8 Drag, Weight, and Thrust Profile for Initial Takeoff Time. ..... 42
Figure 31: Theoretical Ideal, Aerospike, and Bell Nozzle Thrust Coefficient Trends Based on Pressure Ratio between the Nozzle Exit Area (Pc) and Ambient Pressure (Pa) ..... 46
Figure 32: Case 1 Velocity Profile ..... 68
Figure 33: Case 1 Altitude Profile ..... 69
Figure 34: Case 1 Drag, Weight, and Thrust Profile ..... 70
Figure 35: Case 2 Velocity Profile ..... 71

Figure 36: Case 2 Altitude Profile ..... 72
Figure 37: Case 2 Drag, Weight, and Thrust Profile ..... 73
Figure 38: Case 3 Velocity Profile..... 74
Figure 39: Case 3 Altitude Profile ..... 75
Figure 40: Case 3 Drag, Weight, and Thrust Profile ..... 76
Figure 41: Case 4 Velocity Profile..... 77
Figure 42: Case 4 Altitude Profile ..... 78
Figure 43: Case 4 Drag, Weight, Thrust Profile ..... 79
Figure 44: Case 5 Velocity Profile..... 80
Figure 45: Case 5 Altitude Profile ..... 81
Figure 46: Case 5 Drag, Weight, and Thrust Profile ..... 82
Figure 47: Case 6 Velocity Profile..... 83
Figure 48: Case 6 Altitude Profile ..... 84
Figure 49: Case 6 Drag, Weight, and Thrust Profile ..... 85
Figure 50: Case 7 Velocity Profile..... 86
Figure 51: Case 7 Altitude Profile ..... 87
Figure 52: Case 7 Drag, Weight, and Thrust Profile ..... 88
Figure 53: Case 8 Velocity Profile..... 89
Figure 54: Case 8 Altitude Profile ..... 90
Figure 55: Case 8 Drag, Weight, and Thrust Profile ..... 91

# CHAPTER I
# INTRODUCTION AND GENERAL INFORMATON

In this chapter, conventional bell nozzle and aerospike nozzle design concepts will be introduced along with an overview to their performance.

## 1.1 Introduction to Aerospike Nozzle

Reducing the cost of space travel is an ongoing launch optimization problem. One accepted method to accomplish this is through single-stage to orbit (SSTO) flight, which reduces the launch weight by simplifying the design. Previous work has evaluated the feasibility of SSTO through new composite propellant tank technology [12] in an effort to reduce the dry mass of the system; with the addition of an updated nozzle design, the propellant mass fraction (PMF, defined in Section 1.2) may be reduced even further, leaving more weight available for payload. The dry mass refers to the mass of the system without the propellant; this includes the structure, engine, instrumentation, payload, etc. The wet mass is the total mass of the system, including the propellant.

### 1.1.1 Design and Purpose

The annular, aerodynamic spike nozzle, also known as an aerospike, is a variable exit area nozzle designed to maintain perfect expansion throughout flight by compensating for the change in ambient pressure as a result of the increasing altitude. The aerospike nozzle is shown in Figure 1 (black trapezoid) with its corresponding exhaust plume conditions. The aerospike design is essentially an inverted nozzle where, instead of the exhaust flow being contained inside a structure, the flow is directed around a structure with the ambient pressure acting as the outer boundary. At low altitudes, when the ambient pressure is highest, the exhaust remains close to the nozzle contour, maintaining isentropic expansion (far left image). The aerospike nozzle is at maximum efficiency when the exhaust gases form a column, parallel to the direction of flight. The middle image of Figure 1 shows the exhaust plume in this parallel direction a short distance downstream. At higher altitudes, recompression shock waves occur inside the plume, forcing the

plume to remain column-shaped in a closed-wake state [24] (far right image), despite the expanding exhaust plume shape. This maintains efficiency because the exhaust gases are not expanding beyond the physical nozzle, but still exerting force, thus producing thrust, on the nozzle itself. The advantages of the aerospike design compared to a constant area nozzle are that it maintains higher efficiency for a greater flight path and that the primary flow is acted upon only by the ambient pressure of the atmosphere. Some disadvantages of the aerospike design include its increased mass, thermal cooling considerations, and increased cost to manufacture due to the complexity of the design.

Other configurations of the annular nozzle design are discussed in Section 3.1.1.2.

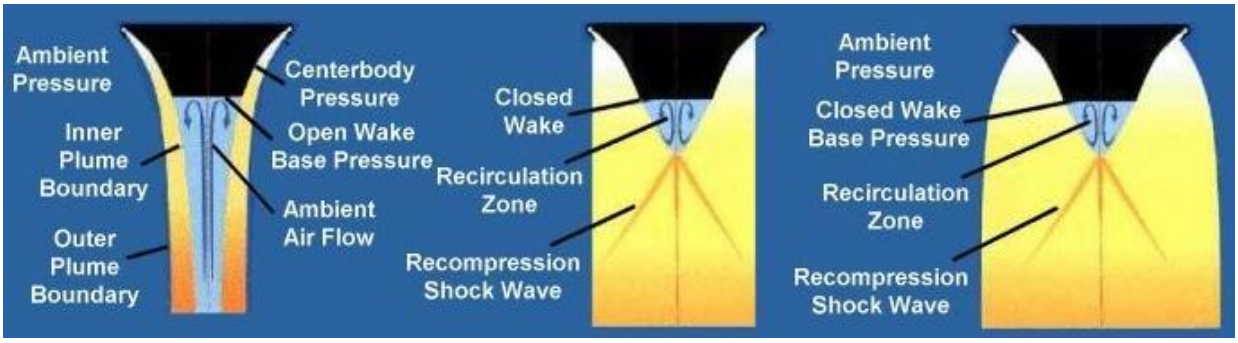



**Figure 1: Aerospike Nozzle, Exhaust Plume Diagram at High (overexpanded), Optimized (perfectly expanded), and Low (underexpanded) Ambient Pressures [1].**

### 1.1.2 Comparison to Bell and Cone Nozzle Designs

Most rockets today have the traditional bell nozzle design on their engines as shown in Figure 2. It is the most efficient, conventional nozzle design currently in use. At lower altitudes, where the ambient pressure is high, the exhaust gases are overexpanded inside the nozzle and compressed radially inwards towards the nozzle exit. In extreme cases this can cause flow separation from the boundary wall within the nozzle, decreasing efficiency. When the exit pressure of the exhaust gases equals that of the ambient, the engine is at maximum efficiency because the thermal energy of the plume that is being converted directly into directed kinetic energy to produce thrust is maximized. As the rocket continues to increase in altitude, the

ambient pressure continues to decrease. The exhaust gases are underexpanded at the nozzle exit, when the ambient pressure is less than the pressure at the nozzle exit, causing the exhaust to continue to expand beyond the nozzle. This external expansion does not exert force on the nozzle wall, so that is thrust lost, decreasing the engine efficiency. This underexpansion is a lost opportunity and would not be a loss by having a larger nozzle exit area to achieve higher nozzle exit velocities, as the aerospike configuration allows. These exhaust plume behaviors describe basic compressible gas expansion, when a gas at high pressure and density is expanded isentropically to larger volumes in order to reduce its pressure and density. In Figure 2, the exhaust gases expanding in a fixed-area nozzle experience overexpansion, then perfect expansion, then underexpansion as altitude is increased. This suggests that a variable nozzle exit area should optimize engine performance if all other parameters are held equal.

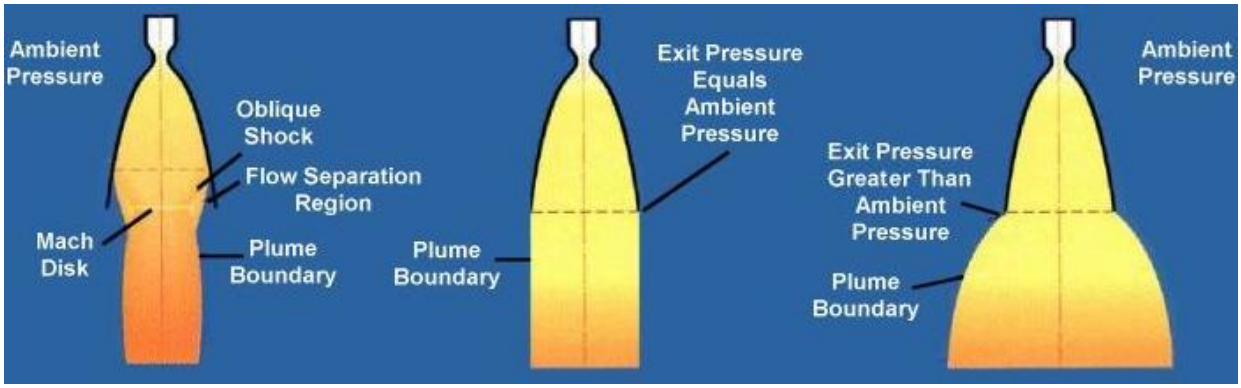



**Figure 2: Bell Nozzle, Exhaust Plume Diagram at High (overexpanded), Optimized (perfectly expanded), and Low (underexpanded) Ambient Pressures [1].**

Prior to the wide-spread use of the bell nozzle, the cone, or conical nozzle was used. The conical nozzle was easy to manufacture and had the flexibility of converting an existing design to higher or lower expansion area ratio without a major overhaul. It is called a conical nozzle because the walls diverge at a constant angle from the throat. The smaller this angle, the greater the thrust because the axial component of the exhaust gases is maximized. However, this requires a longer and heavier cone design. If size and weight are minimized by increasing the angle of

expansion, then performance at low altitudes where the ambient pressure is highest decreases. This causes overexpansion and induces flow separation. Figure 3 shows the exhaust plume behavior at overexpansion, perfect expansion, and underexpansion.

The focus of this work will be to compare the bell nozzle to the aerospike design, as the bell is more efficient than the cone and more commonly used.

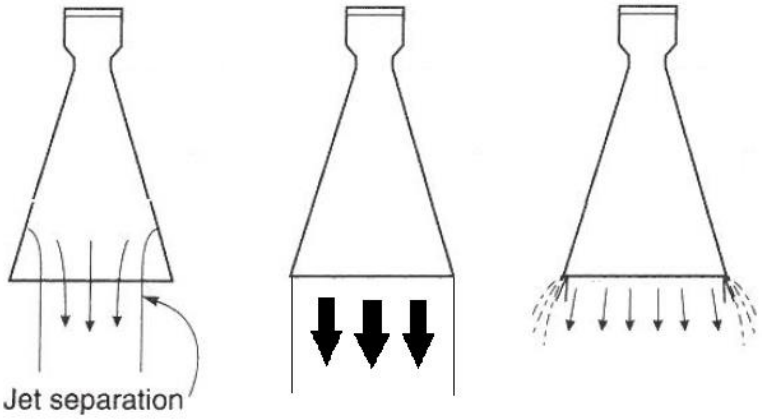



**Figure 3: Conical Nozzle, Exhaust Plume Diagram at High (overexpanded), Optimized (perfectly expanded), and Low (underexpanded) Ambient Pressures [37].**

## 1.2 Thesis Objective

The objective of this thesis is to revisit the possible application of using an aerospike engine nozzle in single-stage to orbit (SSTO) rocket flight, a task not widely undertaken since the 1990s. Recent advances in material science [12] make SSTO more practical than initial research indicated, if an optimized launch trajectory requiring a lower propellant mass fraction (PMF) than that of conventional unmanned rockets may be achieved. When characterizing engine performance, the PMF is taken into consideration because it represents the portion of the initial, total mass that does not make it to orbit, essentially representing the percentage of the total weight that is the propellant used to reach that orbit. The lower the PMF, the less fuel was consumed in order to reach the same orbit, hence leaving more mass for the payload.

This work evaluates the usefulness and potential of an aerospike nozzle to achieve SSTO, and by using Optimal Trajectories by Implicit Simulation (OTIS) [34], a trajectory modeling and analysis code provided by NASA Kennedy Space Center, compares the aerospike design to existing bell nozzle engines in its performance capabilities, specifically, in lowering the PMF as affected by the nozzle exit area to reach a circular orbit at an altitude of 750 km.

### 1.2.1 Thesis Significance

As spaceflight continues to move from projects sponsored by the government to the private sector, the necessity for lowering costs increases. Launching satellites into low Earth orbit (LEO) is one such area where costs may be more easily reduced than for manned missions. The most efficient way to accomplish this is through SSTO flight; however, until now, the cost per pound in such an endeavor was not achievable via a reduction from two-stage flight using a bell nozzle. If an aerospike nozzle design for SSTO can be more efficient through a greater payload capacity at a lower cost than two-stage flight for unmanned payloads to LEO, then the versatility of private sector spaceflight will increase as well as allowing for more defense, communication, and weather satellites, for the same overall cost.

## 1.3 Thesis Organization

Chapter II of this work explains previous projects that investigated SSTO flight, aerospike technology, and the attempts to effectively integrate the aerospike nozzle design into either space or aircraft. Chapter III details the science and engineering necessary to understand the work presented in this thesis. Here, rocket flight parameters are discussed, as well as how OTIS implements design conditions. Chapter IV presents the trajectory results for the eight cases modeled and evaluates their performance. Concluding remarks and observations are made in Chapter V, along with recommendations on future works.

# CHAPTER II
# LITERATURE REVIEW

The purpose of this chapter is to provide an overview on previous work done in the areas of single-stage to orbit flight and the research performed on linear, aerospike nozzles. This chapter also outlines any ongoing projects or work on this technology.

## 2.1 Single-Stage to Orbit Flight

When the United States first decided to dedicate a focused effort towards space flight in the late 1950s, the idea of SSTO was already under consideration as a possible method to achieve orbit. At the time however, it was deemed infeasible due to material and technological limitations of the time. SSTO technology remained on the back burner until the Challenger disaster in 1986. As a result of this event, all rocket technology was reevaluated, and for the next decade, a serious effort was made into the analysis and feasibility of SSTO [27].

The primary focus of SSTO development in the mid-1990s focused on multiple-propellant engines, proposing that either dual mixture engines (oxygen and hydrogen propellants) [32], or that tri-propellant engines would increase performance of new engines [26] or existing engines [28]. Many private corporations were hesitant to commence development of this technology until the conclusion of the joint NASA/Lockheed Martin X-33 project [36] (see Section 2.2.1). Finally, Dorrington of the University of London said at the turn of the century that only expendable SSTO technology was possible and that cheaper engines with greater reliability would need to be developed in order to truly make SSTO feasible [8]. The author feels that the ongoing advances in materials technology increases the feasibility of SSTO technology.

### 2.1.1 Georgia Tech *Hyperion*

One example of the evaluation of SSTO was a Georgia Institute of Technology project sponsored by NASA Marshall Space Flight Center entitled *Hyperion* [32]. The primary purpose of this project was to determine if a rocket-based combined cycle (RBCC) could be used to produce a vehicle that could reduce the cost of space flight. Georgia Tech proposed a plan for a horizontal takeoff and horizontal landing (HTHL) vehicle for SSTO that uses five ejector

scramjet RBCC engines, combusting LOX/LH2. Their concept is presented in Figure 4 and Figure 5. The basic design for *Hyperion* incorporated both advanced propulsion techniques as well as metal composites.

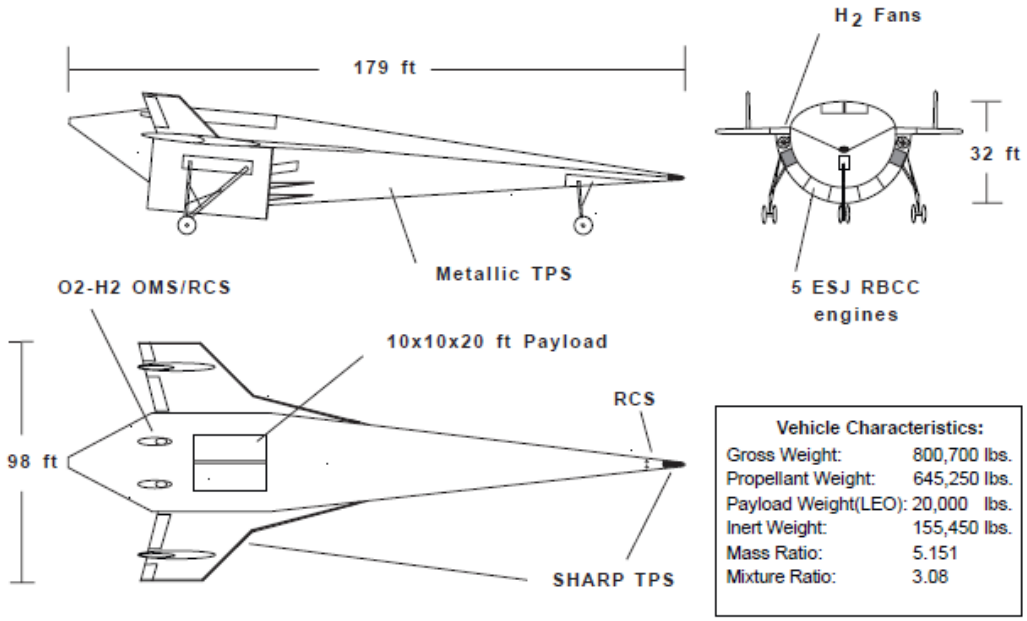



**Figure 4: *Hyperion* Configuration [32]**



**Figure 5: *Hyperion* Artist Rendering of RBCC Ascent [32]**

Georgia Tech used the Simulated Combined Cycle Rocket Engine Analysis Module (SCCREAM), a one-dimensional analysis code outputting an engine deck for use in a trajectory simulation program. The trajectory analysis was performed in the Program to Optimize Simulated Trajectories (POST) [32], a NASA/Lockheed Martin counterpart to OTIS. The trajectory constraint was a dynamic pressure boundary of 2,000 psf during the ramjet and scramjet modes, when the *Hyperion* flies between Mach 3 and 9, as any higher pressure loading would increase airframe weight and cooling requirements. Transition to the all-rocket mode is completed by Mach 10. This vehicle was designed to be low cost and reusable at about 150 flights a year at $1.64M a flight in 1999. Georgia Tech determined that the probability of achieving a viable *Hyperion* was low as it did not present a reduction in cost of existing vehicles, thus a prototype was never constructed.

### 2.1.2 NASA GTX

In addition to the funding NASA provided to the Georgia Institute of Technology, NASA Glenn Research Center also researched into a vertical launched, horizontal landing, SSTO vehicle using an RBCC engine concept called GTX[1]. The basic concept of the GTX is shown in Figure 6 with details of the propulsion design in Figure 7.

The initial designs and tests in 2001 focused on using the rocket engine for the vertical takeoff until about Mach 2.5. The rocket is then ramped off, while operating a subsonic combustion ramjet of LOX/LH2 until Mach 6, at which point the engine operates with supersonic combustion, i.e. a scramjet. For the final ascent into orbit, the air-breathing engine is closed, and the rocket re-ignites to orbit [39]. The altitude-compensating thruster nozzle shown in Figure 7 is a factor of the arrangement of nozzles that acts as an expansion surface when operating at high speeds and as altitude compensation at low speeds [35].

In 2002, NASA Glenn published work investigating how adding a solid rocket motor (SRM) to the GTX design would increase performance. For this study, they used OTIS to look at the thrust, flight path angle, altitude, and weight changes from the baseline case to the augmented case with the addition of the SRMs. They determined that the additional weight of the GEM 46

[1] GTX is not an acronym standing for anything in particular.

SRM would not significantly compromise the feasibility of SSTO while providing the sought-after additional weight [35].

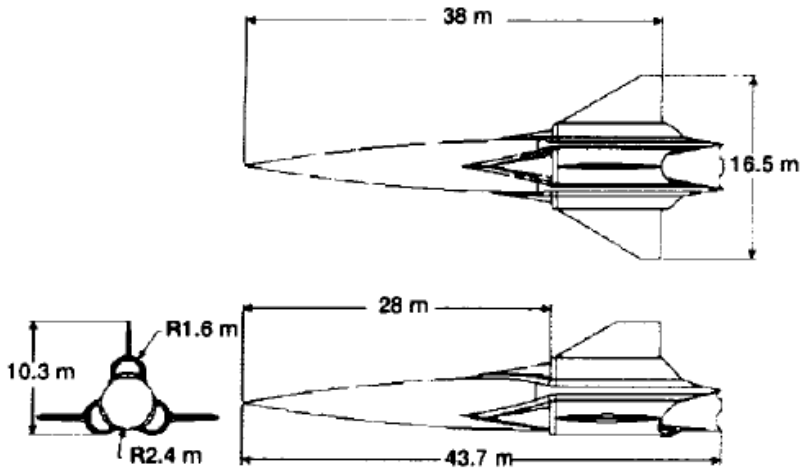



**Figure 6: NASA GTX Vehicle Concept [38]**

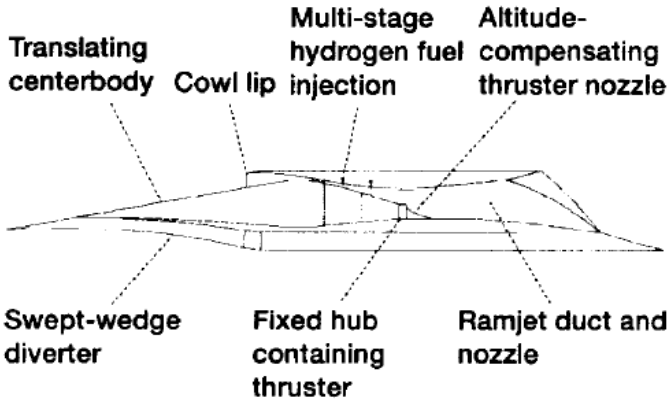



**Figure 7: GTX Propulsion Pod [39]**

The final publication on the GTX design was to demonstrate the propulsion system performance of the ram to scramjet transition and to validate the vehicle's aerodynamic and propulsion airframe integration by providing a demonstrator in order to test the engine

performance [22]. This demonstrator vehicle model is shown in Figure 8. Although the vehicle was never flown, a trajectory analysis of the ground tests using OTIS was performed, and it was deemed appropriate that experimental data was needed to validate the results. However, the cost of this data collection was estimated to be $325M, and would further provide a benchmark for high speed, air-breathing propulsion and future hypersonic work [22].

The author was unable to find any further work on the GTX vehicle, so this RBCC propulsion technique for SSTO was never fully realized.

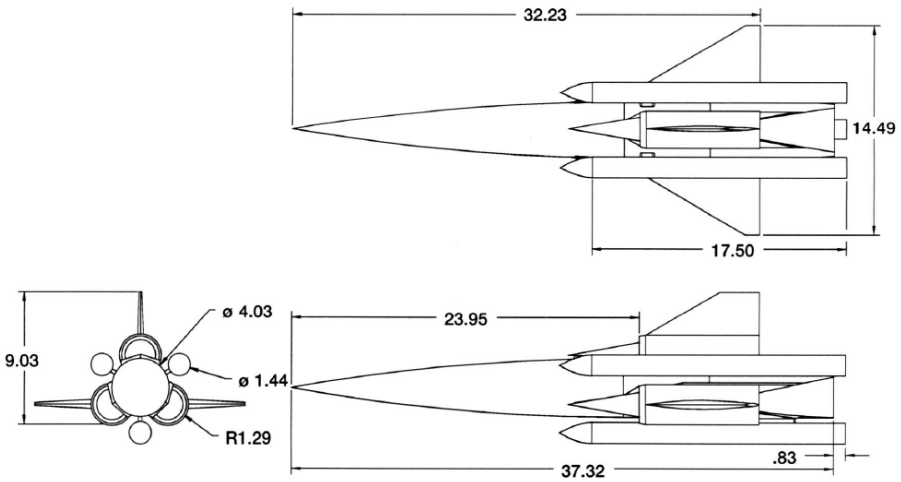



**Figure 8: GTX Flight Demonstrator (dimensions in feet) [22]**

## 2.2 Linear Aerospike Nozzles

The aerospike nozzle design and development began in earnest in the early 1970s with projects primarily taken on by Rocketdyne, NASA, and the U.S. Air Force. One of the first projects was awarded to Rocketdyne by the U.S. Air Force to develop and test an annular aerospike thrust chamber, first reported on in 1973 [25]. In this report, previous contract work is cited for aerospike thrust chamber tests at varying thrust levels; this includes initial tests of a linear aerospike engine configuration, which the author of this thesis was unable to find in the open literature. In 1974, the aerospike thrust chamber work continued with fabrication and

testing of the completed system [16]. Rocketdyne successfully demonstrated the flightweight aerospike thrust chamber, establishing a technology baseline.

One of the first comprehensive studies of using the linear aerospike engine for SSTO and reusable applications came in 1977, also conducted by Rocketdyne [20]. They provide the design and data for a dual-fuel, split combustor engine as shown in Figure 9. Using the materials technology level of the Space Shuttle Main Engine, Rocketdyne determined that the linear aerospike engine was versatile for a wide range of thrust levels.

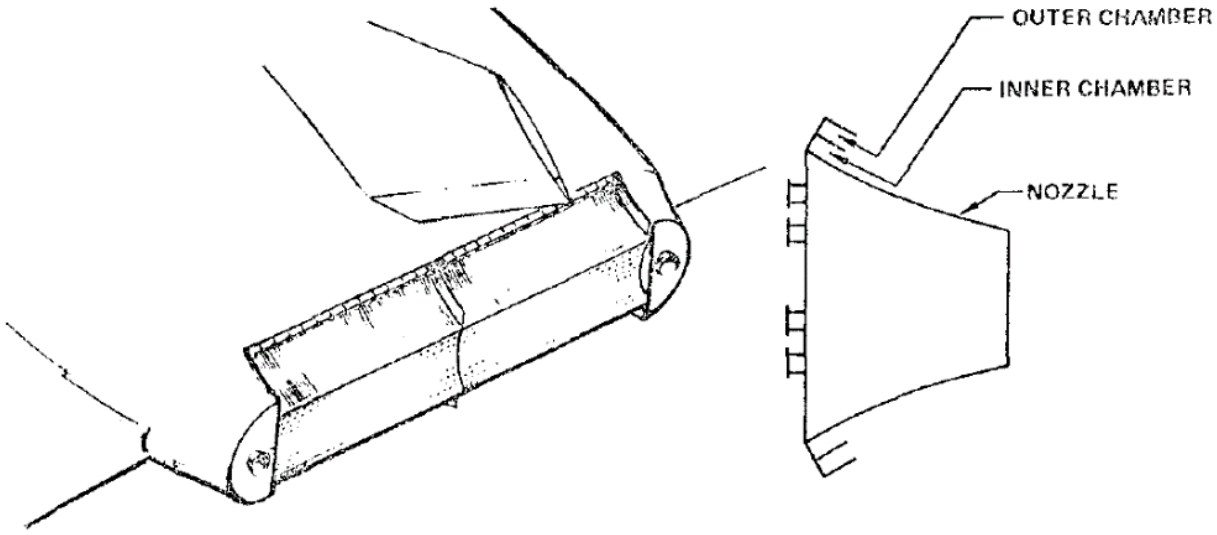



**Figure 9: Rocketdyne Linear Aerospike Nozzle Concept [20].**

The aerospike technology was not closely evaluated again until the mid-1990s due to the establishment of the Linear Aerospike SR-71 Experiment (LASRE) program to support Lockheed Martin's development of the X-33.

### 2.2.1 NASA/Lockheed Martin Linear Aerospike SR-71 Experiment (LASRE)

In 1997, Rocketdyne, now a division of Boeing, published their results for the Linear Aerospike SR-71 Experiment (LASRE) program to demonstrate the performance of the linear

aerospike on a lifting body to specifically simulate the X-33 [24]. This was accomplished by mounting a 20% scale, X-33 forebody onto an SR-71 (Lockheed Martin Blackbird) to determine the magnitude of the slipstream effect at the proper altitude and Mach number conditions before starting hot fire tests of the engine. The slipstream effect refers to the degradation of engine performance due to the air moving over the lifting body interacting with the outer boundary of the exhaust plume. The data from this test was used to validate computational fluid dynamic (CFD) codes for future vehicle design and optimization. The X-33 was the subscale technology demonstrator for a NASA-Lockheed Martin joint project known as the Venture Star. The Venture Star was a proposed, SSTO reusable launch system that was never fully developed due to complications with the weight associated with the LASRE and X-33 programs [9]. The major study on the LASRE project and its application for the Venture Star was a trajectory optimization study in how to generate a parametric model for optimizing aerospike designs [21]. NASA Langley Research Center was able to successfully generate an aerospike engine database by using POST and integrated the resulting parametric model into a multidisciplinary framework in order to determine alternate designs. In 2001, Lockheed Martin was able to perform a hot fire test, shown in Figure 10.

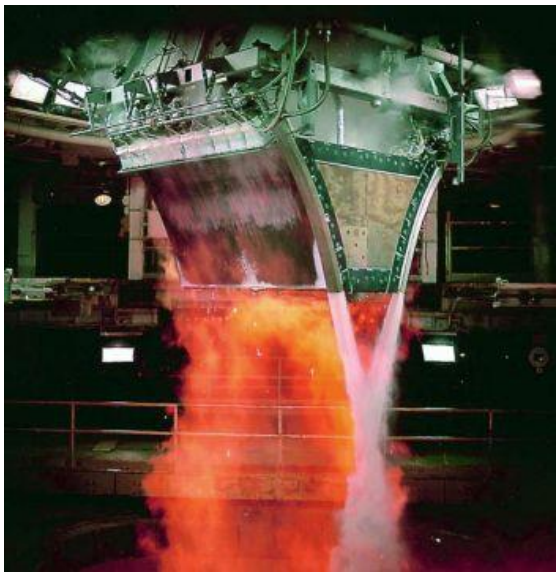


**Figure 10: Lockheed Martin Linear Aerospike Hot Fire Test as Part of the LASRE Program [1].**

### 2.2.2 Aerospike Study since LASRE/X-33

With the attention that NASA was generating about aerospike nozzle engines and their application for SSTO flight, the international community and universities began a more in-depth study of the technology beginning in the late 1990s, moving into the early 2000s. In 1997, universities in Munich, Germany evaluated the data published from Rocketdyne's Linear Test Bed from the 1970s and argued that the linear aerospike design was too optimistic with too many assumptions to make it a realistic option at altitude conditions [10]. Japan and China then published their interests in classifying the aerospike nozzle. The National Aerospace Laboratory (KRC) in Japan investigated the thrust losses of the linear aerospike design and proposed a method for predicting the thrust coefficient of an engine [40]. In 2001 and 2003, the Beijing University of Aeronautics and Astronautics published work on experimental and numerical methods of the aerospike design [44], the parametric optimization of a solid-propellant aerospike engine [43], and a new, tile-shaped plug design [42]. The University of Tokyo did some CFD modeling to evaluate the heating of the linear aerospike nozzle surface [41], which related the heat-flux distribution to the viscid-inviscid flowfield near the nozzle surface. The Japanese Aerospace Exploration Agency (JAXA) continued the in-depth characterization of the aerospike as recently as 2014 by successfully testing the flowfields of aerospike nozzles under the presence of external flow in wind tunnel experiments [38].

California State University at Long Beach investigated using a liquid-propellant aerospike engine for use in their Nanosat Launch Vehicles (NLV) or Small Launch Vehicles (SLV) and to collect aerospike flight data at a fraction of the cost of the X-33 program [6] to show the feasibility of using an all-aluminum, pressure-fed fuel tank instead of the more risky cryogenic composite tank [5]. The final work of California State University was to design and test a multi-thrust chamber aerospike nozzle to characterize the slipstream effect [4] in 2008. Their successful firing of a test engine, shown in Figure 11, led to an advanced design with curved, instead of linear, thrusters (Figure 12), with computational modeling in 2013 [29].

The author was unable to confirm if California State University is continuing this work.



**Figure 11: California State University Aerospike Engine Test Stand [4].**

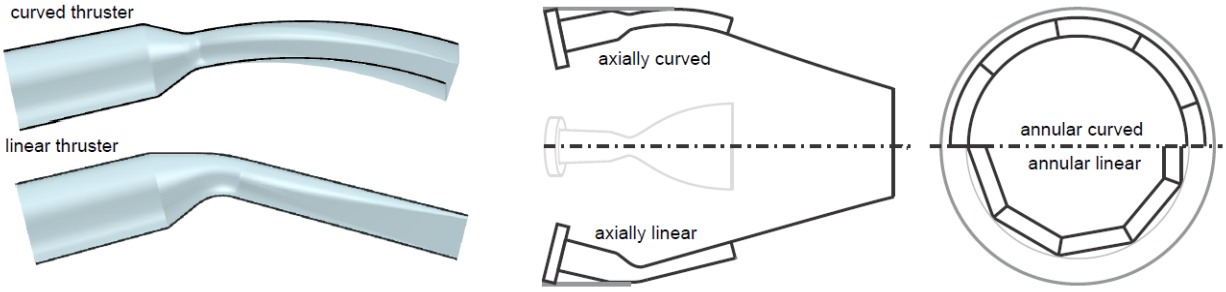



**Figure 12: California State University Curved vs. Linear Aerospike Thruster Design [29].**

## 2.3 Current Work

Since the lack of progress associated with the LASRE and X-33 projects in 2001, there has been little funding dedicated to the continued development of the linear aerospike engine. Furthermore, a lack of advancement in materials science has impeded the progress into SSTO technology.

### 2.3.1 SKYLON Spaceplane

Reaction Engines, Ltd., a British corporation founded in 1989, has developed the concept of a SKYLON spaceplane to act as a horizontal takeoff, horizontal landing, SSTO vehicle that uses two of their in-house developed SABRE engines [14]. SABRE is an air-breathing rocket based combined cycle (RBCC) engine. It uses the oxygen in the air at low altitudes combined with liquid hydrogen fuel for combustion, then switches to a conventional rocket mode at high altitudes using on-board liquid oxygen as the oxidizer. This reduces the weight of the vehicle allowing for greater payloads. With the SABRE engines, SKYLON is designed to carry up to 9.5 tons of payload to a 460 kilometer altitude. This technology has yet to be fully tested or integrated at the time of this thesis.

### 2.3.2 Firefly

A relatively new company, Firefly, has just emerged proposing a satellite launch design entitled *Firefly Alpha* [11]. This 2-stage, carbon composite structure is designed to launch a 400 kg payload to low Earth orbit (LEO). The first propulsion stage uses a plug-cluster aerospike design[2] with a liquid oxygen and methane propellant. There have been no published details on their design, but what details they do have is provided on the company website.

[2] See Figure 16 in Section 3.1.1.2.

# CHAPTER III
# MATERIALS AND METHODS

This chapter presents the basic engineering theory behind launch vehicles, as well as the methodology and assumptions in modeling the launch vehicle trajectories in OTIS.

## 3.1 Theory

Analysis and the implementation of the results presented in Chapter IV combine both compressible flow dynamics and orbital mechanics, the basics of which are detailed in this section.

### 3.1.1 Compressible Gas Dynamics

The foundation of analysis for rocket nozzle flow is embedded in compressible gas dynamics [2]; the primary use for this thesis involves property relations between the nozzle throat and the nozzle exit. The basics of nozzle theory are presented below.

#### *3.1.1.1 Nozzle Theory*

There are a few characteristic parameters to describe the dynamics of compressible fluid flow as applied to a rocket engine nozzle. The first, the Mach number, *M*, describes the relationship of the local speed, *V*, to the local speed of sound, *a*, as shown in Equation 1. A Mach number less than one describes the subsonic flow regime, equal to one is the sonic condition, and between one and approximately five is supersonic. A Mach number greater than about five is considered hypersonic, with non-negligible thermodynamic considerations associated with non-calorically perfect gases such as a chemically reacting flow.

$$M = V/a \tag{1}$$

The basic configuration for a rocket engine nozzle is shown in Figure 13. For the cases evaluated in this thesis, the fuel was liquid hydrogen (LH2), and the oxidizer was liquid oxygen (LOX). It was assumed that the conditions in the combustion chamber remained constant, such

that the resulting exhaust gas was ideal and calorically perfect under a constant pressure. This requires the assumption of non-reacting flow during nozzle expansion. This is commonly called "frozen flow", since the assumptions imply that no chemical change takes place throughout the nozzle once combustion occurs in the chamber due to the high gas velocities in the nozzle expansion, and that the mass fractions remain constant throughout the nozzle. The other extreme is called "equilibrium flow", where reactions occur at a rate so high that conditions continuously adjust in order to maintain equilibrium at the local pressure and enthalpy levels; this makes the entire process reversible [2].

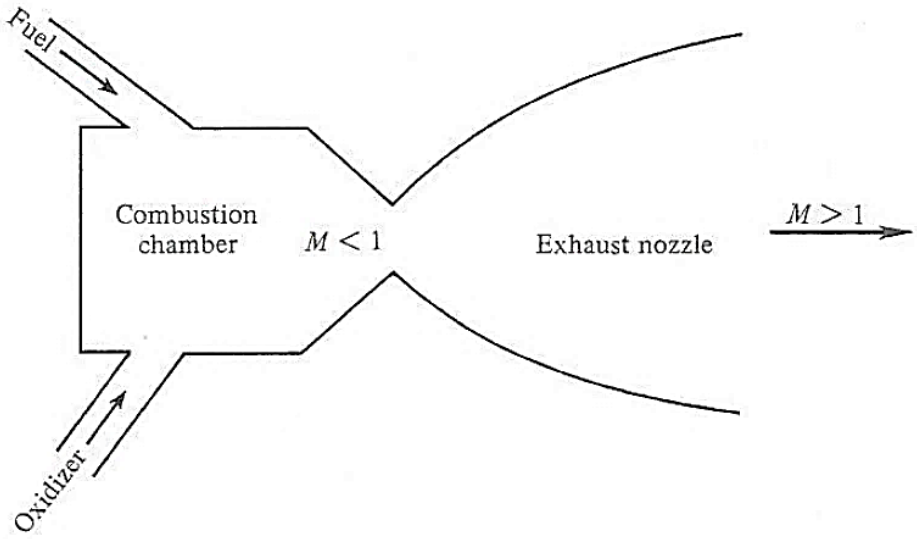



**Figure 13: Rocket Engine Basic Design [2].**

The Mach number in the combustion chamber remains subsonic and accelerates isentropically as the flow approaches the throat. When the exhaust gases reach the throat, the flow reaches a sonic condition where the cross-sectional area is the smallest. The contour of the exhaust nozzle then expands the flow to either supersonic or hypersonic speeds. This is the converging-diverging nozzle, first used by Carl G. P. de Lavel in a steam turbine for marine applications [2].

For the purpose of the study in this thesis, the following parameters were assumed to remain constant for each engine configuration: nozzle throat temperature, nozzle throat pressure, and nozzle throat speed of sound. These were assumed to remain constant so the frozen flow assumption would still apply. With the equilibrium flow, the constant specific heats would change with both pressure and temperature, increasing the complexity of the calculations. It is common and reasonable in launch vehicle analysis to assume frozen flow [2]. The thermally ideal gas relation, provided in Equation 2, was also assumed to be applicable with $P$, the pressure, $v$, the mass specific volume, $\rho$, the density, $R$, the universal gas constant, and $T$, the absolute temperature.

$$Pv = \rho RT \tag{2}$$

There are several characteristic equations that define the relationship of particular parameters between the throat, nozzle exit, and combustion chamber locations. These are summarized below in Equations 3 – 5 for a thermally and calorically perfect gas. The superscript, *, indicates sonic conditions at the throat, while the subscript, $_0$, represents the chamber (stagnation) conditions, with $\gamma$ being the specific heat ratio:

$$P^* = P_0[(\gamma + 1)/2]^{-\gamma/(\gamma-1)} \tag{3}$$

$$T^* = T_0[2/(\gamma + 1)] \tag{4}$$

$$a^* = \sqrt{\gamma RT^*} \tag{5}$$

The isentropic pressure ratio, Equation 6, between the chamber and the nozzle exit is written in terms of the Mach number, $M$, as well as the area-Mach relation equation, Equation 7, which relates the nozzle exit, $A_e$, and throat, $A^*$, areas.

$$P_0/P = [1 + ((\gamma - 1)/2)M^2]^{\gamma/(\gamma-1)} \tag{6}$$

$$A_e/A^* = (1/M^2)[(2/(\gamma + 1))(1 + ((\gamma - 1)/2)M^2)]^{(\gamma+1)/(\gamma-1)} \tag{7}$$

These equations relate nozzle local (exit) pressure and area to chamber (stagnation) values for perfect expansion flow of an optimal nozzle profile, forming the basis for nozzle theory and analysis.

#### *3.1.1.2 Nozzle Designs*

There are three primary categories of rocket nozzle configurations: cone, bell, and annular. These designs are presented in Figure 14, with the "Spike" representing the annular configuration.

The cone, or conical nozzle, design was the first developed for rocket flight. As described in Section 1.1.2, it was easy to manufacture and adjust for varying design criteria.

The bell nozzle was developed as a way to take advantage of the optimal characteristics of the cone. The bell nozzle design primarily consists of two sections as seen in Figure 14, the portion right at the exit of the throat and that at the bottom of the bell. At the throat exit, the initial divergent region uses fast-expansion to create a more uniform exhaust gas flow. The contour of the nozzle wall is more gradual than that of the conical nozzle to prevent oblique shocks, which would negatively impact performance. The divergent angle closer to the nozzle exit is smaller than that at the throat exit, so as to allow for the length of the bell nozzle to be shorter than the conical nozzle [17]. Through the changing divergence angle, the bell design minimizes weight and maximizes performance.

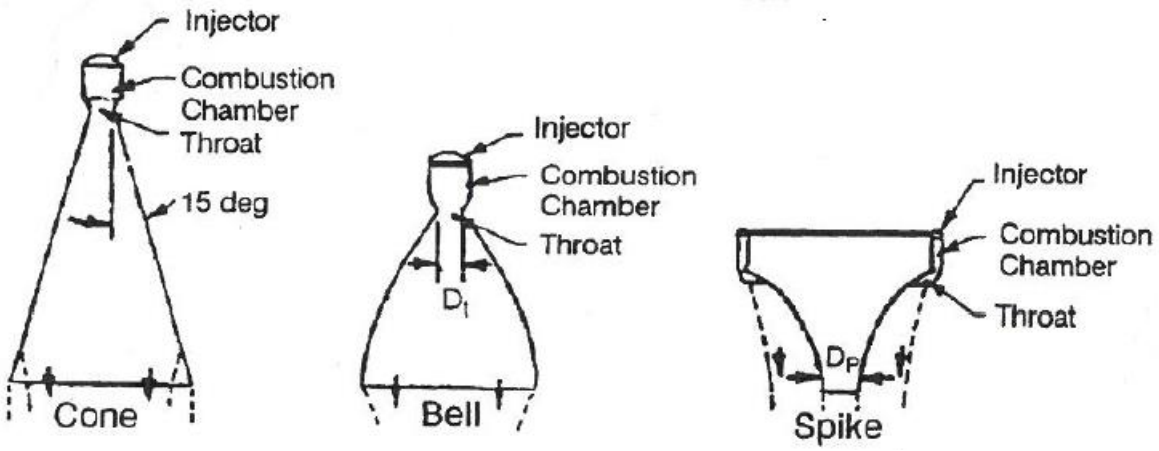



**Figure 14: Cone, Bell, and Aerospike Basic Configurations [17].**

The last configuration is called an annular nozzle because the combustion occurs along a ring (annulus) around the base of the nozzle. The plug or spike refers to the solid piece that blocks the flow from what would be the center of a traditional conical or bell nozzle. This was first attempted in a plug cluster design with a conical spike [17]. This spike prevents turbulent mixing in the exhaust flow that would occur in its absence, while maintaining isentropic expansion. A cross-section of this design is shown in Figure 15.

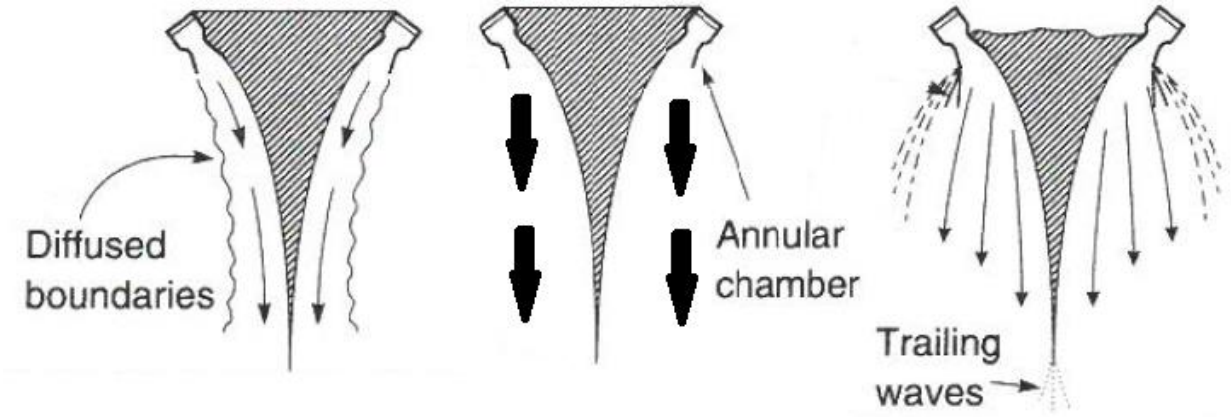



**Figure 15: Cross-section of Conical Plug Spike Nozzle, Exhaust Plume Diagram at High (overexpanded), Optimized (perfectly expanded), and Low (underexpanded) Ambient Pressures [37].**

However, this would require a relatively long, thus heavy, spike. In order to save on mass, the truncated spike was introduced as shown in Figure 16 in a plug cluster configuration [3]. This reduces efficiency, however, by causing a turbulent wake and recirculation at the base of the spike at high altitudes due to viscous effects that generate entropy, increasing drag, as shown in the recirculation regions in Figure 17.

A way to alleviate the induced drag at the base of the spike is to reconfigure from a conical design to a linear one in the form of the linear aerodynamic spike, also known as a linear aerospike. This has the combustion chambers in a line along two sides of the nozzle, allowing the use of lower-cost, modular combustors. This increases efficiency over the conical, truncated spike because it ultimately limits the recirculation area at the truncation by limiting the three-

dimensional effects to a more two-dimensional design. This general design is shown in Figure 18.

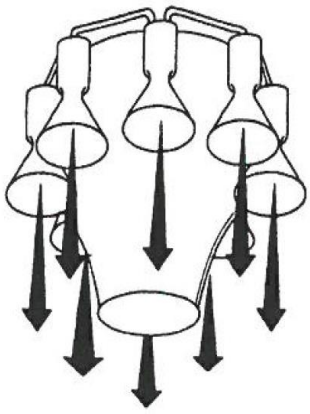


**Figure 16: Truncated, Conical Spike [17].**

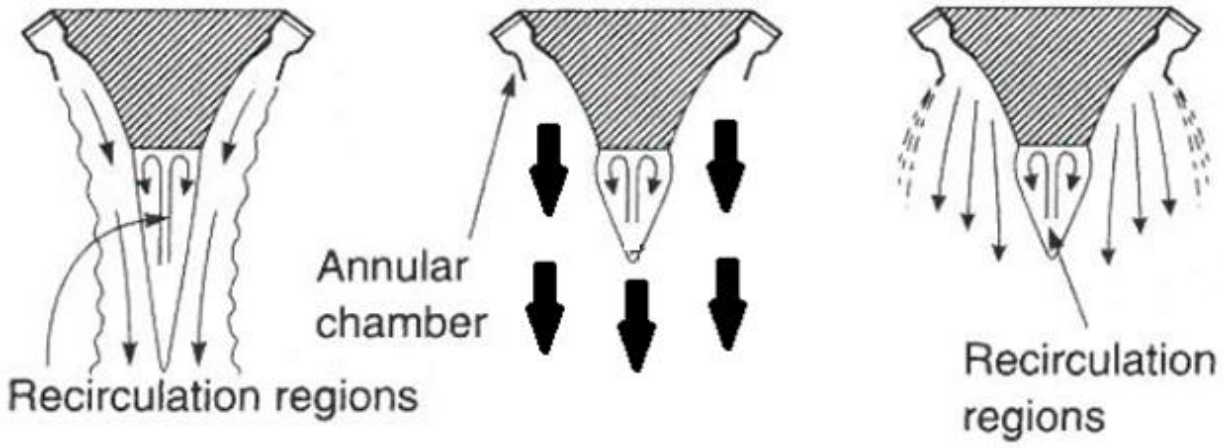



**Figure 17: Cross-Section of Conical, Truncated Plug Spike Nozzle, Exhaust Plume Diagram at High (overexpanded), Optimized (perfectly expanded), and Low (underexpanded) Ambient Pressures [37].**

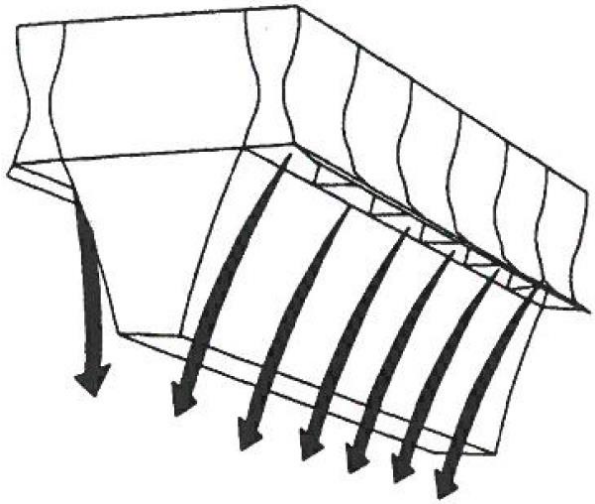


**Figure 18: Truncated, Linear Aerospike [17].**

A more in-depth depiction of the linear aerospike under altitude conditions is given in Figure 19.

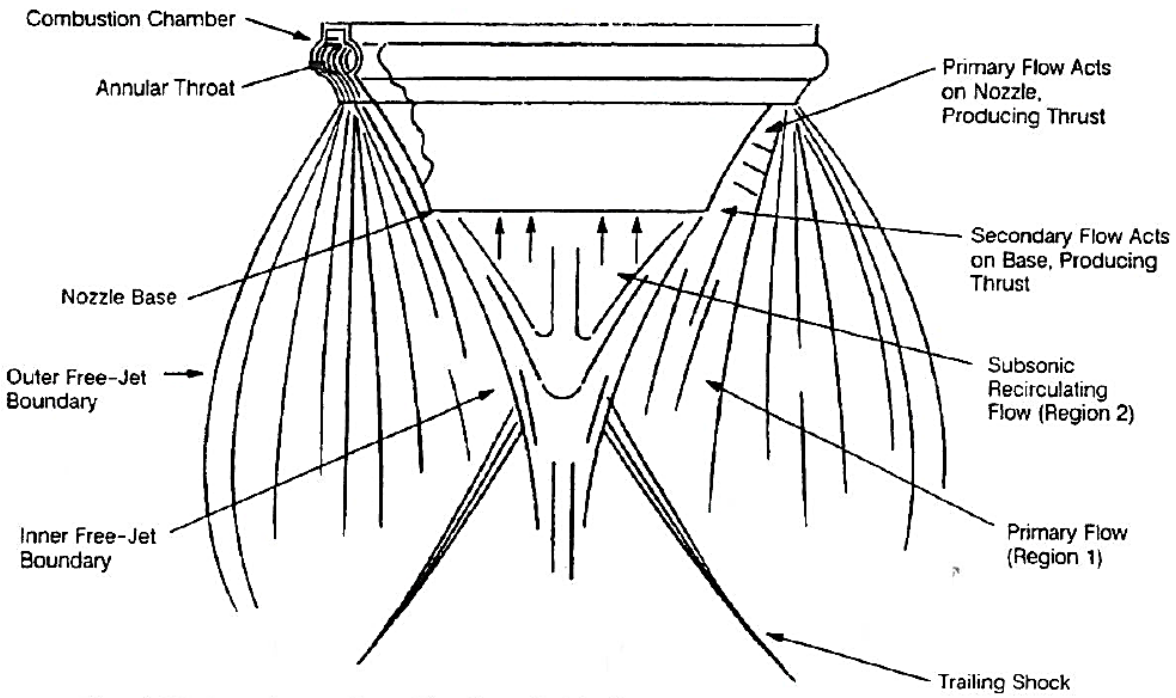



**Figure 19: Linear Aerospike Nozzle Design under Altitude Conditions [17].**

The primary, high pressure gas exhaust flow exits a combustion chamber and further expands along the surface contour of the linear, truncated spike, shown in Figure 19. The primary flow provides the majority of the thrust and is determined from the throat, the nozzle wall contour, and the ambient pressure. The LOX/LH2 propellant enters the system through multiple injection points along the linear sides of the truncated spike. The pressure on the nozzle base contributes additional thrust. A secondary flow ejected from the base of the truncated spike may also increase the base pressure (back pressure on the truncated spike base area that contributes to the total force accelerating the engine) and is roughly 1-2% of the total flow [37]. The free-jet boundary that serves as the outer surface of the primary flow is influenced by the ambient pressure. At lower altitudes (sea level), the compression of the outer free-jet increases the static pressure on the walls of the truncated spike, also increasing the base pressure [37]. As the rocket increases in altitude, the ambient pressure decreases and the outer free-jet expands outwards. This gives the advantage of higher expansion area ratios for a given length (about 1/3 the length of bell nozzles [37]), increasing performance. Furthermore, the expanding diverging flow exerts a decreasing pressure on the contour of the aerospike, similar to the diverging nozzle flow in the conventional bell. However, despite the aerospike being a shorter structure than the bell, this results in high cooling requirements, a heavier structure, and manufacturing difficulties when compared to the bell nozzle design. It is important to note that there is a lack of proven flight experience and reliability to the aerospike design, as only a few, and only ground tests, have been performed (see Chapter II).

Other than the truncated annular and linear aerospike designs, there are other ways to achieve altitude compensation. The most basic ones are described in a NASA Marshall Space Flight Center study done in 1997 [30], the cross-sections of which are provided in Figure 20. A more specific example of the mechanical translating bell nozzle is the extendable exit cone (EEC), as shown in Figure 21, which allows for the perfect expansion at three different design altitudes. Many of these designs have never been tested due to their complexity of maintaining perfect expansion throughout flight.

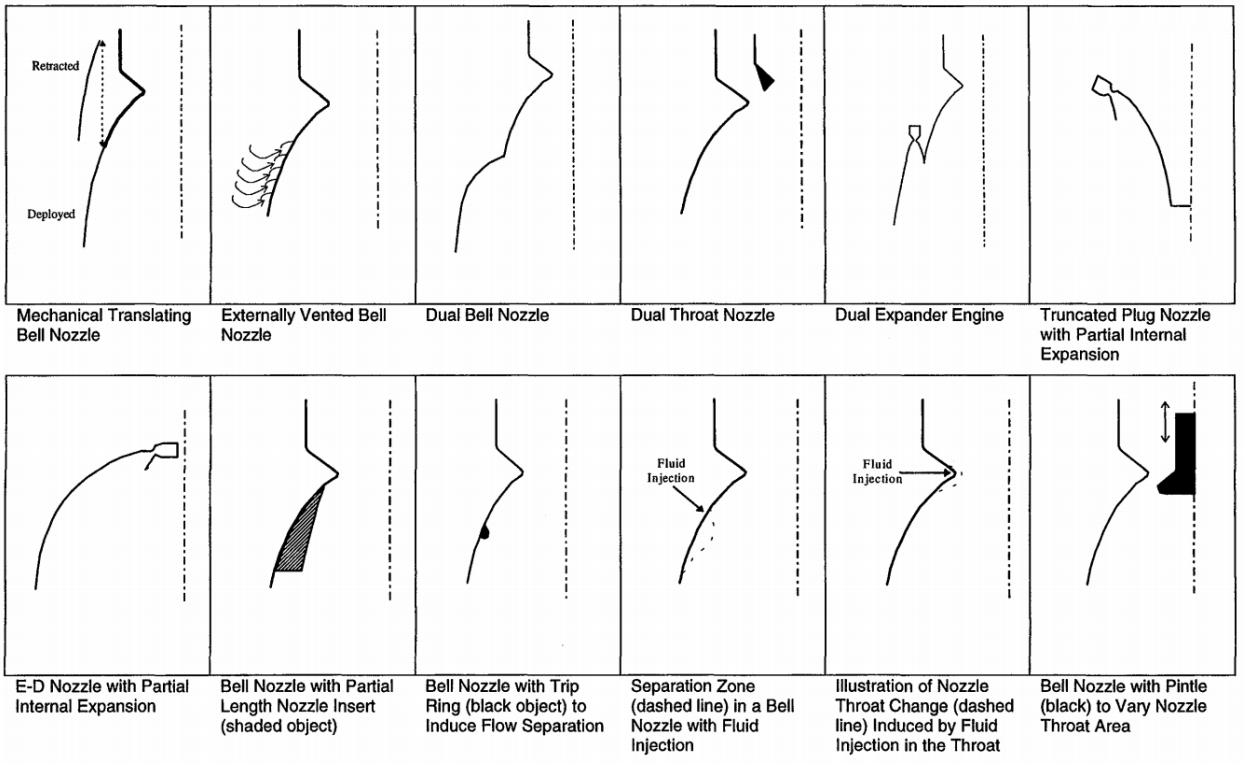



**Figure 20: Cross-Section of Various Altitude Compensating Nozzle Designs [30].**

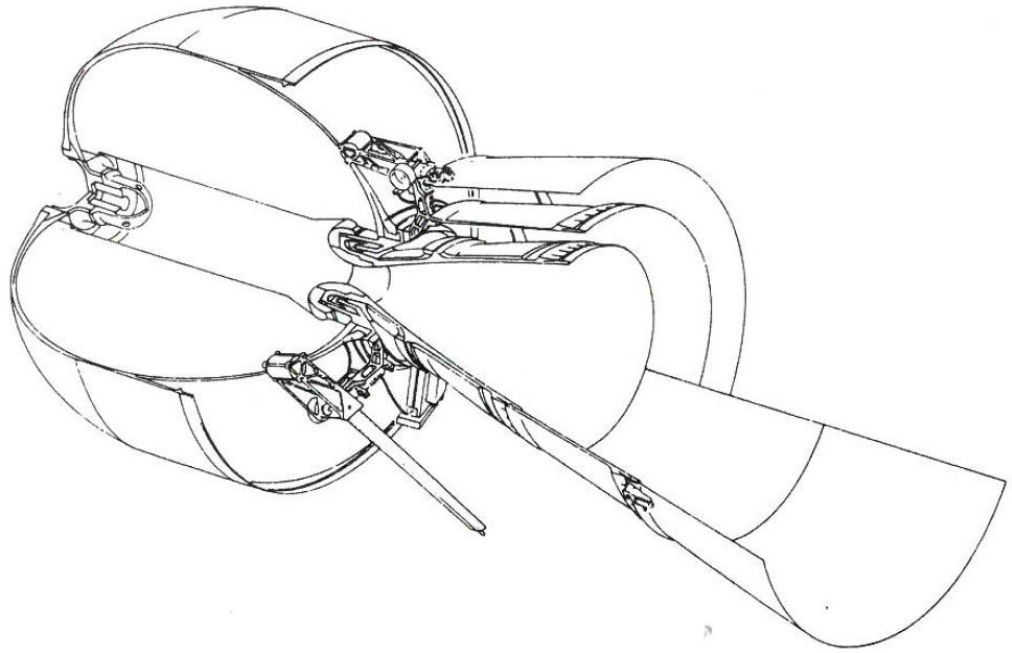


**Figure 21: Extendable Exit Cone Altitude Compensation Nozzle [31].**

### 3.1.2 Launch Vehicle Mechanics

The purpose of a rocket engine is to use the chemical energy from combusting propellant, LOX/LH2 for the purpose of this thesis, to produce a large quantity of high pressure gas, which is expanded and accelerated through a nozzle to provide thrust. This principle is based on Newton's balance of momentum which states that when mass is ejected from a system (the propellant) in one direction, the mass left behind acquires a velocity in the opposite direction (the rocket and payload). This section introduces the fundamental equations that describe rocket trajectories and performance.

#### *3.1.2.1 Basic Equations*

The basis for describing the trajectory of a rocket is presented in Figure 22. The engines at the base of the rocket produce the thrust, *T*, acting in the direction of the velocity vector, *v*. In the figure, the velocity is broken into a tangential and normal unit vectors; the tangential vector is in the same direction as the velocity, while the normal vector is perpendicular to the velocity direction and points towards the center of curvature, *C*. The drag force, *D*, is an aerodynamic force acting opposite to the velocity. The drag forces depend on the dynamic pressure, the drag coefficient, and a reference surface area. The angle, *a*, in Figure 22, is the flight path angle, described in relation to the trajectory model in Section 3.2.1.

The dynamic pressure, *q*, defines the kinetic energy per unit volume of the fluid as a function of the density, ρ, and the local speed, *V*, shown in Equation 8.

$$q = {}^{1}/_{2}\,\rho V^{2} \tag{8}$$

The overall thrust, *T*, is defined in Equation 9 with $u_e$, the nozzle exit velocity, $A_e$, the nozzle exit area, and $P_e$, the nozzle exit pressure. The mass flow rate, $\dot{m}$, is the rate of the combusted gases moving through the nozzle. The static pressure, *P*, is the local ambient pressure at altitude.

$$T = \dot{m}u_e + A_e(P_e - P) \tag{9}$$

For the purpose of this thesis, the vacuum thrust is used in the trajectory modeling program, OTIS. The vacuum thrust is the rocket engine thrust when the ambient pressure, *P*, is assumed to be negligible [7], i.e. zero, in the vacuum of space.

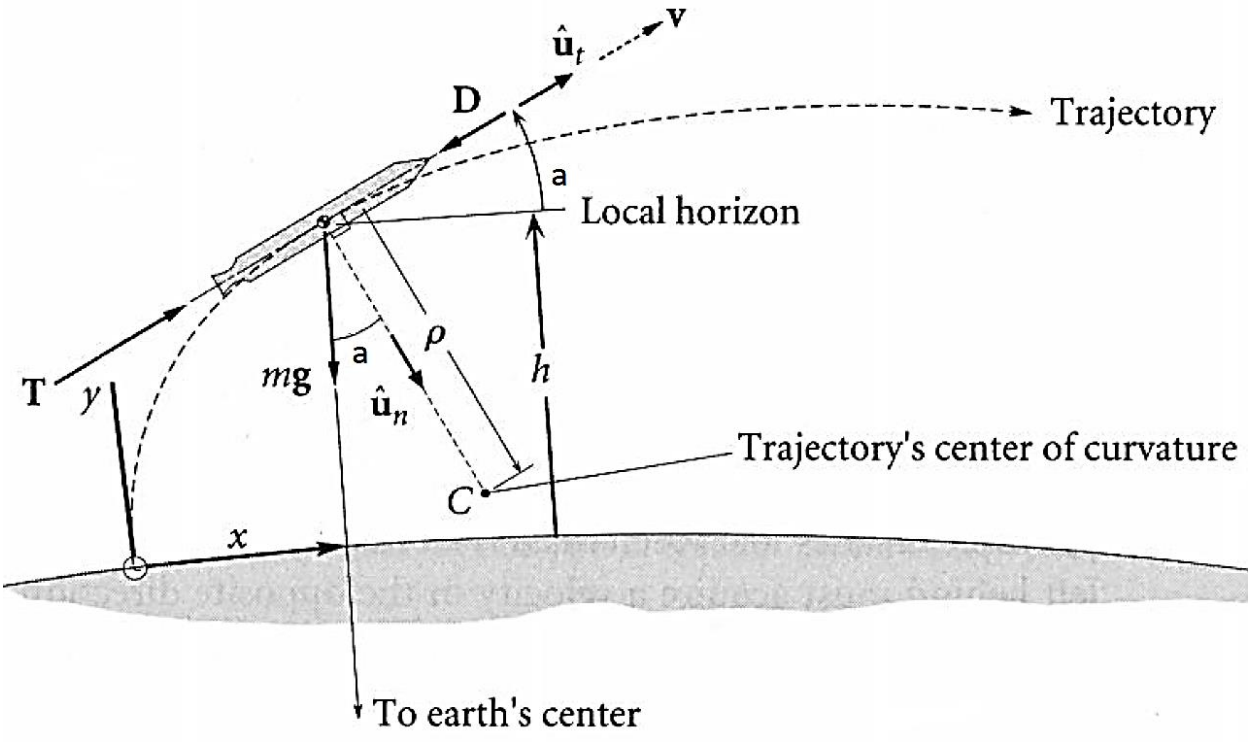



**Figure 22: Launch Vehicle Trajectory Diagram [7]**

The general equation of motion for a launch vehicle in a gravitational field is presented in Equation 10, with *m*, the mass of the rocket, $T_{vac}$, the vacuum thrust, and $F_g$, the local gravitational force [19].

$$m\frac{dv}{dt} = T_{vac} + F_g \tag{10}$$

If the assumption that the gravitational field is negligible compared to the thrust and that the engine operates at a constant $u_e$, then integrating Equation 10 gives what is known as the rocket or delta-v equation:

$$\Delta v = u_e ln\frac{m_i}{m_f} \tag{11}$$

The change in velocity, $\Delta v$, is the magnitude achieved through the ejection of the combusted fuel to achieve a particular maneuver. For example, the $\Delta v$ required to escape Earth's gravitational field from the surface is $1.12 \times 10^4$ m/sec [19]. For the purpose of this thesis, this equation assumes that all of the fuel has been expunged, as $m_i$ is the initial, total, wet mass and $m_f$ is the final, total, dry mass.

#### *3.1.2.2 Engine/Rocket Performance Parameters*

Another way to describe a rocket engine is through performance parameters such as a vacuum thrust to initial weight (thrust-to-weight) ratio. Heavy lift rockets tend to have thrust-to-weight ratios greater than 3.0 because of the greater difficulty to steer at lower altitudes; however, higher ratios generate more drag at lower altitudes due to their greater acceleration and increase the force on payloads at the end of burnouts due to the increased deceleration. In this thesis, a constant value of 3.06 was chosen based on the higher thrust trajectory cases. The linear aerospike engine, in order to minimize gravity losses where this nozzle configuration is most efficient and to increase the control of this larger craft, requires a larger rocket body diameter than the bell nozzle. For consistency, this larger thrust-to-weight ratio was maintained for the lower thrust cases as discussed in Section 4.1 by increasing the total, initial weight of the rocket. This ensures that reasonable comparisons between the two cases are made. Accepted values of thrust-to-weight ratios for non-heavy lift launch vehicles center around 1.5 [13].

Performance parameters, in addition to the vacuum thrust, that were used to describe the rocket engine in the trajectory analysis were vacuum specific impulse, $I_{sp}$, and nozzle exit area. The specific impulse is the thrust per sea-level weight rate per second of propellant consumption and is a measure of engine efficiency. For example, for an engine with an $I_{sp}$ of 400 seconds, the engine will produce 400 lbs of thrust for every pound of fuel injected into the combustion chamber per second. This means that when comparing two engines, the engine with the higher $I_{sp}$ value will produce the same amount of thrust, but consume less fuel than an engine with a lower $I_{sp}$ value. To calculate the vacuum $I_{sp}$ in this thesis, the vacuum thrust is used instead of the sea-level thrust as shown in Equation 12. This is the form used in OTIS (see Section 3.2). The vacuum specific impulse has a higher value than that of sea level, since the ambient pressure factors into the thrust equation. In a vacuum (or near-vacuum), the ambient pressure is much

lower, increasing the thrust value as seen in Equation 9. At sea level, the ambient pressure is frequently higher than that of the nozzle exit pressure, decreasing the thrust value, thus decreasing the specific impulse.

$$I_{sp,vac} = T_{vac}/(\dot{m}g) \tag{12}$$

The final performance parameter, which serves as the basis for trajectory comparison and optimization in this thesis, is the propellant mass fraction (PMF). The PMF represents what percentage of the total mass (weight) that is propellant consumed during flight [13]; this was calculated for each trajectory by using Equation 13.

$$PMF\ (\%) = [(W_i - W_f)/W_i]\ x\ 100 \tag{13}$$

In this equation, it is assumed that all propellant is consumed during flight so that the difference between the initial weight, $W_i$, and the final weight, $W_f$, is the propellant weight. Thus, as the PMF decreases, less propellant is consumed to reach the same altitude, allowing for delivery of greater payloads. The differences in the individual initial weight between trajectories for the cases described in Chapter IV are resolved by maintaining the constant thrust-to-weight ratio, ensuring comparison of equal mass launch vehicles for all test cases.

### 3.1.3 Calculating Effective Nozzle Exit Area of an Aerospike

A direct method for calculating the rocket nozzle exit area based on ambient pressure at an altitude was required in order to implement the altitude compensation factor of the aerospike engine nozzle into the OTIS trajectory analysis program described in Section 3.2. This was done primarily through assumptions made to apply compressible gas dynamic relations to the engine nozzle. Other than assuming perfect expansion throughout flight, the propellant gas, as a result of combusting the LOX/LH2 fuel, was assumed to be ideal, isentropic, and calorically perfect (frozen flow). Therefore, the chamber pressure, specific heat ratio, nozzle throat temperature, nozzle throat pressure, and nozzle throat speed of sound remain constant. Further applying conservation of mass, the mass flow rate, $\dot{m}$, of the exhaust gas would be the same as that at the choked nozzle throat, $\dot{m}^*$, which is a function of the vacuum thrust, $T_{vac}$, vacuum specific

impulse, $I_{sp}$, and gravity, $g$, shown in Equation 14. All calculations were done in standard SI units and converted into English units as needed for input into the trajectory program while assuming choked, nozzle flow.

$$\dot{m} = T_{vac}/(I_{sp} * g) = \dot{m}^* = \rho^* a^* A^* \tag{14}$$

Conditions at the nozzle throat are determined from the previous thermally and/or calorically perfect gas relations in Equations 3-7, so that the constant throat area, $A^*$, may be solved in Equation 14. Equation 15 represents the throat (sonic) density form of the ideal gas law for a thermally perfect gas, Equation 2.

$$\rho^* = P^*/(R\,T^*) \tag{15}$$

From Equations 6, 7, 14 and 15, this yields the exit area, $A$, with a constant nozzle throat area, $A^*$, and chamber pressure, $P_0$, that is only dependent on the ambient pressure, $P$, at the current altitude, presented in Equation 16. Equation 16 is the basis for the calculations of the nozzle exit area for all altitude-compensating cases presented in Chapter IV.

$$\frac{A}{A^*} = \left(\frac{2}{\gamma+1}\right)^{(\gamma+1)/(2\gamma-2)} \left(\frac{P_0}{P}\right)^{(\gamma+1)/(2\gamma)} \left\{\left[\left(\frac{P_0}{P}\right)^{(\gamma+1)/\gamma} - 1\right]\frac{2}{\gamma-1}\right\}^{-1/2} \tag{16}$$

## 3.2 Optimal Trajectories by Implicit Simulation (OTIS)

The trajectory program used for the analysis and optimization of different rocket configurations is the Optimal Trajectories by Implicit Simulation (OTIS) [34] provided for use by NASA Kennedy Space Center. Despite its name, OTIS is capable of performing both implicit and explicit trajectory analysis, but for the purpose of time and simplicity, all solutions presented in this thesis were run explicitly using FORTRAN, which allows scripting that can be used to control computer commands. A basic knowledge and understanding of orbital mechanics is required to operate OTIS, as it may provide non-physical solutions without indicating an error in the simulation.

### 3.2.1 Implementation & Design

OTIS requires two different input files: OTISIN and PHASIN. OTISIN is used to define the user-specified number of phases that comprise the rocket trajectory, the phase names, the coordinate system, whether the solution is explicit or implicit, and the output variables. There can be as many PHASIN inputs as necessary, and this is where the majority of the scripting that controls OTIS occurs. Aerodynamic forces were programmed through a constant drag coefficient of 0.2, and controls were the pitch, yaw, and roll, directions as shown in Figure 23, if the velocity vector were in the positive x-direction (orientated along the rocket velocity vector). Engine parameters were defined through the vacuum thrust, vacuum $I_{sp}$, and nozzle exit area. A time step and total time were also defined and, unless stated otherwise, OTIS assumes a launch from Earth.

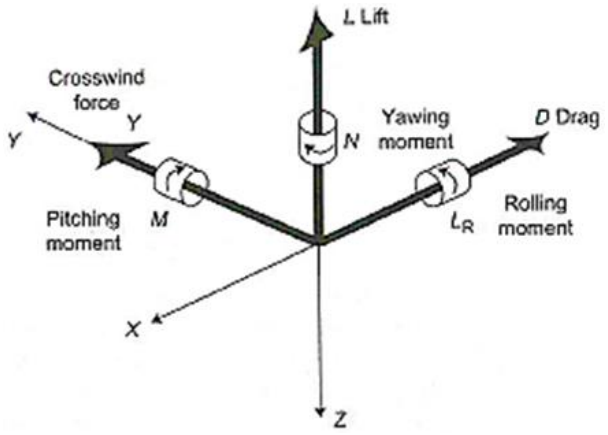



**Figure 23: Aerodynamic Force Direction Diagram [15].**

The first PHASIN phase needs several initial state variables, the majority of which were kept constant between case studies (see Chapter IV). These constant state variables were initial velocity, flight path angle, heading angle, latitude, and longitude. OTIS identifies some discontinuities in the initial velocity, flight path angle, and heading angle if not given a value, or directed at exactly 90 degrees. In this thesis, the initial velocity was given a value of 100

ft/second, about 0.4% of the orbital velocity at the target altitude of 750 kilometers, to correct this discontinuity. Additionally, the flight path and heading angles were given values of 89 degrees, as opposed to 90 degrees. The initial flight path angle represents the rocket sitting vertically on the launch pad, while the heading angle describes the direction of flight from zero degrees North. All cases modeled were eastern launches so as to use the rotational moment of the earth to help achieve orbital velocity at the target altitude. Since the Earth naturally rotates East at 1,041 miles per hour at the sea level equator, a western launch would have to immediately overcome this rotational motion, in addition to gravitational forces in order to achieve the same altitude, thus requiring additional propellant. This is not a normal heading that rockets typically fly as the trajectory would not have the center of the Earth as its intersecting orbital plane once in orbit. This was a design constraint implemented by the contractor, and remains constant for each trajectory case evaluated. A more typical heading for a launch at this location would result in an orbital inclination of 28.5 degrees. The latitude and longitude used in this study are the coordinates for NASA Kennedy Space Center, at sea level.

There can be several parameters used to end one phase in OTIS and enter another; the most basic of which is a function of the total phase time. However, stopping conditions based on altitude, velocity, orbital velocity, etc., are also possible. OTIS can process the assignment of several different phase-stopping conditions and will stop the phase and move on to the next phase of the trajectory whenever one of them is reached.

The output variables defined in OTISIN are shown on the terminal when a simulation is running, but several output files are created during each run for later evaluation; one of these easily exports to a Microsoft Excel file for plotting. OTIS defaults all inputs and outputs into English base units unless programmed otherwise.

There are three general categories that the PHASIN files fall within when modeling an SSTO trajectory: primary burn, coasting, and circularization burn. All cases modeled assume that the engine may be turned off and then on again for a brief burn to ensure a user-defined orbit is reached.

### 3.2.2 Bell Nozzle

For every phase where the engine is firing, an engine entry with the vacuum thrust, vacuum $I_{sp}$, and nozzle exit area must be specified. For all cases modeling a bell nozzle, these three parameters do not change throughout the flight. Note that the values of these parameters correspond to a traditional bell nozzle rocket motor and would differ for other bell-nozzled rocket motors, as well as other motor types.

### 3.2.3 Aerospike Nozzle

The only engine variable that changed for the altitude compensating cases, as described in the next section, was the nozzle exit area. Based on the equations presented previously, after a few seconds of flight, the ambient pressure based on the altitude of the rocket was used to update the effective nozzle exit area at the current altitude by using Equation 16, for the next OTIS phase. An average of 10 second phases was used based on verification runs with shorter phase times, as small as 3 seconds, so that the nozzle exit area would be adjusted at a rate to achieve greater accuracy. Very little difference was observed in the optimization of the flight trajectory for phase times less than 10 seconds. Furthermore, since the annular nozzle design provides reduced improvements in performance at higher altitudes, the more rapidly changing nozzle exit area at those higher altitudes as a result of any longer phase times, had less impact on the trajectory than if there were longer phase times at lower altitudes[3].

## 3.3 Trajectory Modeling Process

As introduced in Chapter I, the performance and efficiency of the rocket trajectory is measured by the propellant mass fraction (PMF) and serves as the basis for optimization and comparison for this work. This process is achieved by changing the nozzle exit area to model altitude compensating effects throughout flight in 10 second increments in addition to observing two specific impulse values common to accepted conventional bell and linear aerospike configurations for rockets of this size. Each rocket trajectory must model the same design goals

[3] A complete OTIS input file is provided in Appendix A for the aerospike nozzle baseline case, Case 1 (Table 1).

of obtaining a circular orbit at a 750 kilometer altitude on the opposite side of the earth from the launch location. Results of this process are presented in Chapter IV.

# CHAPTER IV
# RESULTS AND DISCUSSION

The focus of this chapter is the presentation of the case results and sample trajectory profiles to form the foundation for optimization comparison and analysis.

## 4.1 Trajectory Analysis and Comparison

A summary of the different rocket configurations considered in this study is presented in Table 1. Cases 1 and 5 in Table 1 describe the linear aerospike and bell nozzle control cases, respectively. The nozzle type classification of constant, limited, or infinite describes the modeled nozzle behavior during flight. A constant nozzle area maintains its value throughout flight; a limited nozzle area indicates that the area changes at lower altitudes, but is then held constant when it reaches the value of the bell nozzle constant area; an infinite nozzle type describes a theoretical aerospike expansion where the nozzle exit area has no upper limit and continues to increase with altitude. These nozzle configurations were chosen to show the effects of a wide-range of nozzle designs on SSTO launch vehicle performance, and were applied in combination with varying thrust and specific impulse values since increasing these rocket engine performance parameters also decreases PMF. An aerospike specific impulse and thrust were chosen based on Mitsubishi's LE-7 engine series [23], and the bell nozzle specific impulse and thrust were based on Pratt & Whitney's RL10A-4 engine [18].

### 4.1.1 Optimizing Trajectory Profiles

Obtaining a successful rocket trajectory is simple with very little input; provided there is enough thrust and a high enough $I_{sp}$, rockets may obtain escape velocity. However, optimizing the launch trajectory is complex. There are two primary ways to optimize a basic rocket trajectory to expend less fuel, lowering the PMF. The first is a gravity turn, where the rocket gradually becomes parallel to the Earth's surface, as opposed to a launch profile that is straight up with the orbital turn occurring quickly near the target altitude. For this thesis, the target altitude was 750 kilometers. This gravity turn is accomplished by adding directional controls to the flight path to change the pitch of the rocket and allowing the gravity of the Earth to influence

the flight path of the rocket. To optimize launch mass, launch vehicles are designed to be relatively weak in bending, shear, and torsion, which are induced by lifting surfaces. Heavy lift launch vehicles build up speed in a nearly vertical trajectory, so that they quickly rise above the dense, lower layers of the atmosphere to reduce the lifting forces. The gravity turn then trades vertical for horizontal speed so that the rocket may reach orbital velocity at altitude [7]. The second launch trajectory optimization technique is to increase the flight time of the rocket to assist with increased efficiency of the gravity turn [37]. By increasing the amount of time the engine burns, gravity has greater opportunity to assist with the turn, resulting in less fuel consumed to reach the same orbital velocity. All comparisons in Sections 4.1.2-4.1.4 were made using this optimizing approach. Another self-check for optimization is that the rocket reaches altitude on the opposite side of the earth from the launch location.

**Table 1: All Trajectory Case Configurations**

| Configuration Designation | Vacuum Thrust (lbs) | Vacuum Isp (sec) | Nozzle Type | Notes |
|---|---|---|---|---|
| Case 1 | 30,000 | 466 | Infinite | Aerospike Datum |
| Case 2 | 30,000 | 466 | Limited | Variable nozzle exit area up to max at bell nozzle area* |
| Case 3 | 15,300 | 437 | Limited | Variable nozzle exit area up to max at bell nozzle area |
| Case 4 | 15,300 | 437 | Infinite | Variable nozzle exit area throughout flight |
| Case 5 | 15,300 | 437 | Constant | Bell Nozzle Datum |
| Case 6 | 15,300 | 466 | Limited | Variable nozzle exit area up to max at bell nozzle area |
| Case 7 | 15,300 | 466 | Infinite | Variable nozzle exit area throughout flight |
| Case 8 | 15,300 | 466 | Constant | Only Isp change from Datum, Case 5 |

*Note: The bell nozzle exit area is 1.8869 $ft^2$

The two primary optimization techniques are evident in velocity and altitude trajectory profiles. For Case 6 (Table 1), Figure 24 and Figure 25 present the velocity trajectory profiles before and after the application of the two optimization techniques, respectively. In these

figures, the designation “VEL” indicates the total velocity, relative to the Earth’s rotational speed at sea level at the equator, “VELI” the absolute orbital velocity, and “VELRAD” the radial component of the velocity throughout flight. By initiating a gravity turn in the trajectory, the magnitude of the radial velocity component decreases from a sharp peak (Figure 24) at about 140 seconds into a more continuous hump for the transition from the primary burn to coasting (Figure 25). Furthermore, the overall and orbital velocity magnitudes at the end of the primary burn increase from Figure 24 to Figure 25 so that there is less velocity loss during coasting, meaning less fuel is consumed during the circularization burn in order to reach and maintain the orbital velocity required at altitude.

The total velocity curve describes the rocket’s total velocity magnitude compared to Earth’s rotation (1,041 mph at sea level, equator). During the primary burn phase of the trajectory, the rocket accelerates continuously at a fast rate, increasing speed. The total velocity curve does not start at zero because of the assigned starting condition of 100 ft/s to avoid discontinuity. During the coasting phase, the velocity decreases at a slow rate until the engine is re-ignited for the circularization burn. The orbital velocity follows the general trend of the overall velocity, and is an important indicator of maintaining altitude. The difference in magnitude between the total and orbital velocities is a result of the different reference frames for each, relative to the rotation of the Earth. For every altitude, there is an associated orbital velocity required to continuously overcome gravity. The purpose of the circularization burn is to keep the rocket oriented correctly at the appropriate altitude and velocity. For the target altitude of 750 km, the absolute orbital velocity is 24,546 ft/s. Finally, the radial velocity is an indicator of the relative position of the rocket trajectory to the surface of the Earth. Maintaining too high of a magnitude indicates a perpendicular direction to the Earth, and the closer to zero it approaches, the more parallel the trajectory. Because the target orbit was circular as opposed to elliptical, the radial velocity should maintain roughly a value of zero at orbit. As previously discussed, the general shape of the radial velocity during the primary burn is a hump with a maximum magnitude roughly 1% of the maximum overall velocity magnitude. By the end of the coasting phase, the rocket should be at the target altitude with a negligibly small radial velocity.

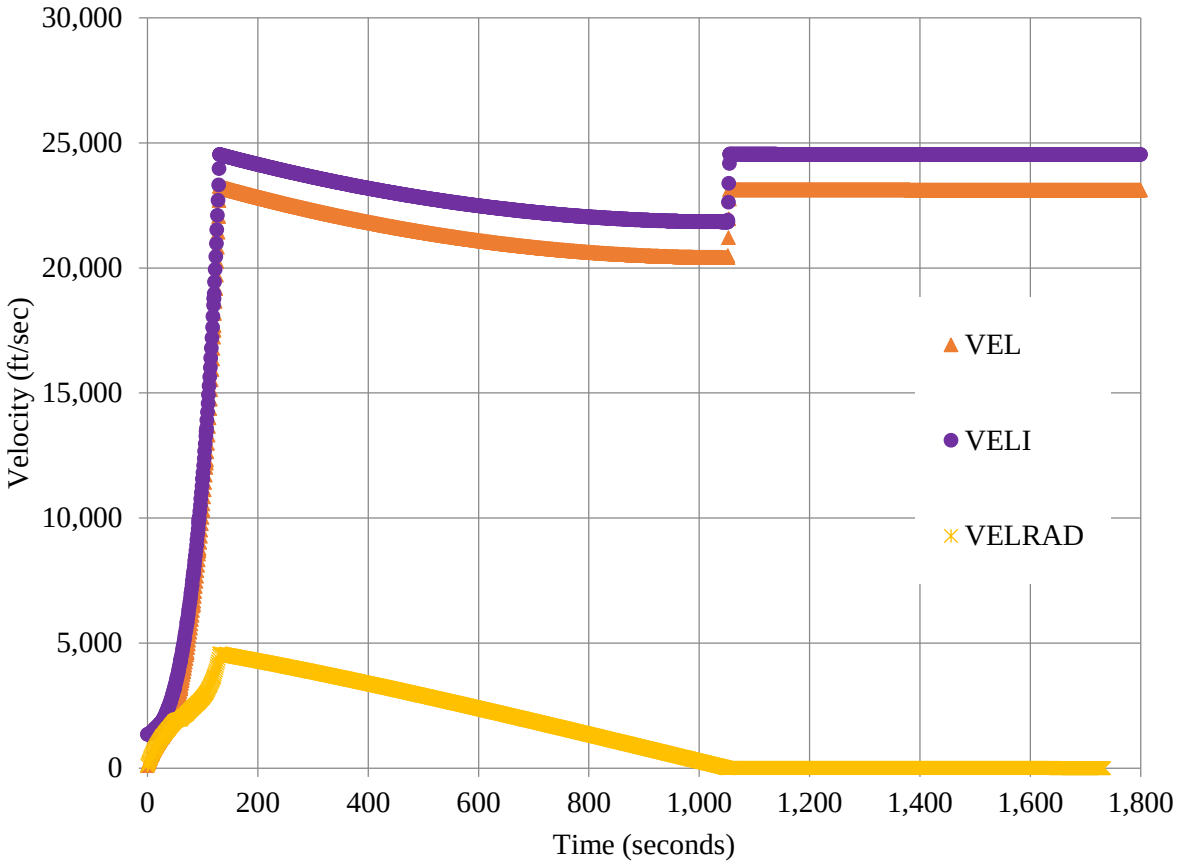



**Figure 24: Case 6 Velocity Profile, Prior to Optimization.**

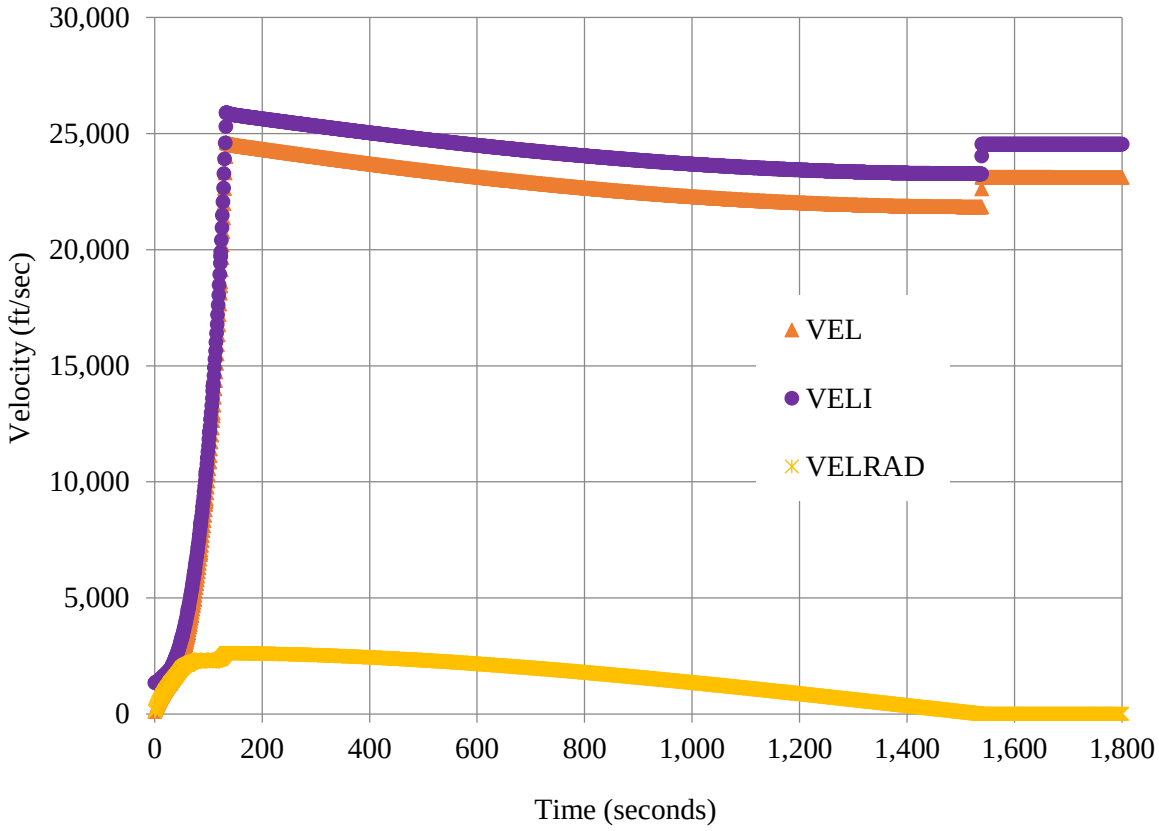



**Figure 25: Case 6 Velocity Profile, After Optimization.**

Both the velocity profiles (Figure 24 and Figure 25) and the altitude profiles, shown in Figure 26 and Figure 27, show an increase in total flight time to target altitude of about 500 seconds, with the addition of the gravity turn assist. Before optimization, the Figure 26 altitude profile has a slight dip in altitude at about 80 seconds into the flight that is not seen in Figure 27, post optimization. This is an indicator that prior to optimization, the rocket experiences greater difficulty in overcoming gravity due to its more vertically severe flight path. The optimized velocity profile in Figure 25 and the altitude profile in Figure 27 are qualitative representations of all cases presented in the following subsections.

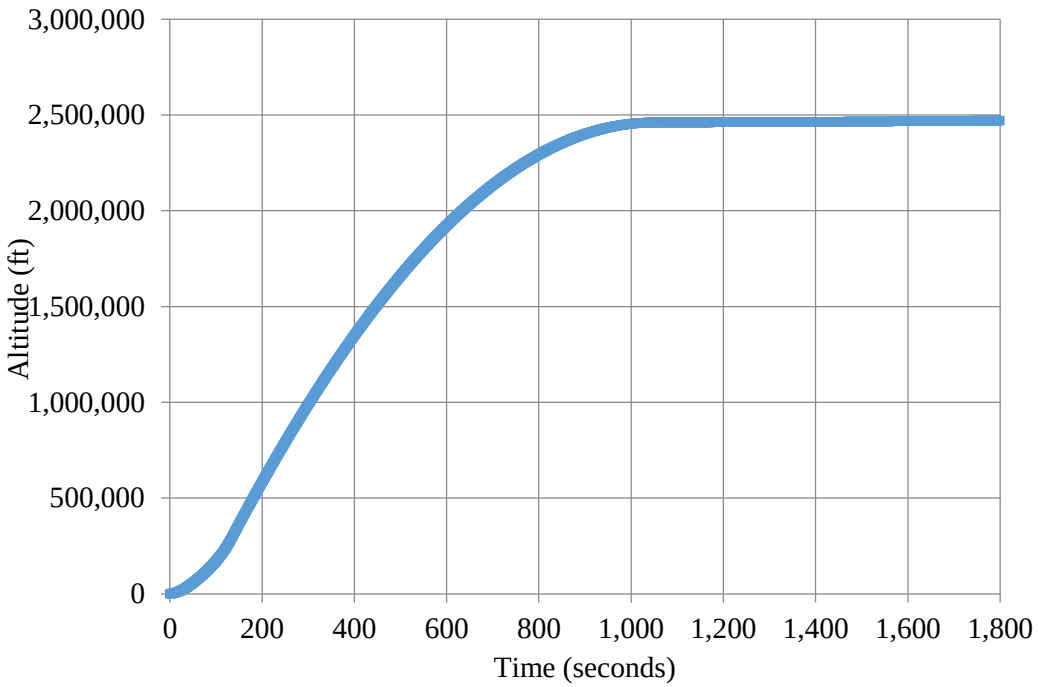



**Figure 26. Case 6 Altitude Profile, Prior to Optimization.**

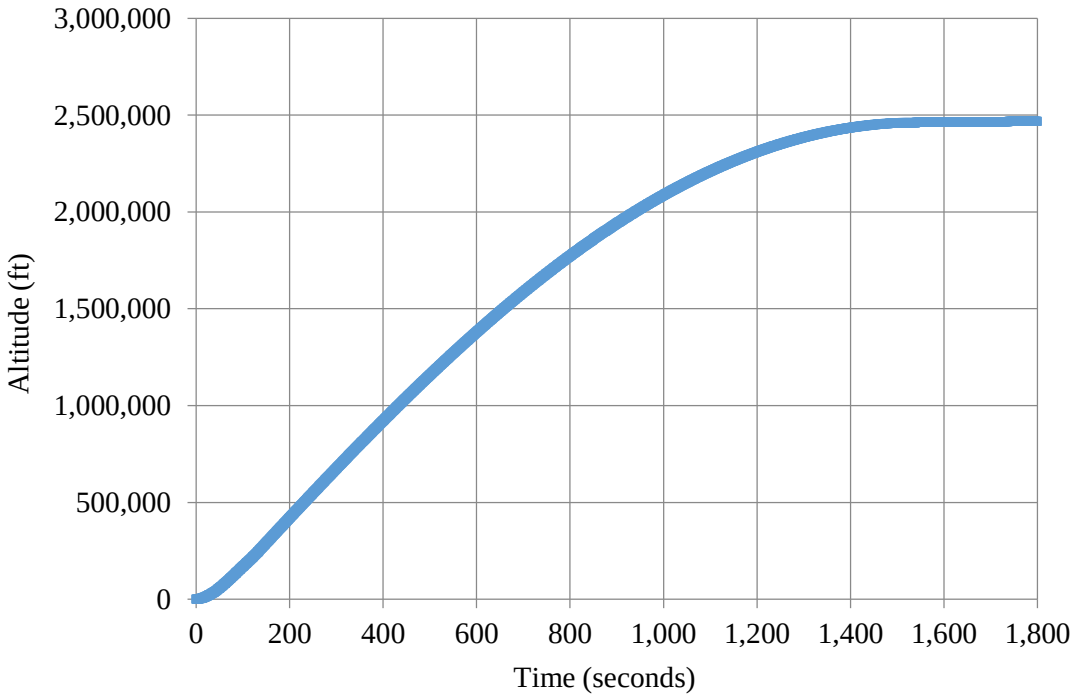



**Figure 27. Case 6 Altitude Profile, After Optimization.**

The last chart of interest is the drag, weight, and thrust profile represented in Figure 28 and Figure 29[4]. These are also representative of the altitude compensating cases and constant nozzle exit area cases, respectively. The drag curve represents the total drag on the system in pounds force based on the constant drag coefficient of 0.2 and the reference surface area for a 6 foot diameter rocket body. The differences in the magnitude of the drag force between the altitude compensating and constant nozzle cases remains on the order of 400 $lbs_f$, and peaks around the time when the gravity turn is initiated. The weight is the total weight of the rocket starting with the initial wet mass and ending with the dry mass. The only difference between Cases 6 and 8 in Figure 28 and Figure 29, respectively, is the limited and constant nozzle configurations. With that one change, there is a 40 $lb_m$ weight savings in propellant burned by applying altitude compensation at lower altitudes verses maintaining and constant nozzle area. Finally, the thrust curves actually show the thrust of the rocket engine at sea level. This is why the thrust levels off at 15,300 $lbs_f$, because the rocket has reached a vacuum state and the engine parameters specify a vacuum thrust. For the altitude compensating case in Figure 28, the thrust varies between the OTIS phases when the nozzle exit area changes incrementally; each section of the thrust curve represents a change in nozzle exit area and the curve remains smooth once it becomes constant. This is a factor of the exit area implementation, rather than a coding flaw.

Knowing and tracking the drag force on the system aids the selection of materials, and knowing where the maximum force occurs helps to reduce its magnitude which will decrease losses by changing the flight path. The starting and ending weight of the system is at the heart of this analysis, since the assumption is that the only loss in weight is the consumed fuel. Finally, monitoring the thrust levels to look for discontinuities is a measure of engine performance for this SSTO configuration and can help optimize the code for a more realistic trajectory model.

Table 2 provides each of the trajectory cases with their corresponding propellant performance parameters. The propellant mass is the difference between the initial and final weight values. The mass reduction is the weight saved when compared to either of the datum cases. As previously mentioned, the configuration of Case 1 and Case 5 represent the datum altitude compensating aerospike and constant nozzle bell cases, respectively. The numbers in

[4] All altitude, velocity, drag, weight, and thrust profiles for each case trajectory may be found in Appendix B.

parenthesis represents the case for which the comparison was made. For example, the mass reduction for Case 2 is 20 $lb_m$ compared to Case 1. For Case 3, it's 163 $lb_m$ compared to Case 5.

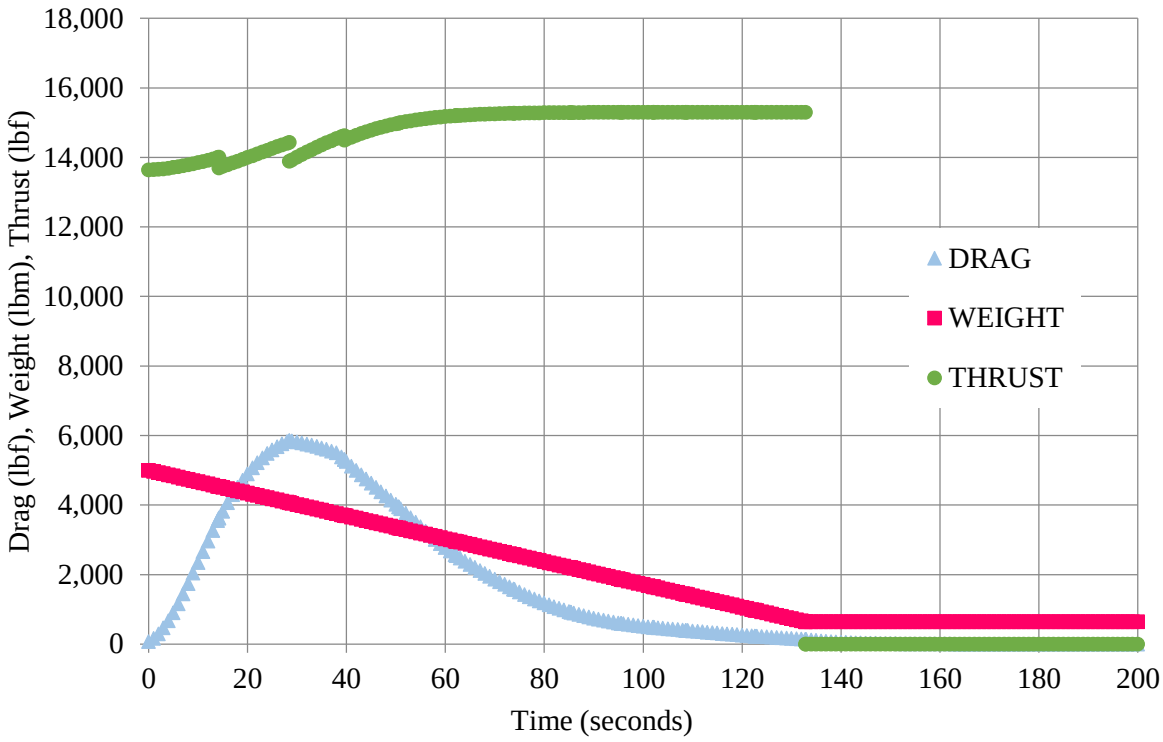



**Figure 28: Case 6 Drag, Weight, and Thrust Profile for Initial Takeoff Time**

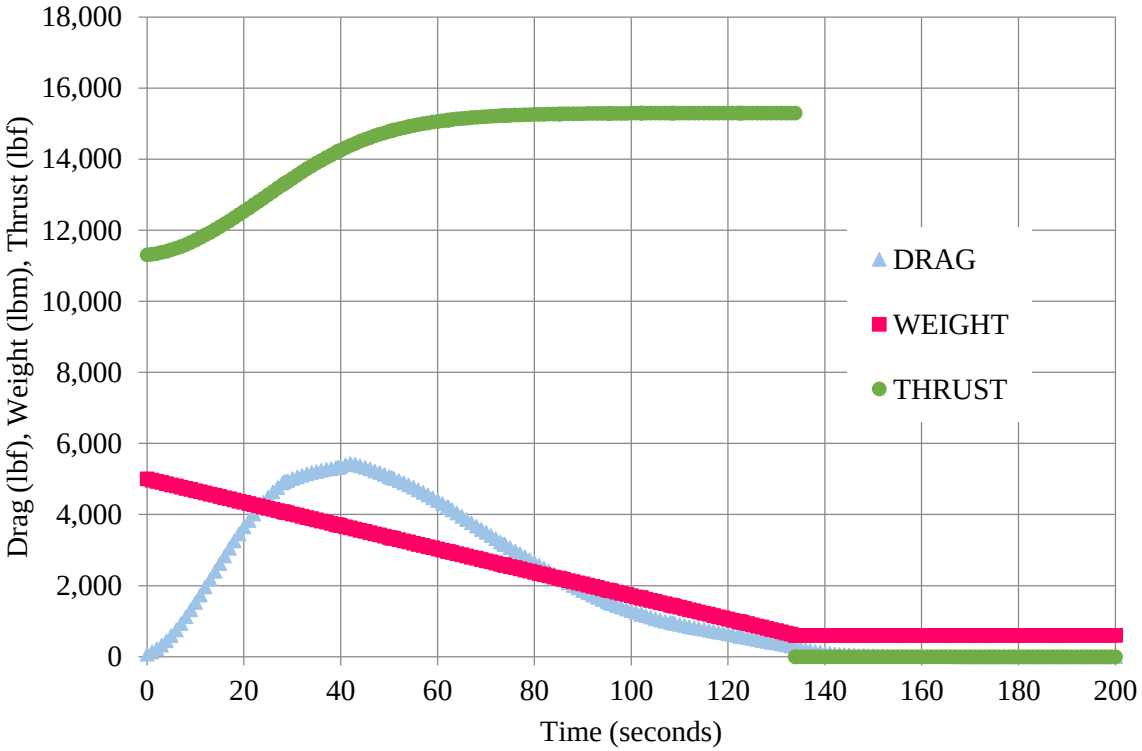



**Figure 29: Case 8 Drag, Weight, and Thrust Profile for Initial Takeoff Time.**

In order to assess the launch cost associated with each case, a reference based on the Minotaur 1 rocket of $222.59 per pound [18] was made and calculated from the total cost of the rocket (excluding labor) and the gross weight. If the propellant mass saved by varying the engine parameters is directly applied to the potential use of the payload, then the mass savings may be considered the money saved from the reduction of the weight of the fuel. This means that, although the aerospike configuration of Cases 1 and 2 have the lowest PMF values, changing an existing, constant bell nozzle configuration to a limited one while maximizing the specific impulse of the engine saves more money, as seen in Cases 6 and 7. In this way, the limited nozzle cases essentially act like an aerospike since they have such similar PMF values, with everything else held constant.

The number of significant figures in this table is based on the degree of precision from the calculations for the nozzle exit area, which were based on the provided values for the combustion chamber.

**Table 2: Trajectory Case Configurations with Propellant Performance Parameters**

| Configuration Designation | Propellant Mass ($lb_m$) | Propellant Mass Reduction ($\Delta lb_m$) | Mass Savings ($) | PMF (%) | PMF Percent Difference from Datum Cases 1, 5 (%) |
|---|---|---|---|---|---|
| Case 1 | 8,560 | --- | --- | 87.31 | --- |
| Case 2 | 8,540 | 20.0 (1) | 4,452 | 87.20 | 0.1260 (1) |
| Case 3 | 4,549 | 163.0 (5) | 36,282 | 90.97 | 3.460 (5) |
| Case 4 | 4,557 | 155.0 (5) | 34,502 | 91.16 | 3.258 (5) |
| Case 5 | 4,712 | --- | --- | 94.23 | --- |
| Case 6 | 4,413 | 299.0 (5) | 66,555 | 88.25 | 1.077 (1), 6.346 (5) |
| Case 7 | 4,424 | 288.0 (5) | 64,106 | 88.48 | 1.340 (1), 6.102 (5) |
| Case 8 | 4,465 | 247.0 (5) | 54,980 | 89.30 | 2.279 (1), 5.232 (5) |

*Note: The numbers in parenthesis represents the case number to which the comparisons were made.

In addition to the propellant performance parameters, the acceleration and drag of the rocket were evaluated. After ignition, the acceleration increases at a steady rate and peaks at the end of the primary burn before the coasting phase. Table 3 provides that maximum value in Earth gravities (1 g = 32.2 $ft/s^2$). The maximum drag was found based on charts such as Figure 28 and Figure 29 and as previously discussed, occurs at the point where the gravity turn begins.

**Table 3: Trajectory Performance Parameters**

| Configuration Designation | Max. Acceleration (g) | Max. Drag ($lb_f$) |
|---|---|---|
| Case 1 | 22.1 | 8,101 |
| Case 2 | 22.1 | 8,053 |
| Case 3 | 29.5 | 5,723 |
| Case 4 | 29.9 | 5,725 |
| Case 5 | 41.5 | 5,463 |
| Case 6 | 23.7 | 5,839 |
| Case 7 | 24.4 | 5,813 |
| Case 8 | 24.9 | 5,432 |

### 4.1.2 Cases 1 & 2

Starting with Cases 1 and 2 (Table 2), the more powerful aerospike engine with a traditional infinite nozzle is compared to a limited nozzle type. The limited nozzle case (Case 2) reduces the PMF by 0.11%, implying that the variable nozzle design is the most efficient at lower altitudes when the ambient pressure is greatest. In addition to decreasing the amount of fuel required to reach orbit, changing the nozzle configuration from an infinite to limited one did not increase the maximum acceleration experienced by the system, and it decreased the magnitude of the total drag.

### 4.1.3 Cases 3, 4, 5

Cases 3 through 5 have the same vacuum thrust and vacuum $I_{sp}$ with the nozzle changing from a limited, to infinite, to constant configuration, respectively. For the purposes of evaluation, Case 5 is considered the baseline, conventional bell nozzle configuration. As expected, this case has the highest PMF, indicating it takes more fuel to obtain altitude than with a varying nozzle. Furthermore, the trend seen between Cases 1 and 2 are also seen between Cases 3 and 4, with a decrease in PMF of 0.19% when going from an infinite to limited nozzle configuration. This represents an over 3% decrease in fuel consumption compared to Case 5. As before, an altitude compensating design decreases the maximum acceleration experienced by the system, in these cases by about 12 g's. That is significant progress if an SSTO design would be considered for manned missions at a future date because it reduces the structural requirements of the rocket, which saves mass. However, making the nozzle variable increases the magnitude of the drag force by about 260 $lb_f$. The primary reason for this is because although the maximum acceleration decreases, it reaches that maximum during the primary burn faster because of the increased efficiency, so at lower altitudes, it experiences more drag due to higher air density.

### 4.1.4 Cases 6, 7, 8

The bell nozzle datum configuration may be further optimized by increasing the $I_{sp}$, as in Cases 6 through 8. The same trends observed in Cases 3 – 5 are also seen in Table 2, with the constant nozzle configuration having the largest PMF, then the infinite, then the limited in decreasing PMF percentage. It is important to look at the PMF differences between Case 5 and

Cases 6 – 8, because that covers both the change in nozzle exit area and change in specific impulse. Generally speaking, increasing the specific impulse of the engine increases its performance; that is why the greatest PMF difference is between Cases 6 and 7 compared to Case 5, because there is both the specific impulse increase and nozzle exit area variation. To a lesser extent than Cases 3 – 5, the maximum acceleration decreases by having a variable nozzle, but to a greater extent, it increases the maximum drag force by a much larger 400 $lb_f$. Just as with Cases 3 – 5, the changing nozzle area increases the rate of acceleration during the primary burn, and with the increased specific impulse value, this overall system becomes more efficient. This is why the maximum acceleration values are less than those of Cases 3 – 5, but also why the maximum drag values are higher than Cases 3 – 5.

## 4.2 Performance Analysis

As Cases 1 and 2 have the most optimized engine parameters of high $I_{sp}$ and altitude compensation, it is reasonable that their PMF magnitudes are the lowest, followed by those in Cases 6 – 8, then Cases 3 – 5. It is possible that the limited nozzle configuration appears to outperform the infinite nozzle only from a margin of error of OTIS and the manual optimization process. If the data is within this margin of error, then the limited altitude compensating nozzle performs the same as the infinite aerospike nozzle. If not, then the results suggest that in order to optimize engine efficiency for SSTO flight, a combination of high performance engine with a limited nozzle design (e.g. EEC or dual bell) that may be maximized at some optimized nozzle exit area ultimately reduces the cost of flight by consuming less propellant and allowing for heavier payloads. The further benefit being that these limited designs could be less complex and easier to manufacture than the linear aerospike. However, it is evident that the variable area nozzles outperform the conventional bell nozzle used in these simulations.

The difference in PMF for the limited and infinite nozzle cases is on the order of 0.2%. It is reasonable to expect the performance of these cases to approach each other, since the benefits of the infinite area diminish at higher altitudes, corresponding to the high pressure ratio data shown in Figure 30. In this figure, the ideal nozzle refers to a theoretical, isentropic, perfectly expanded nozzle while the figure source implies that the aerospike and bell nozzle curves are taken from empirical data [17]. This covers the general operating range from sea level to a

vacuum, where the ambient pressure becomes zero. The thrust coefficient is a dimensionless parameter used to characterize engine performance. It is a function of the combustion chamber pressure (also considered at the nozzle entrance), the nozzle throat area, the specific heat, the nozzle area ratio, and the pressure across the nozzle [37].

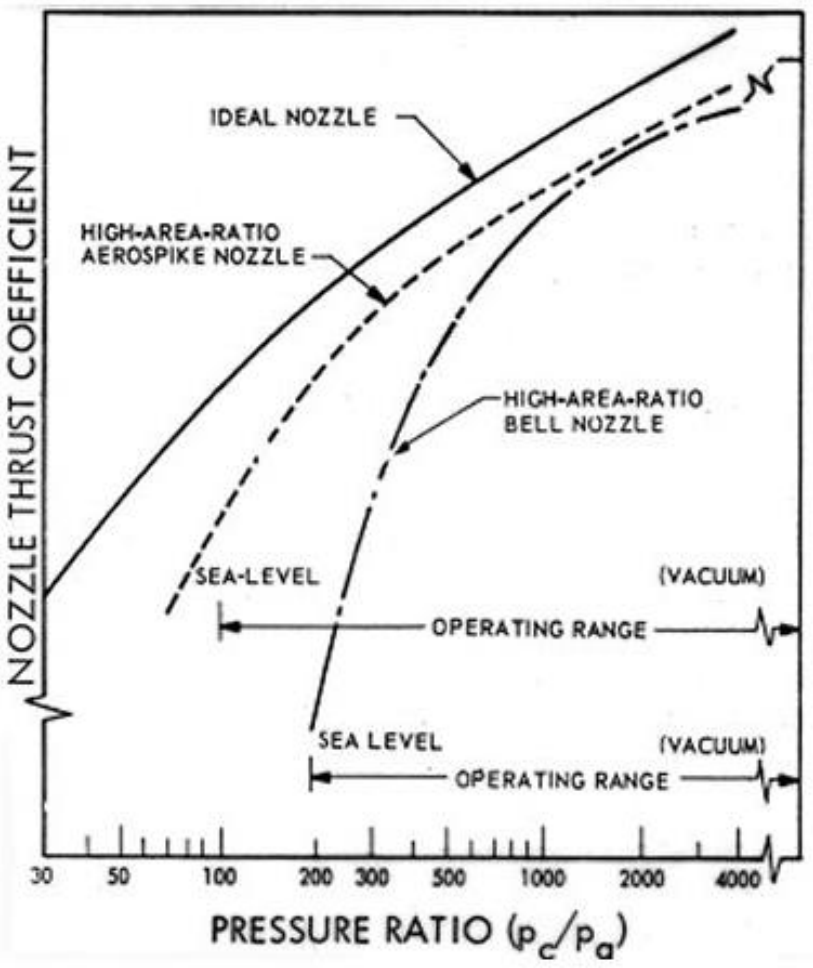



**Figure 30: Theoretical Ideal, Aerospike, and Bell Nozzle Thrust Coefficient Trends Based on Pressure Ratio between the Nozzle Exit Area (Pc) and Ambient Pressure (Pa) [17].**

If the relationship between the limited and infinite nozzle cases were the result of a physical effect, it could possibly be due to complex expansion and compression shock

interactions, which were not included in the trajectory modeling for this thesis. One of the reasons the aerospike configuration is able to maintain a higher thrust and efficiency value is because the exhaust plume remains more parallel to the flight path of the rocket with fewer losses due to expansion waves at the nozzle exit, as described in Chapter I with Figure 1 and Figure 2. These expansion waves are small compared to the recompression shock waves that result from the truncation of the nozzle, maintaining the plume shape. However, by limiting the maximum expansion to a specified exit area, the effects of the expansion waves would not have as significant an impact on the thrust of the rocket at higher altitudes, where the ambient pressure no longer helps to conform the flow. This would allow more of the flow to apply thrust directly on the nozzle for a longer period of time, despite the zero ambient pressure. This higher-altitude performance would also increase with a longer bell shape. The details of such complex processes need to be confirmed through more detailed simulation and experiment.

# CHAPTER V
# CONCLUSIONS AND RECOMMENDATIONS

In this thesis, the efficiency of a conventional bell nozzle to an altitude compensating nozzle for single-stage to orbit flight was evaluated based on the trajectory model in the Optimal Trajectories by Implicit Simulation program.

## 5.1 Which Nozzle Performs Better?

With new technology that focuses on the feasibility of SSTO being developed, the evaluation of rocket nozzles may further optimize this method of space travel. The use of an annular, aerodynamic spike nozzle, instead of the traditional bell design, optimizes an unmanned, heavy launch vehicle by lowering the propellant mass fraction (PMF) up to 7% from conventional rocket engine designs. The results suggest that implementing a design such as the nozzle variability, if only applied at lower altitudes, further decreases the PMF than if the nozzle expanded to infinity; but the improvement is small and may fall within the uncertainty of OTIS' results. Aerospike engines inherently have a higher specific impulse value than bell nozzle designs, and the results show that this can have a significant impact on performance. This would not decrease the material and structural endurance of the vehicle because, although there is increased drag at lower altitudes, this drag is countered by lower acceleration, which reduces the dynamic forces on the vehicle. By varying the nozzle exit area based on the ambient pressure, the engine performs much closer to the ideal, isentropic, perfect expansion model than the traditional bell. The infinitely expanding exhaust plume at vacuum conditions theoretically applies force other than in the direction of flight, lowering the engine performance at those altitudes. Containing the flow at a maximum area would alleviate these effects. However, the losses associated with flow separation inside the bell nozzle at low altitudes are much greater than the losses of thrust of the aerospike at high altitudes. One way to confirm this would be to simulate an infinitely expanding nozzle for a trans-planetary flight.

By combining weight saving materials techniques with more advanced rocket nozzle designs, not only would SSTO become more feasible and practical, it would open up space travel to many more companies or individuals for scientific advancement or tourism.

## 5.2 Recommendations

Further work would include the trajectory analysis and optimization of what altitude a nozzle expansion maximum should occur and what annular design most effectively accomplishes this simulated configuration. This would need to include the losses associated with the nozzle design to ensure that the differences in performance are outside the uncertainty of the simulation results. OTIS is also capable of implementing weather conditions into the model for a more robust design. Future modeling should also include comparisons of bell and aerospike nozzles for interplanetary missions, to further assess their performance outside planetary atmospheric conditions. In addition, further experimental ground tests of the aerospike in conditions ranging from sea level to vacuum would provide data to confirm the trends observed in this thesis.

# LIST OF REFERENCES

[1] Alexander, G., Brown, A., Jackson, D., Scott, J., Swanson, M., and VanderWyst, A., "Altitude Compensation," Aerospace Web [online database], URL: http://www.aerospaceweb.org/design/aerospike/compensation.shtml [cited 1 January 2015].

[2] Anderson, John D., *Modern Compressible Flow with Historical Perspective,* 3rd ed., McGraw Hill, New York, 2003.

[3] Aukerman, Carl A., "Plug Nozzles—The Ultimate Customer Driven Propulsion System," NASA S3-25266, Aug. 1991.

[4] Baker, Matthew, Shibuya, Akihiro, Verma, Deepak, Bostwick, Christopher, Skaar, Paul, and Besnard, Eric, "Flight Test and Analysis of a Multi-Chamber Aerospike Engine," *44th Joint Propulsion Conference and Exhibit,* AIAA/ASME/SAE/ASEE, Harford, CT, July 2008.

[5] Besnard, Eric and Garvey, John, "Aerospike Engines for Nanosat and Small Launch Vehicles (NLV/SLV)," *Space 2004 Conference and Exhibit*, AIAA, San Diego, CA, Sept. 2004.

[6] Besnard, Eric, and Garvey, John, "Development and Flight-Testing of Liquid Propellant Aerospike Engines," *40th Joint Propulsion Conference and Exhibit,* AIAA/ASME/SAE/ASEE, For Lauderdale, FL, July 2004.

[7] Curtis, Howard D, *Orbital Mechanics for Engineering Students*, Elsevier Ltd., Oxford, England, UK, 2005.

[8] Dorrington, G.E., "The Possibility of Near-Term Commercial Single-Stage-to-Orbit Vehicles," *35th Joint Propulsion Conference and Exhibit,* AIAA/ASME/SAE/ASEE, Los Angeles, CA, June 1999.

[9] Ehrlich, Jr., Carl F., "Why the X-33 Venture Star Gave SSTO a Bad Name," *SPACE 3009 Conference and Exposition,* AIAA, Pasadena, CA, 2009.

[10] Fick, Michael, and Schmucker, Robert H., "Linear Aerospike Engine Performance Evaluation," AIAA 3305, Washington, D.C., 1997.

[11] "Firefly Alpha," Firefly [company website], URL: http://www.fireflyspace.com/vehicles/firefly-a [cited 20 November 2014].

[12] Gloyer, Paul W., Lewis, Tim S., and Taylor, Zachary R., "ACE: Practical SSTO," *AIAA Space 2014 Conference,* AIAA 4401, Washington, D.C., 2014.

[13] Hale, Francis J., *Introduction to Space Flight,* Prentice-Hall, Inc., Upper Saddle River, 1994.

[14] Hempsell, Mark, "SKYLON Users' Manual," Reaction Engines, Ltd., Abingdon, Oxfordshire, Great Britain, 2014.

[15] Houghton, E. L., Carpenter, P. W., Collicott, Steven H., and Valentine, Daniel T., *Aerodynamics for Engineering Students*, 6th ed., Elsevier, Waltham, MA, USA, 2013, pp. 40.

[16] Huang, D.H., "Aerospike Engine Technology Demonstration for Space Propulsion," *10th Propulsion Conference*, AIAA/SAE, San Diego, CA, 1974.

[17] Huzel, Dieter K., Huang, David H., *Modern Engineering for Design of Liquid-Propellant Rocket Engines*, Progress in Astronautics and Aeronautics, Vol. 147, AIAA, Washington, D.C., 1992.

[18] Isakowitz, Steven J., Hopkins, Joshua B., and Hopkins, Joseph P., Jr., *International Reference Guide to Space Launch Systems*, 4th ed., AIAA, Washington, D.C., 2004.

[19] Jahn, Robert G., *Physics of Electric Propulsion*, Dover Publications, Inc., Mineola, NY, 1968.

[20] Kirby, F.M., and Martinez, A., "Linear Aerospike Engine," *13th Propulsion Conference*, AIAA/SAE, Orlando, FL, 1977.

[21] Korte, J.J., "Parametric Model of an Aerospike Rocket Engine," *38th Aerospace Sciences Meeting & Exhibit*, AIAA 1044, Reno, NV, Jan. 2000.

[22] Krivanek, Thomas M., Roche, Joseph M., and Riehl, John P., "Affordable Flight Demonstration of the GTX Air-Breathing SSTO Vehicle Concept," *Combustion, Airbreathing Propulsion, Propulsion Systems Hazards, and Modelling and Simulations Subcommittees Joint Meeting*, NASA/TM-2003-212315, NASA Glenn Research Center, Cleveland, OH, 2003.

[23] Kumakawa, A., Onodera, T., and Yoshida, M., "A Study of Aerospike-Nozzle Engines," AIAA 3526, Washington, D.C., 1998.

[24] Kutin, M.S., "Linear Aerospike SR-71 Experiment (LASRE) Rocket Engine," AIAA 3319, Washington, D.C., 1997.

[25] Lamont, E. A., "The Aerospike Engine System for the Space Tug-A Status Report," *9th Propulsion Conference*, AIAA/SAE, Las Vagas, NV, 1973.

[26] Limerick, Charles D., "Rocket Propulsion for Single Stage to Orbit," *30th Joint Propulsion Conference*, AIAA/ASME/SAE/ASEE, Indianapolis, IN, June 1994.

[27] Martin, James, "History of Propulsion for Single-Stage-to-Orbit and Multiple-Stage Vehicles," *AIAA Journal of Propulsion and Power,* Vol. 11, No. 1, 1995, pp. 98-104.

[28] Masciarelli, James, Peterson, Wayne, Robertson, Edward, Teixeira, Charles, and Templin, Kevin, "Single Stage to Orbit Vehicles: Issues and Sensitivities," *Space Programs and Technologies Conference,* AIAA, Huntsville, AL, Sept. 1994.

[29] Meiss, Jan-Hendrick, and Besnard, Eric, "Advanced Design of a Mult-Thruster LOX/Propylene Aerospike Engine," *49th Joint Propulsion Conference*, AIAA/ASME/SAE/ASEE, San Jose, CA, 2013.

[30] Muss, J.A., Nguyen, T.V., Reske, E.J., and McDaniels, D.M., "Evaluation of Altitude Compensating Nozzle Concepts for RLV," AIAA 3222, Washington, D.C., 1997.

[31] Oates, Gordon C., *Aerothermodynamics of Gas Turbine and Rocket Propulsion, 3rd ed.*, AIAA Education Series, Washington, D.C., 1997.

[32] Olds, J., Bradford, J., Charania, A., Ledsinger, L., McCormick, D., and Sorensen, K., "*Hyperion*: An SSTO Vision Vehicle Concept Utilizing Rocket-Based Combined Cycle Propulsion," *9th International Space Planes and Hypersonic Systems and Technologies Conference,* AIAA 4944, Washington, D.C., 1999.

[33] Parsley, Randy C., "Single-Stage-to-Orbit Propulsion Technologies," *25th Joint Propulsion Conference,* AIAA/ASME/SAE/ASEE, Monterey, CA, July 1989.

[34] Riehl, John, "Optimal Trajectories by Implicit Simulation (OTIS) Users' Manual," Vol. 2, NASA Glenn Research Center, Cleveland, OH, 2008.

[35] Riehl, John, and Trefny, Charles, "SRM-Assisted Trajectory for the GTX Reference Vehicle," *Combustion, Airbreathing Propulsion, Propulsion Systems Hazards, and Modelling and Simulations Subcommittees Joint Meeting*, NASA/TM-2002-211599, NASA Glenn Research Center, Cleveland, OH, 2002.

[36] Sponable, J.M, "Assessing Single Stage to Orbit Feasibility," *31st Joint Propulsion Conference and Exhibit,* AIAA/ASME/SAE/ASEE, San Diego, CA, July 1995.

[37] Sutton, George P., and Biblarz, Oscar, *Rocket Prolusion Elements,* 8th ed., John Wiley & Sons, Inc., Hoboken, 2010.

[38] Takahashi, Hidemi, Tomioka, Sadatake, Tomita, Takeo, and Sakuranaka, Noboru, "Flowfield Characterization of Linear Aerospike Nozzles," *52nd Aerospace Sciences Meeting and Exhibit,* AIAA, National Harbor, MD, Jan. 2014.

[39] Thomas, Scott R., Palac, Donald T., Trefny, Charles J., and Roche, Joseph M., "Performance Evaluation of the NASA GTX RBCC Flowpath," *Fifteenth International Symposium on Airbreathing Engines,* NASA/TM-2001-210953, NASA Glenn Research Center, Cleveland, OH, 2001.

[40] Tomita, Takeo, Takahashi, Mamoru, Onodera, Takuo, and Tamura, Hiroshi, "Thrust Loss due to Desing of Linear Aerospike Nozzles," *36th Joint Propulsion Conference and Exhibit,* AIAA/ASME/SAE/ASEE, Huntsville, AL, July 2000.

[41] Tsutsumi, Seiji, Yamaguchi, Kazuo, Teramoto, Susumu, and Nagashima, Toshio, "Clustering Effects on Performance and Heating of a Linear Aerospike Nozzle," *45th Aerospace Sciences Meeting and Exhibit,* AIAA, Reno, NV, Jan. 2007.

[42] Wuye, Dia, Yu, Liu, Xianchen, Cheng, and Bin, Ma, "Analytical and Experimental Studies of Tile-Shaped Aerospike Nozzles," *AIAA Journal of Propulsion and Power,* Vol. 19, No. 4, 2003, pp. 640-645.

[43] Wuye, Dai, Yu, Liu, Xianchen, Cheng and Haibin, Tang, "Aerospike Nozzle Performance Study and Its Contour Optimization," *37th Joint Propulsion Conference and Exhibit,* AIAA/ASME/ASE/ASEE, Salt Lake City, UT, July 2001.

[44] Yu, Liu, Guozhou, Zhang, Wuye, Dai, and Bin, Ma, "Experimental Investigation on Aeropsike Nozzle in Different Structures and Working Conditions," *37th Joint Propulsion Conference and Exhibit,* AIAA/ASME/SAE/ASEE, Salt Lake City, UT, July 2001.

# APPENDICES

# APPENDIX A

Sample OTIS input file of the aerospike infinite nozzle configuration (Case 1).

```
!Aerospike Datum, Case 1
        !750 km Altitude target
        !Isp,vac = 466 seconds
        !Thrust,vac = 30,000 lbs

!The exclamation mark indicates a comment, not to be interpreted as an OTIS
command or input.

!The first input file is the "OTISIN" where general information about the entire trajectory
is programmed.

        $OTISIN

!Must integrate either explicitly or implicitly. All cases were explicitly integrated, hence
the "T" for true.
        expint_flg=T,
        impopt_flg=F,

!Spherical Coordinates labelling is turned on.
        sph_flg=T,

!Allows specific values to be determined
        RANG_FLG=T,

!The number of phases to be run. Because the trajectory is complete, this is the total
number of phases created.
        phase_num= 17,

!Each phase must have its own unique name, fully listed here.
        phase_nam='ph001','ph002','ph003','ph004','ph005','ph006','ph007','ph008','ph00
9','ph010','ph011','ph012','ph013','ph014','ph015','ph016','ph017',

!Define output terms in order of which you'd like them. These show up in both the
terminal screen as well as in output files.
        outblk_nam='TIME','ALT','VEL','VELI','VELRAD','VELTHT','VELPHI','ACCT','GAM
D','AZMD','LATD','LOND',
'ALPHAD','DRAG','WEIGHT','THRUST',

!End OTISIN phase.
        $END
```

```
!There is no specific "PHASIN" command to start running each of the phases. Each
phase begins with the "PHASIN" command, then the phase name of what you'd like to
run. You must program the phases in the order listed in the "phase_nam" command in
"OTISIN".

!Phase One
        $PHASIN
        ph_nam='ph001'

!Delta time step for this phase in seconds.
        outblk_dt= 1,

!Define aerodynamic forces if any. This defines a drag coefficient, which is held
constant.
        aero(1) = "TYPE=CD:DEF=0.2",

!Reference surface aera (6ft=D) in ft^2 for the rocket body.
        sref ='28.27433388'

!Defining the engine parameters. Because this is SSTO, there is only the one engine
defined by the vacuum thrust, vacuum Isp, and nozzle exit area. This nozzle "AEXIT"
changes with each phase based on the current altitude of the rocket.
        ENGINE(1)="TYPE_T=TVAC:DEF_T=30000:TYPE_F=ISP:DEF_F=466.0:AEXIT
=0.784709929",

!Initial Conditions are defined by the below state variables.
!Velocity (ft/s)
        state(1)='ic_val= 100',
!Heading Angle (From 0 degrees north--Eastern launch)
        state(2)='ic_val= 89',
!Flight Path Angle (Singularity if flight path angle is 90)
        state(3)='ic_val= 89.5',
!Altitude (ft)
        state(4)='ic_val= 0',
!Longitude (Kennedy Space Center)
        state(5)='ic_val= 80.5528',
!Latitude (Kennedy Space Center)
        state(6)='ic_val= 28.4750',
!Weight (lbs)
        state(7)='ic_val=9804',

!Total Phase Time (sec). This is kept relatively small for frequent updates of the nozzle
exit area. A smaller phase time did not significantly alter the optimization or
performance of the trajectory when compared to the other cases.
```

```
        tp='val=10',

        $END

!Phase Two
        $PHASIN
        ph_nam='ph002'

!Delta time step
        outblk_dt= 1,

!Define aerodynamic forces.
        aero(1) = "TYPE=CD:DEF=0.2",

!Reference surface aera (6ft=D)
        sref ='28.27433388'

!Engine Parameters
        ENGINE(1)="TYPE_T=TVAC:DEF_T=30000:TYPE_F=ISP:DEF_F=466.0:AEXIT
=0.890913558",

!Phase Time (sec)
        tp='val=10',

        $END

!Phase Three
        $PHASIN
        ph_nam='ph003'

        outblk_dt= 1,

        aero(1) = "TYPE=CD:DEF=0.2",

        sref ='28.27433388'

!Engine Parameters
        ENGINE(1)="TYPE_T=TVAC:DEF_T=30000:TYPE_F=ISP:DEF_F=466.0:AEXIT
=1.21488431",

        tp='val=10',

        $END
```

```
!Phase Four
        $PHASIN
        ph_nam='ph004'

        outblk_dt= 1,

        aero(1) = "TYPE=CD:DEF=0.2",

        sref ='28.27433388'

!Engine Parameters
        ENGINE(1)="TYPE_T=TVAC:DEF_T=30000:TYPE_F=ISP:DEF_F=466.0:AEXIT
=1.96466285",

!Phase Time (sec). Some phase times were adjusted in order to reach the target
altitude.
        tp='val=8.47',

        $END

!Phase Five
        $PHASIN
        ph_nam='ph005'

        outblk_dt=1,

        aero(1) = "TYPE=CD:DEF=0.2",

        sref ='28.27433388'

!Engine Parameters
        ENGINE(1)="TYPE_T=TVAC:DEF_T=30000:TYPE_F=ISP:DEF_F=466.0:AEXIT
=3.406524571",

!After the rocket gains a certain altitude, the gravity turn may be implemented as
discussed in Chapter III of this thesis. This is the first phase where the manual controls
are implemented to force the rocket into this gravity turn. The OTIS input must be in
radians, hence the conversion in the definition. A negative degree/radian control pushes
the rocket nose (alpha) back towards the ground.

!Controls
        control(1)="NAM=ALPHA:DEF=-0.01745329255*40.0",
        control(2)="NAM=BETA:DEF=-0.0174532925*0",
        control(3)="NAM=SIGMA:DEF=-0.0174532925*0",
```

```
        tp='val=10',

        $END

!Phase Six
        $PHASIN
        ph_nam='ph006'

        outblk_dt=1,

        aero(1) = "TYPE=CD:DEF=0.2",

        sref ='28.27433388'

!Engine Parameters
        ENGINE(1)="TYPE_T=TVAC:DEF_T=30000:TYPE_F=ISP:DEF_F=466.0:AEXIT
=7.549753157",

!Controls
        control(1)="NAM=ALPHA:DEF=-0.01745329255*33",
        control(2)="NAM=BETA:DEF=-0.0174532925*0",
        control(3)="NAM=SIGMA:DEF=-0.0174532925*0",

        tp='val=10',

        $END

!Phase Seven
        $PHASIN
        ph_nam='ph007'

        outblk_dt=1,

        aero(1) = "TYPE=CD:DEF=0.2",

        sref ='28.27433388'

!Engine Parameters
        ENGINE(1)="TYPE_T=TVAC:DEF_T=30000:TYPE_F=ISP:DEF_F=466.0:AEXIT
=18.32868554",
```

```
!Controls
        control(1)="NAM=ALPHA:DEF=-0.01745329255*28",
        control(2)="NAM=BETA:DEF=-0.0174532925*0",
        control(3)="NAM=SIGMA:DEF=-0.0174532925*0",

        tp='val=10',

        $END

!Phase Eight
        $PHASIN
        ph_nam='ph008'

        outblk_dt= 1,

        aero(1)="TYPE=CD:DEF=0.2",

        sref ='28.27433388'

!Engine Parameters
        ENGINE(1)="TYPE_T=TVAC:DEF_T=30000:TYPE_F=ISP:DEF_F=466.0:AEXIT
=46.6061258",

!Controls
        control(1)="NAM=ALPHA:DEF=-0.0174532925*20",
        control(2)="NAM=BETA:DEF=-0.0174532925*0",
        control(3)="NAM=SIGMA:DEF=-0.0174532925*0",

        tp='val=10',

        $END

!Phase Nine
        $PHASIN
        ph_nam='ph009'

        outblk_dt= 1,

        aero(1)="TYPE=CD:DEF=0.2",

        sref ='28.27433388'
```

```
!Engine Parameters
        ENGINE(1)="TYPE_T=TVAC:DEF_T=30000:TYPE_F=ISP:DEF_F=466.0:AEXIT
=119.6098817",

!Controls
        control(1)="NAM=ALPHA:DEF=-0.0174532925*15",
        control(2)="NAM=BETA:DEF=-0.0174532925*0",
        control(3)="NAM=SIGMA:DEF=-0.0174532925*0",

        tp='val=10',

        $END

!Phase Ten
        $PHASIN
        ph_nam='ph010'

        outblk_dt= 1,

        aero(1)="TYPE=CD:DEF=0.2",

        sref ='28.27433388'

!Engine Parameters
        ENGINE(1)="TYPE_T=TVAC:DEF_T=30000:TYPE_F=ISP:DEF_F=466.0:AEXIT
=306.3193875",

!Controls
        control(1)="NAM=ALPHA:DEF=-0.0174532925*10",
        control(2)="NAM=BETA:DEF=-0.0174532925*0",
        control(3)="NAM=SIGMA:DEF=-0.0174532925*0",

        tp='val=10',

        $END

!Phase Eleven
        $PHASIN
        ph_nam='ph011'

        outblk_dt= 1,

        aero(1) = "TYPE=CD:DEF=0.2",
```

```
        sref ='28.27433388'

!Engine Parameters
        ENGINE(1)="TYPE_T=TVAC:DEF_T=30000:TYPE_F=ISP:DEF_F=466.0:AEXIT
=785.2196984",

!Controls
        control(1)="NAM=ALPHA:DEF=-0.0174532925*10",
        control(2)="NAM=BETA:DEF=-0.0174532925*0",
        control(3)="NAM=SIGMA:DEF=-0.0174532925*0",

        tp='val=10',

        $END

!Phase Twelve
        $PHASIN
        ph_nam='ph012'

        outblk_dt= 1,

        aero(1) = "TYPE=CD:DEF=0.2",

        sref ='28.27433388'

!Engine Parameters
        ENGINE(1)="TYPE_T=TVAC:DEF_T=30000:TYPE_F=ISP:DEF_F=466.0:AEXIT
=2001.752761",

!Controls
        control(1)="NAM=ALPHA:DEF=-0.0174532925*8",
        control(2)="NAM=BETA:DEF=-0.0174532925*0",
        control(3)="NAM=SIGMA:DEF=-0.0174532925*0",

        tp='val=10',

        $END

!Phase Thirteen
        $PHASIN
        ph_nam='ph013'

        outblk_dt= 1,
```

```
        aero(1) = "TYPE=CD:DEF=0.2",

        sref ='28.27433388'

!Engine Parameters
        ENGINE(1)="TYPE_T=TVAC:DEF_T=30000:TYPE_F=ISP:DEF_F=466.0:AEXIT
=4986.596519",

!Controls
        control(1)="NAM=ALPHA:DEF=-0.0174532925*7",
        control(2)="NAM=BETA:DEF=-0.0174532925*0",
        control(3)="NAM=SIGMA:DEF=-0.0174532925*0",

        tp='val=10',

        $END

!Phase Fourteen
        $PHASIN
        ph_nam='ph014'

        outblk_dt= 1,

        aero(1) = "TYPE=CD:DEF=0.2",

        sref ='28.27433388'

!Engine Parameters
        ENGINE(1)="TYPE_T=TVAC:DEF_T=30000:TYPE_F=ISP:DEF_F=466.0:AEXIT
=12175.92107",

!Controls
        control(1)="NAM=ALPHA:DEF=-0.0174532925*6",
        control(2)="NAM=BETA:DEF=-0.0174532925*0",
        control(3)="NAM=SIGMA:DEF=-0.0174532925*0",

        tp='val=2.80',

        $END
```

```
!Phase Fifteen
!This phase is known as the "coasting" phase where the engine is temporarily turned off
to allow for deceleration to the correct altitude to be reached. The cumulative phases
before this one are called the primary burn phases, and the phase immediately after this
is the circularization burn.
        $PHASIN
        ph_nam='ph015'

        outblk_dt= 1,

        aero(1) = "TYPE=CD:DEF=0.2",

        sref ='28.27433388'

!This total phase time must be long enough for the radial velocity of the rocket to reach
very close to zero, indicating that the rocket is moving parallel to the Earth's surface. By
the end of this phase, the rocket should also be at altitude, 750 kilometers for this
thesis. Once this point is reached, the rocket performs the circularization burn.
        tp='val=1400.63',

        $END

!Phase Sixteen
!Circularization Burn
        $PHASIN
        ph_nam='ph016'

        outblk_dt=1,

        aero(1)="TYPE=CD:DEF=0.2",

        sref ='28.27433388'

!Keeping the engine nozzle exit area the same as before with the assumption that the
engine will burn for a very short period of time in a near-vacuum.
        ENGINE(1)="TYPE_T=TVAC:DEF_T=30000:TYPE_F=ISP:DEF_F=466.0:AEXIT
=12175.92107",

!Controls. Some slight control change may need to be made in order to keep the rocket
in a more circular, as opposed to elliptical orbit.
        control(1)="NAM=ALPHA:DEF=-0.01745329255*-0.5"
        control(2)="NAM=BETA:DEF=-0.0174532925*0"
        control(3)="NAM=SIGMA:DEF=-0.0174532925*0"
```

```
!Make long enough so stopping conditions (below) may be met.
        tp='val=500',

!Stopping Condition for this phase is the orbital velocity needed to maintain the 750 km
altitude in ft/s.
        stp_nam='VELI',
        stp_val=24546.0,

        $END

!Phase Seventeen
!This final phase was added to be able to make sure the rocket stays in a stable,
circular orbit at the target altitude for many cycles around the Earth.
        $PHASIN
        ph_nam='ph017'

        outblk_dt= 1,

        tp='val=9000',

        $END

!Exit the Program so OTIS does not look for any more information and can export the
results.
        exit
```

# APPENDIX B

All trajectory case altitude, velocity, drag, weight, and thrust data
(Case numbers reference Table 1, reprinted here for convenience)

| Configuration Designation | Vacuum Thrust (lbs) | Vacuum Isp (sec) | Nozzle Type | Notes |
|---|---|---|---|---|
| Case 1 | 30,000 | 466 | Infinite | Aerospike Datum |
| Case 2 | 30,000 | 466 | Limited | Variable nozzle exit area up to max at bell nozzle area |
| Case 3 | 15,300 | 437 | Limited | Variable nozzle exit area up to max at bell nozzle area |
| Case 4 | 15,300 | 437 | Infinite | Variable nozzle exit area throughout flight |
| Case 5 | 15,300 | 437 | Constant | Bell Nozzle Datum |
| Case 6 | 15,300 | 466 | Limited | Variable nozzle exit area up to max at bell nozzle area |
| Case 7 | 15,300 | 466 | Infinite | Variable nozzle exit area throughout flight |
| Case 8 | 15,300 | 466 | Constant | Only Isp change from Datum, Case 5 |

Please see Chapter IV for the assessment of the general features of the following trajectory plots.

As a reminder for the velocity plots, “VEL” is the total velocity relative to the rotation of the earth, “VELI” is the absolute orbital velocity, and “VELRAD” is the radial velocity relative to the Earth’s rotation.

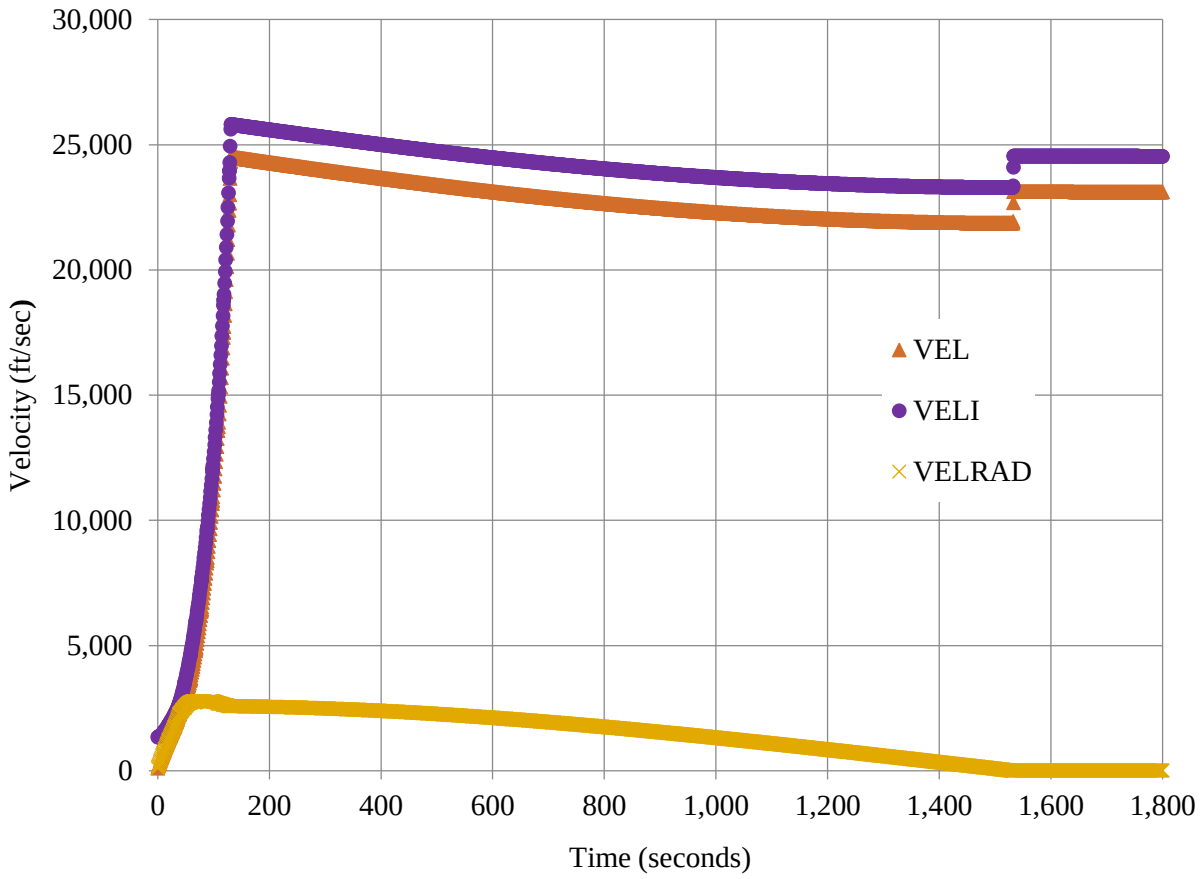



**Figure 31: Case 1 Velocity Profile**

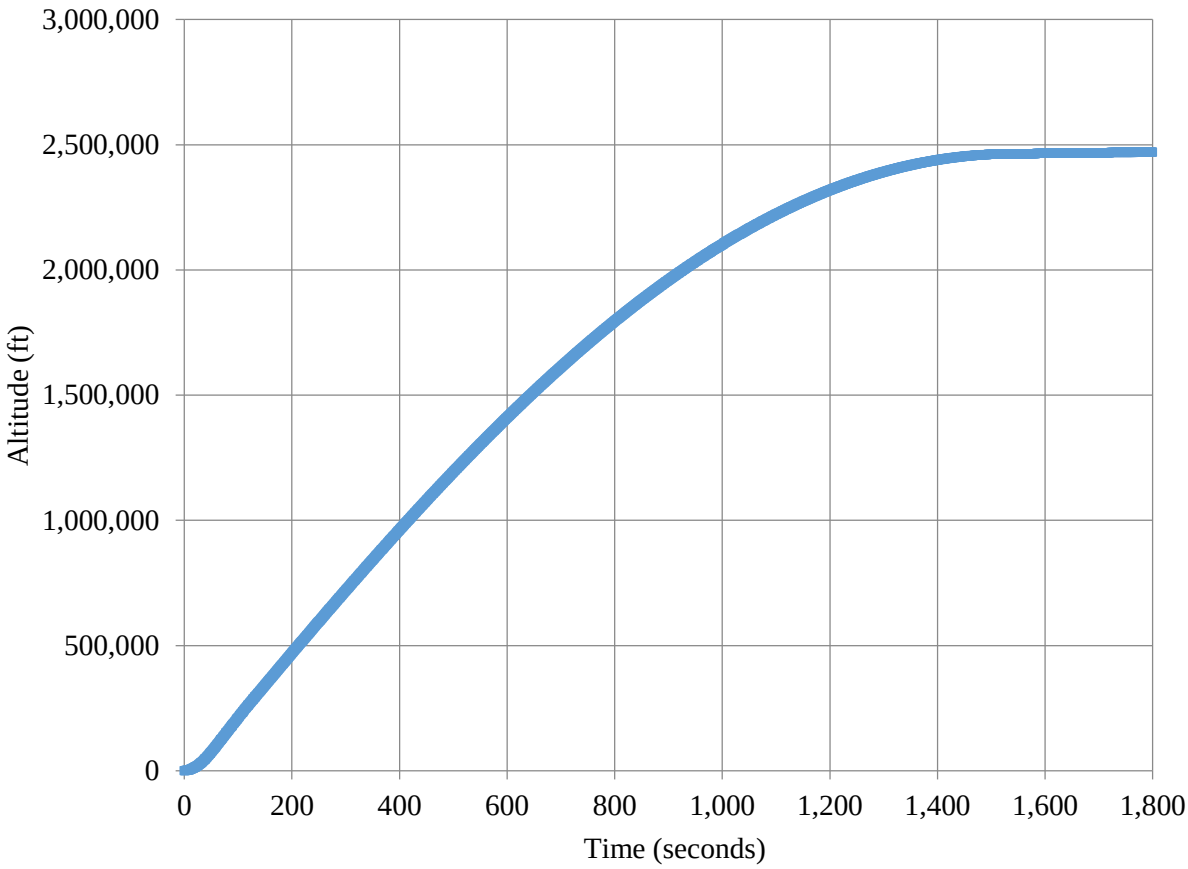



**Figure 32: Case 1 Altitude Profile**

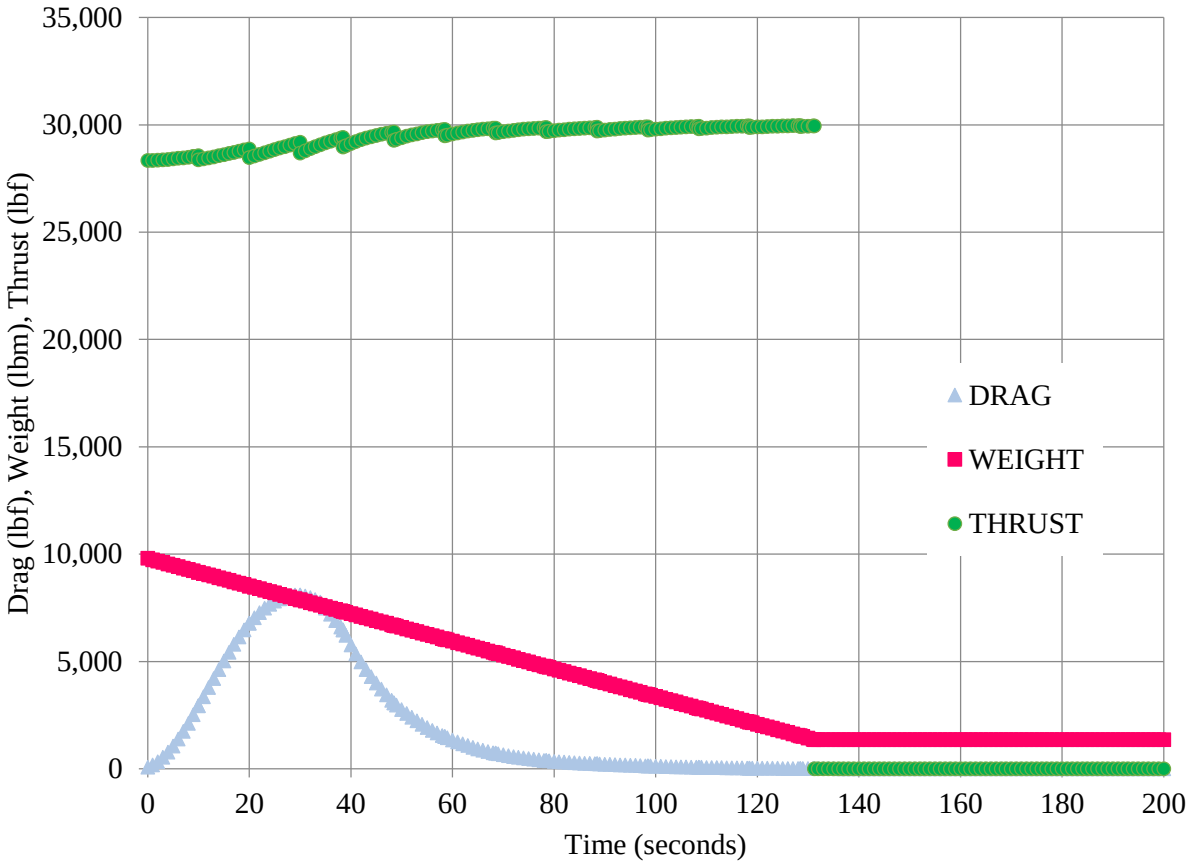



**Figure 33: Case 1 Drag, Weight, and Thrust Profile**

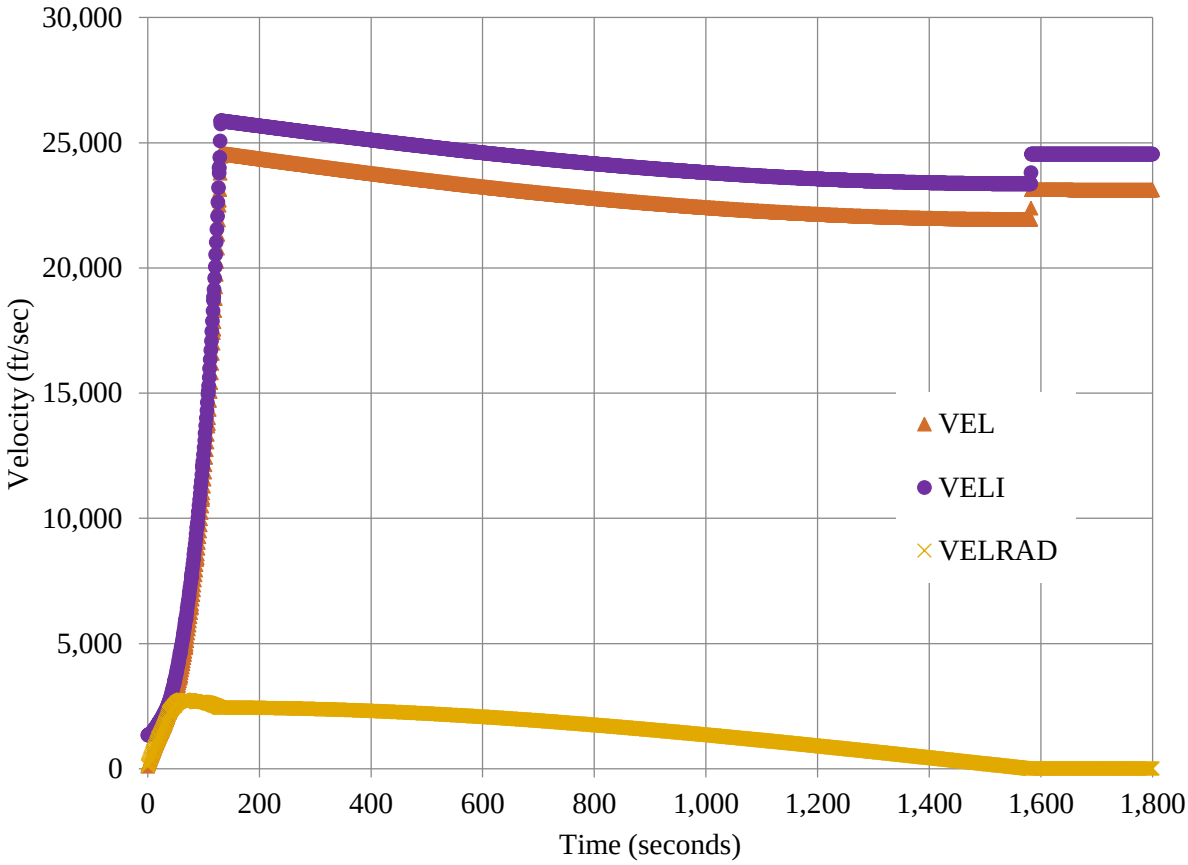



**Figure 34: Case 2 Velocity Profile**

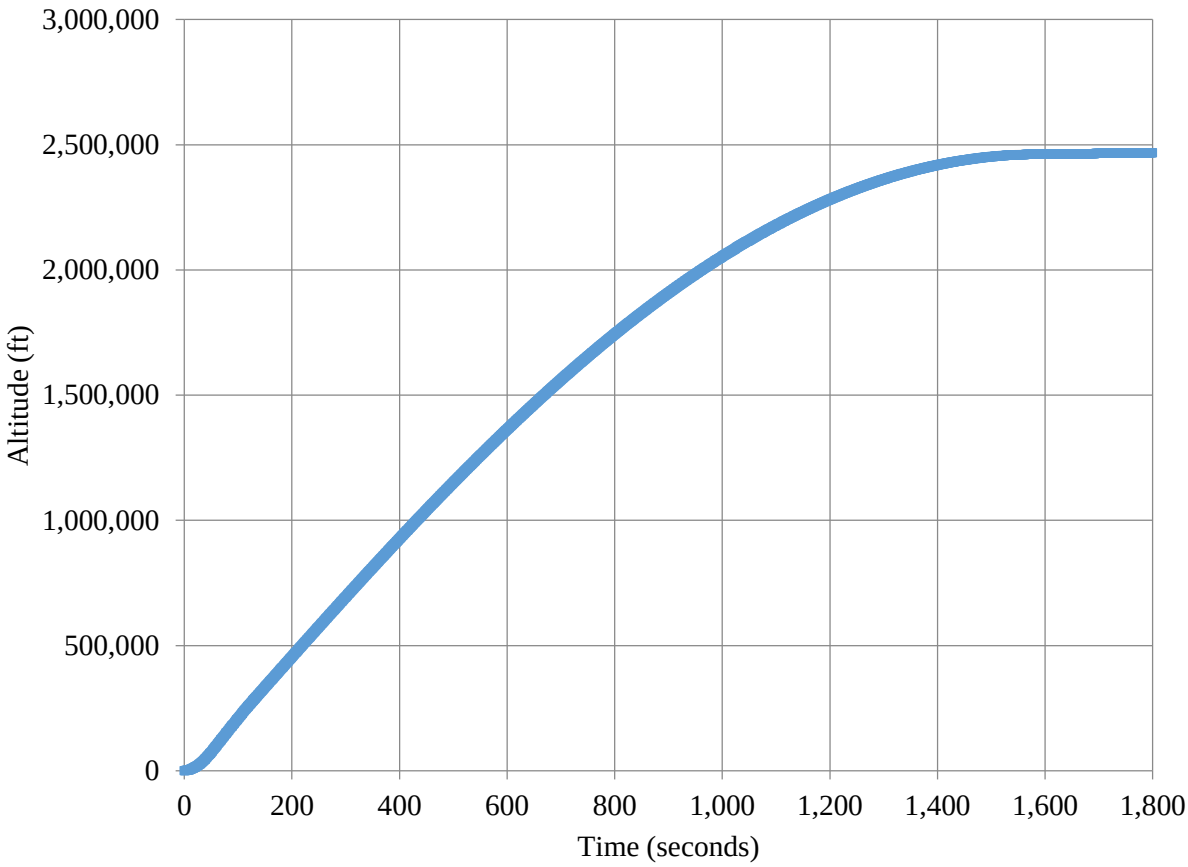



**Figure 35: Case 2 Altitude Profile**

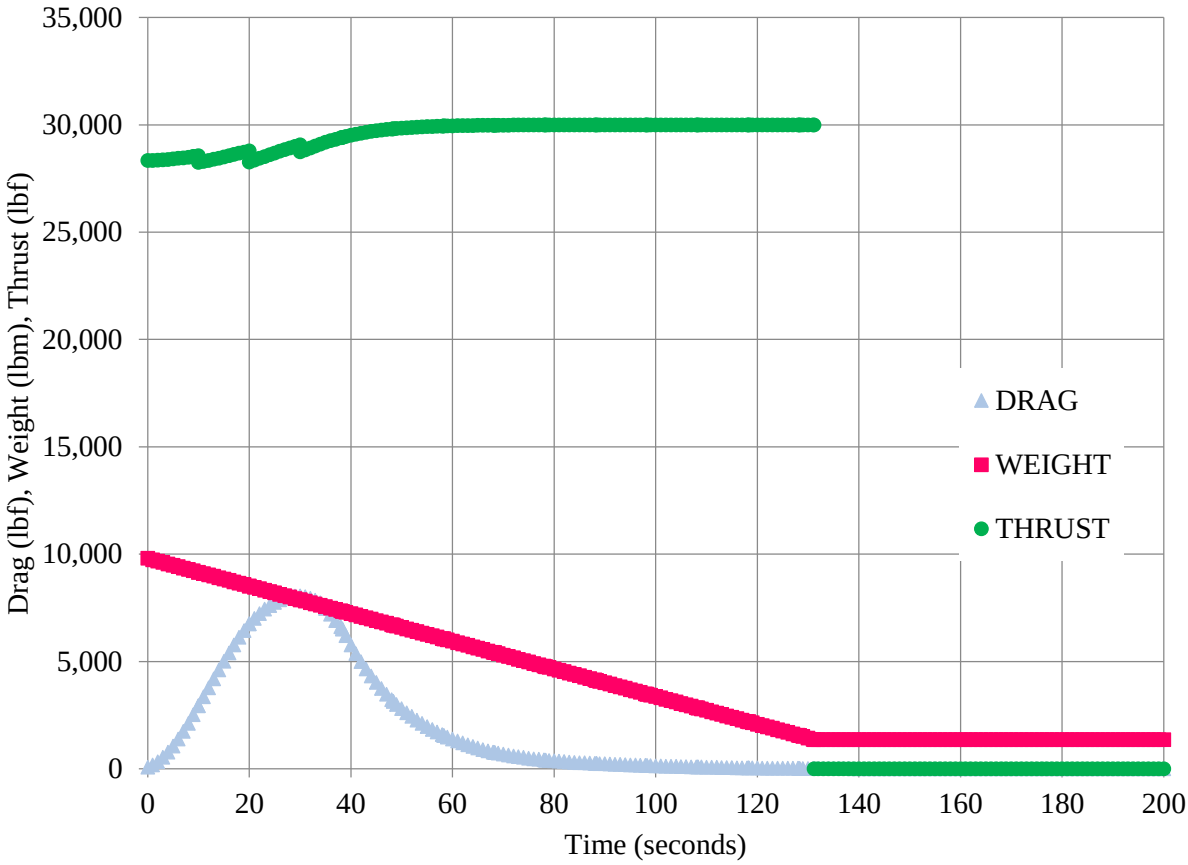



**Figure 36: Case 2 Drag, Weight, and Thrust Profile**

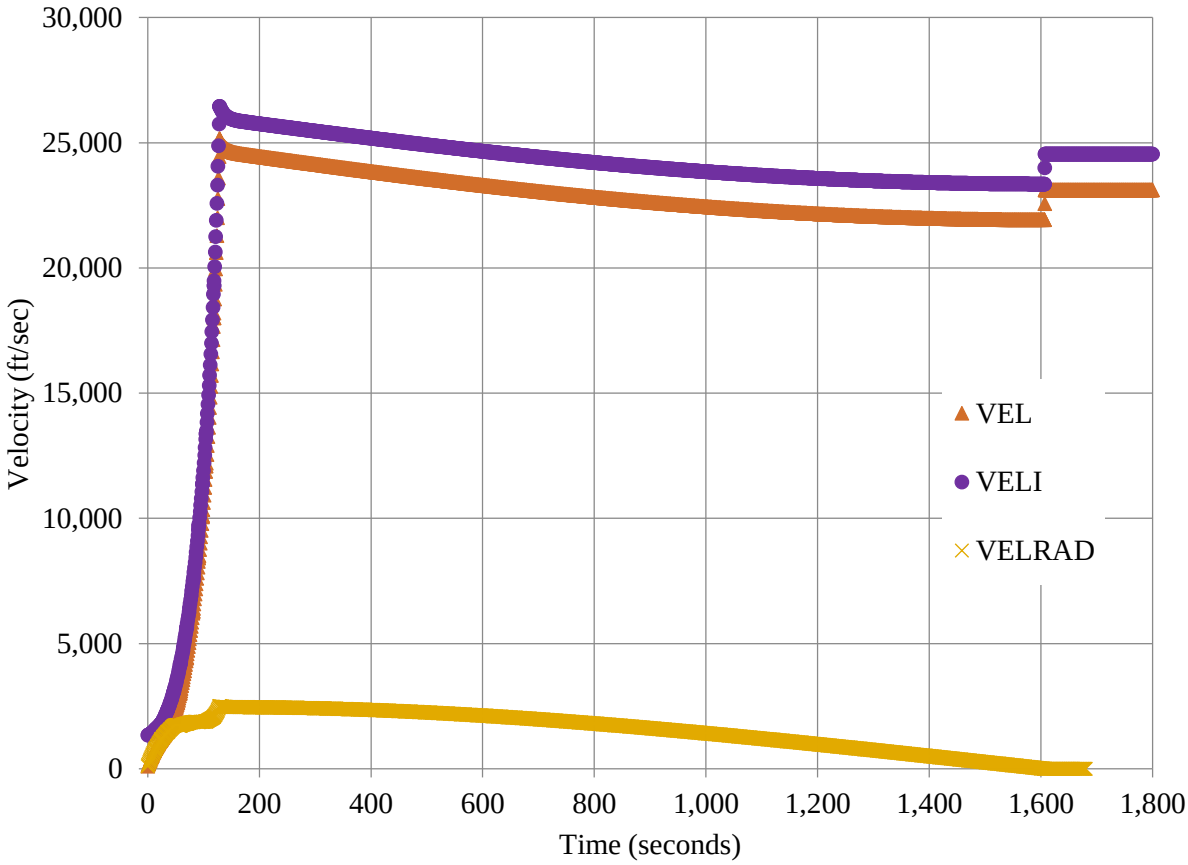



**Figure 37: Case 3 Velocity Profile**

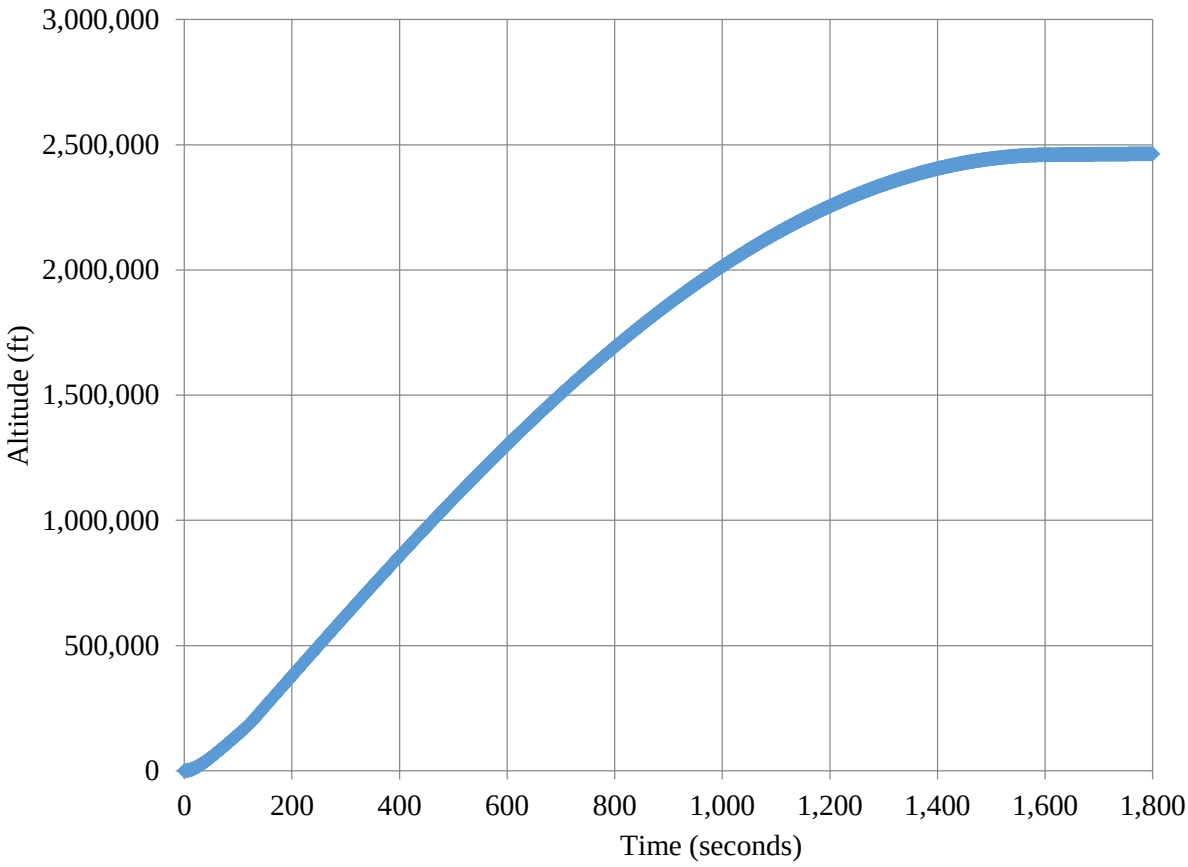



**Figure 38: Case 3 Altitude Profile**

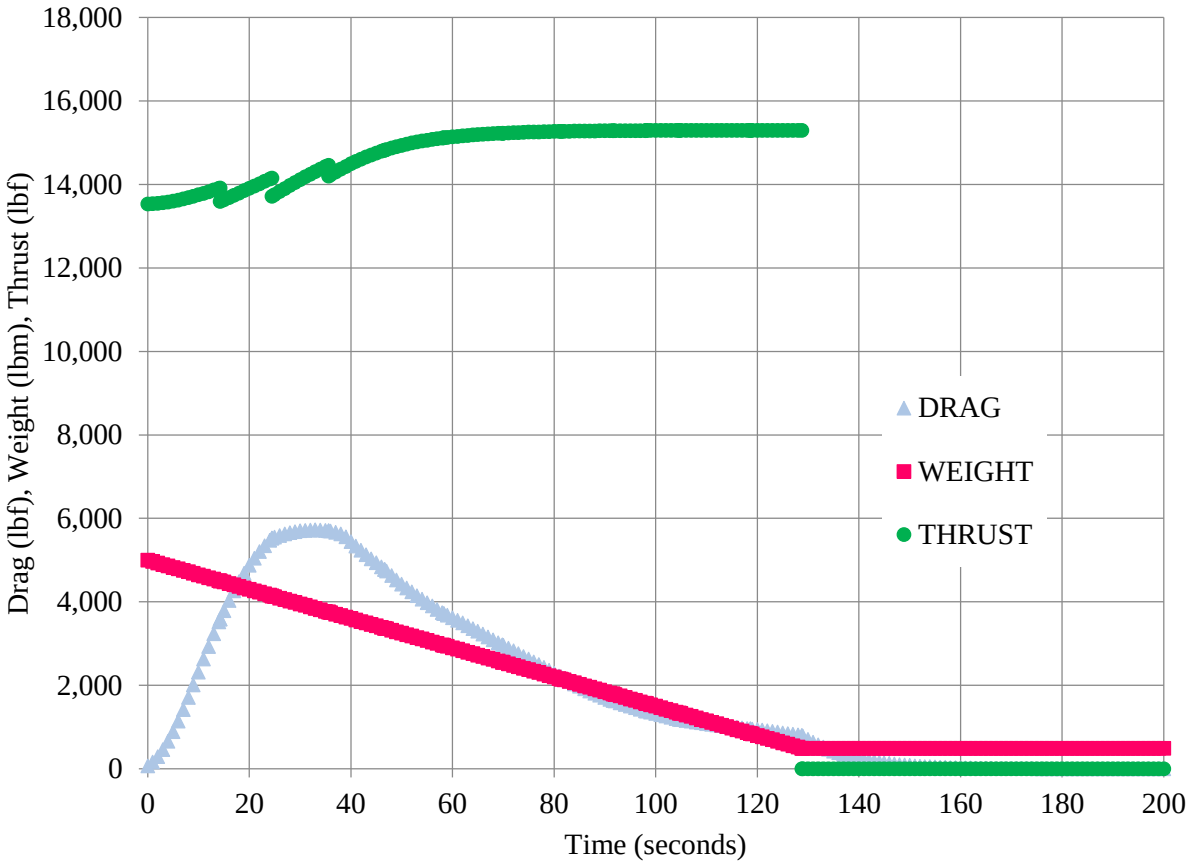



**Figure 39: Case 3 Drag, Weight, and Thrust Profile**

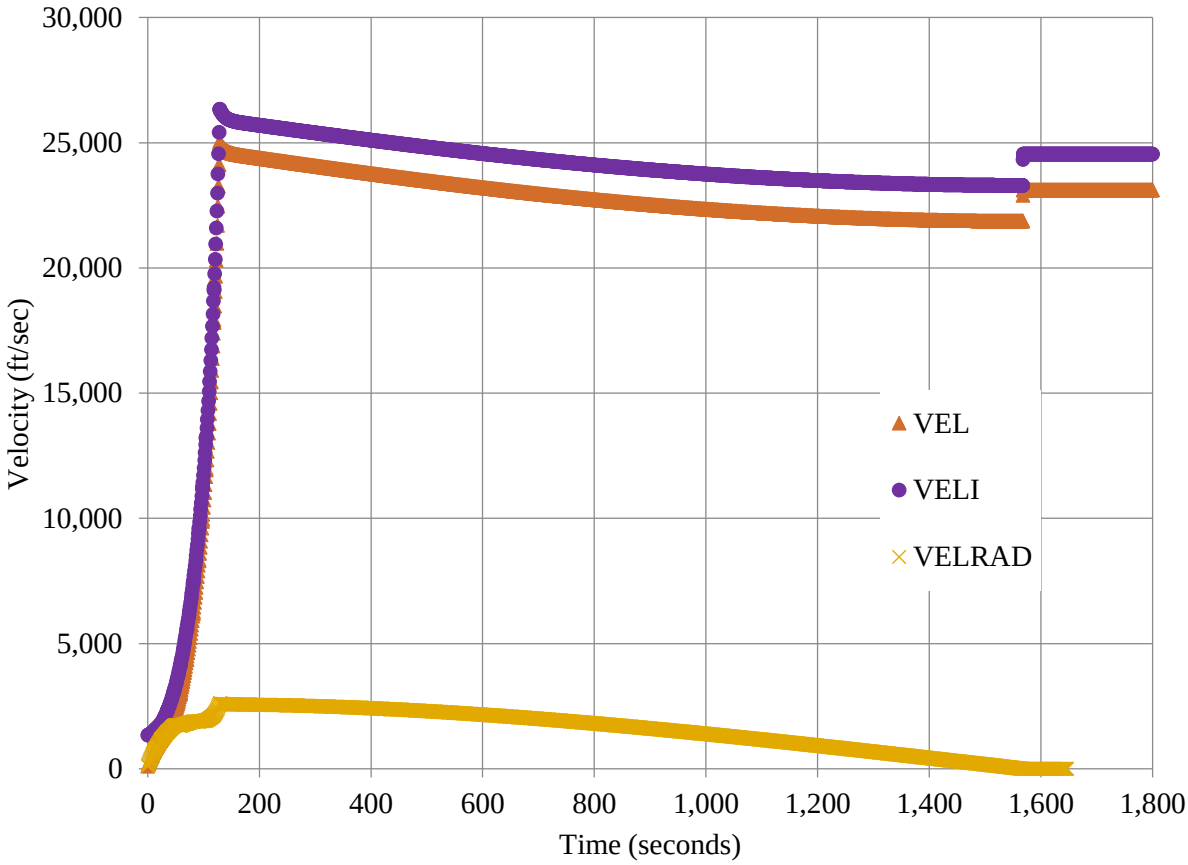



**Figure 40: Case 4 Velocity Profile**

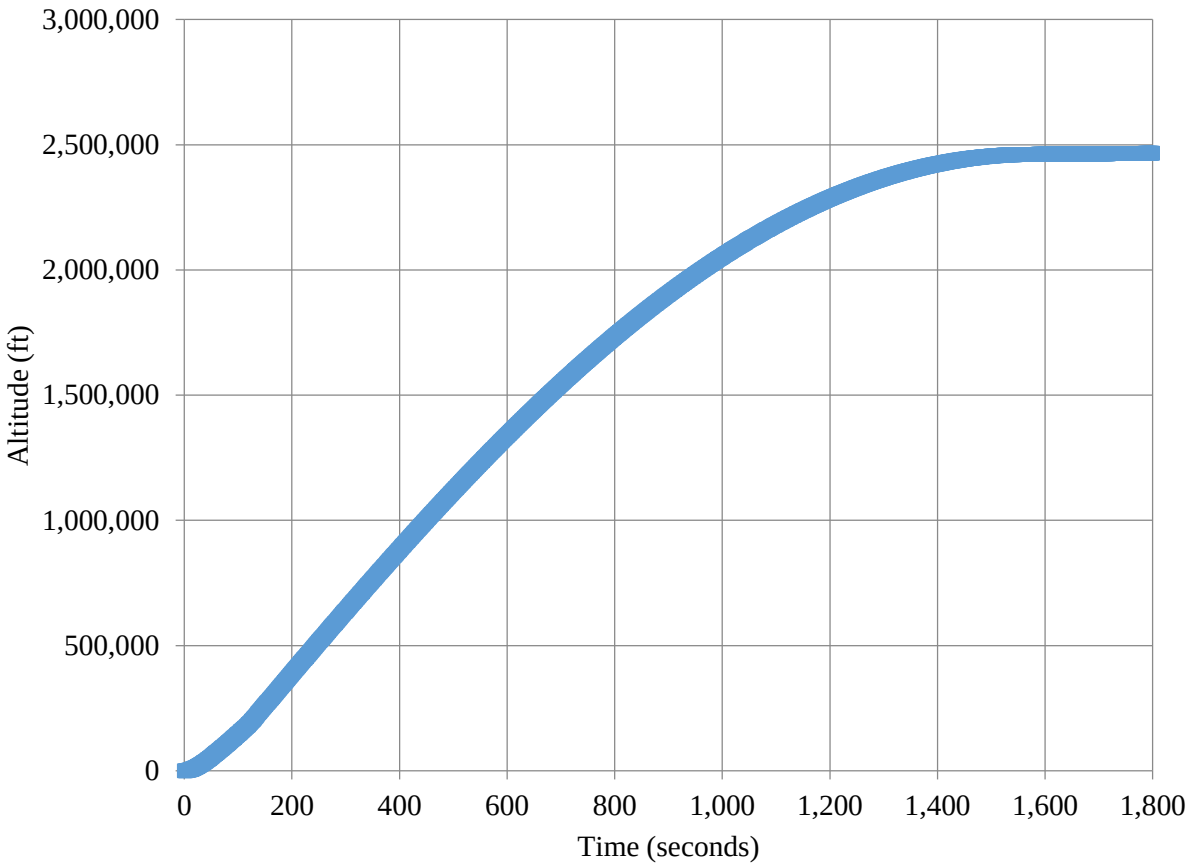



**Figure 41: Case 4 Altitude Profile**

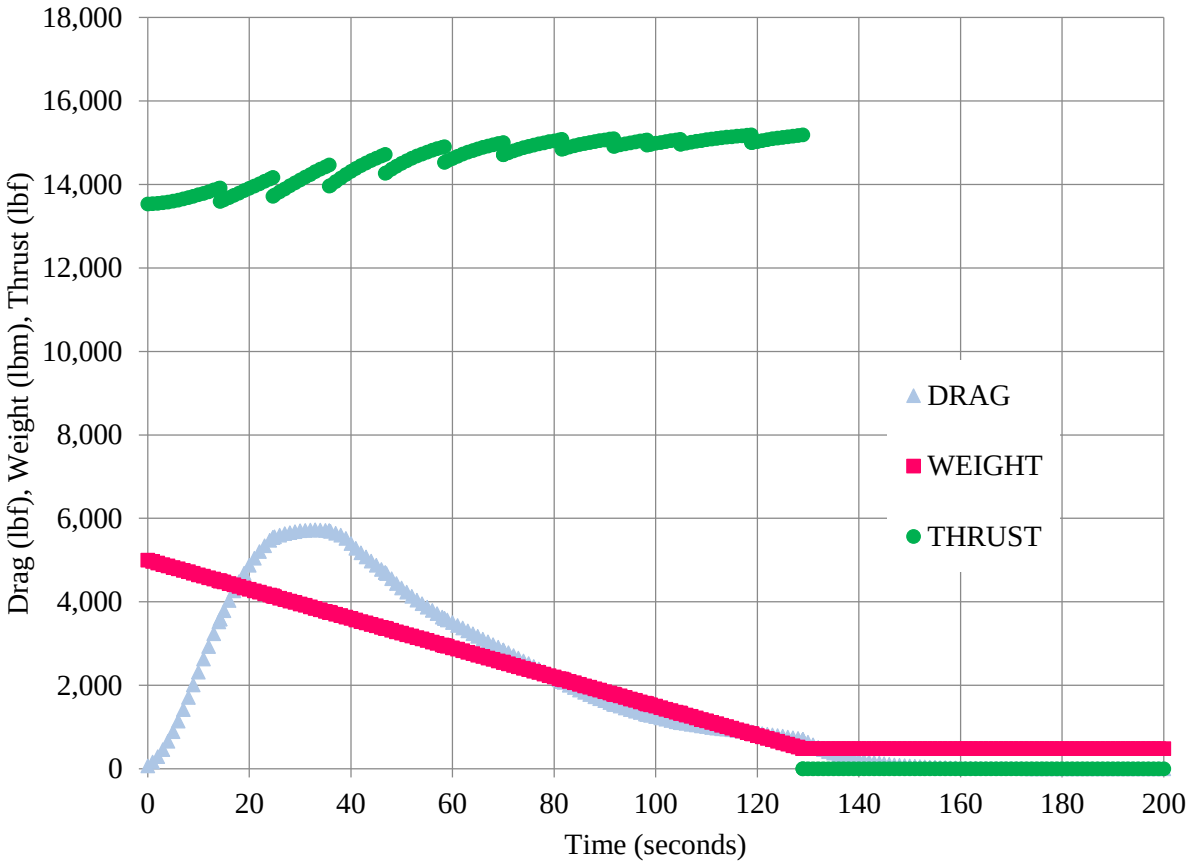



**Figure 42: Case 4 Drag, Weight, Thrust Profile**

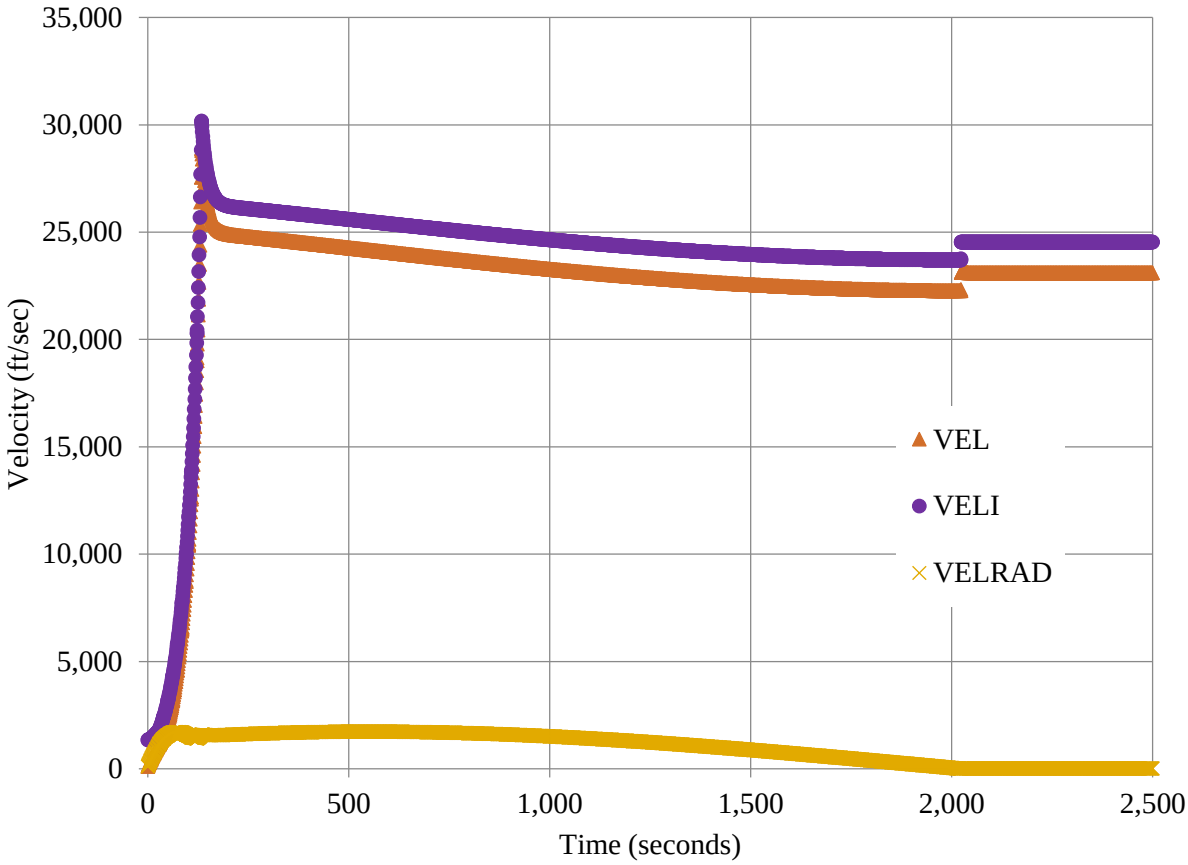



**Figure 43: Case 5 Velocity Profile**

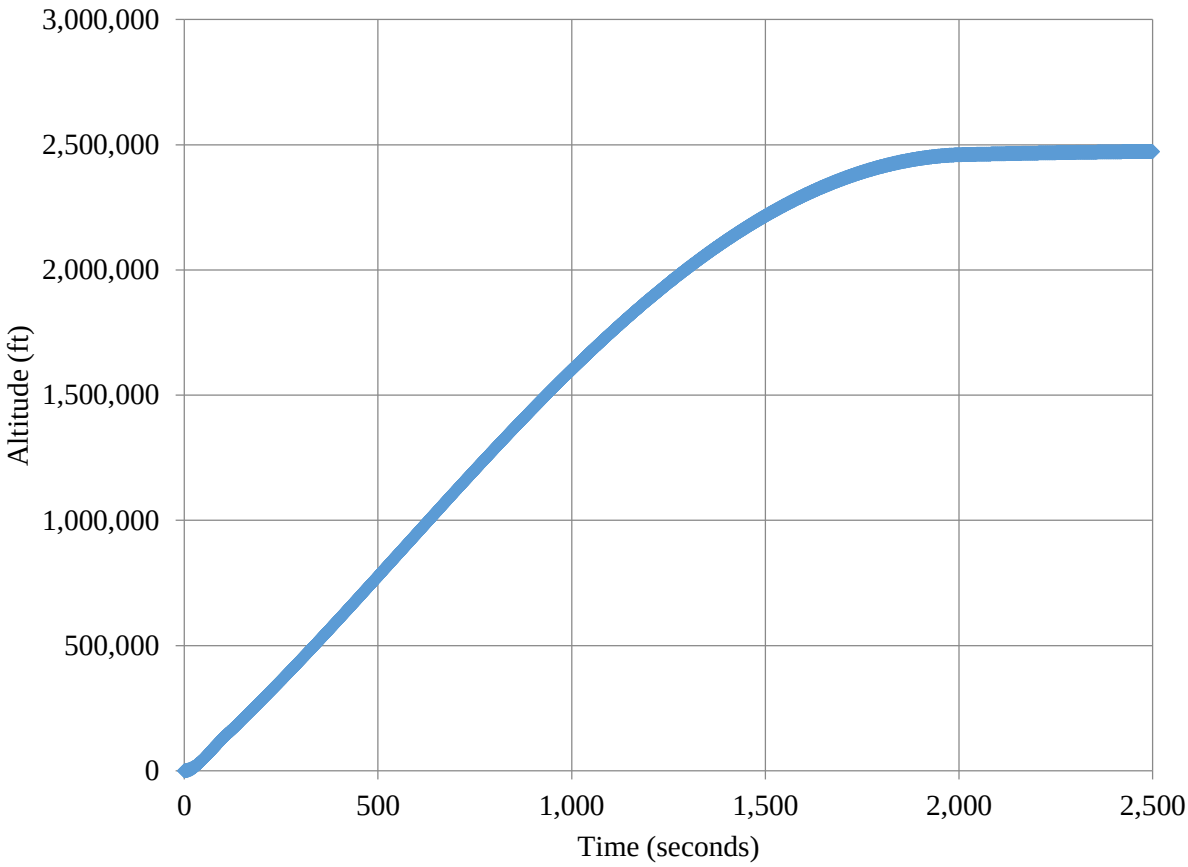



**Figure 44: Case 5 Altitude Profile**

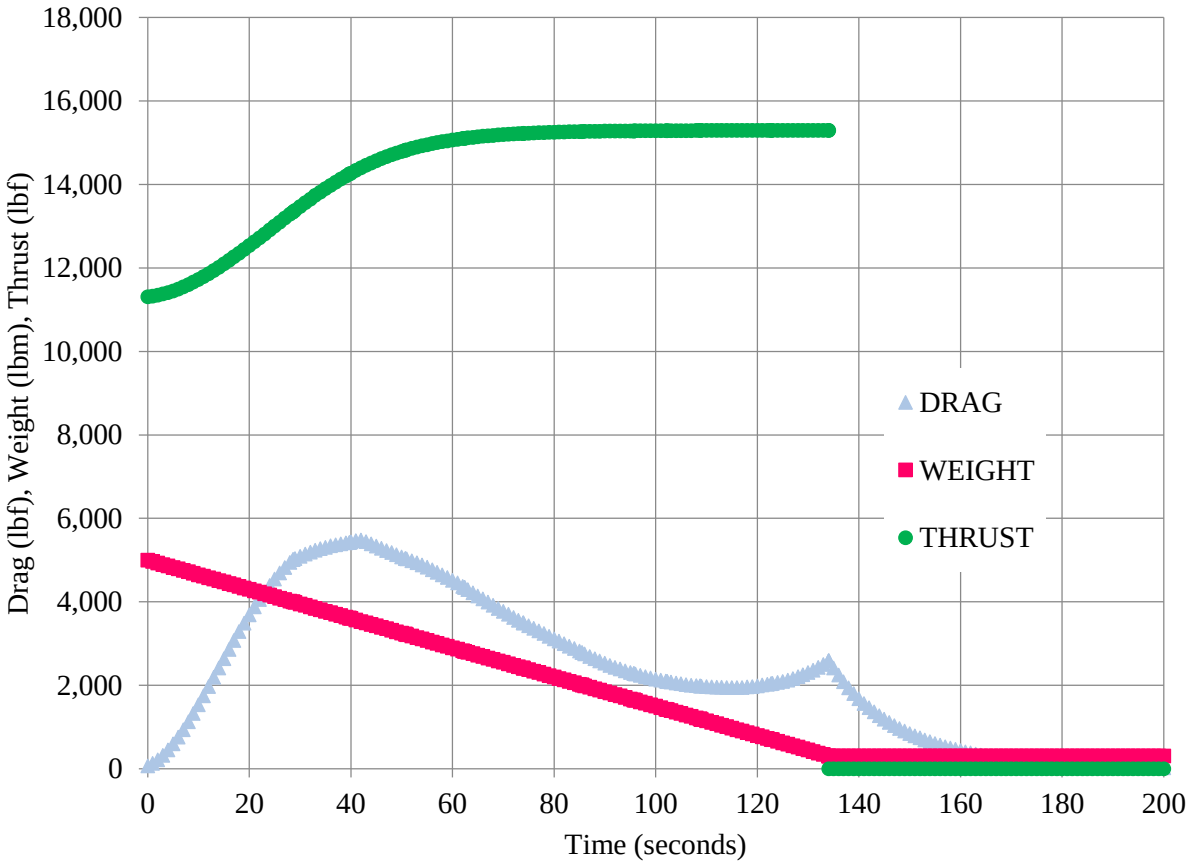



**Figure 45: Case 5 Drag, Weight, and Thrust Profile**

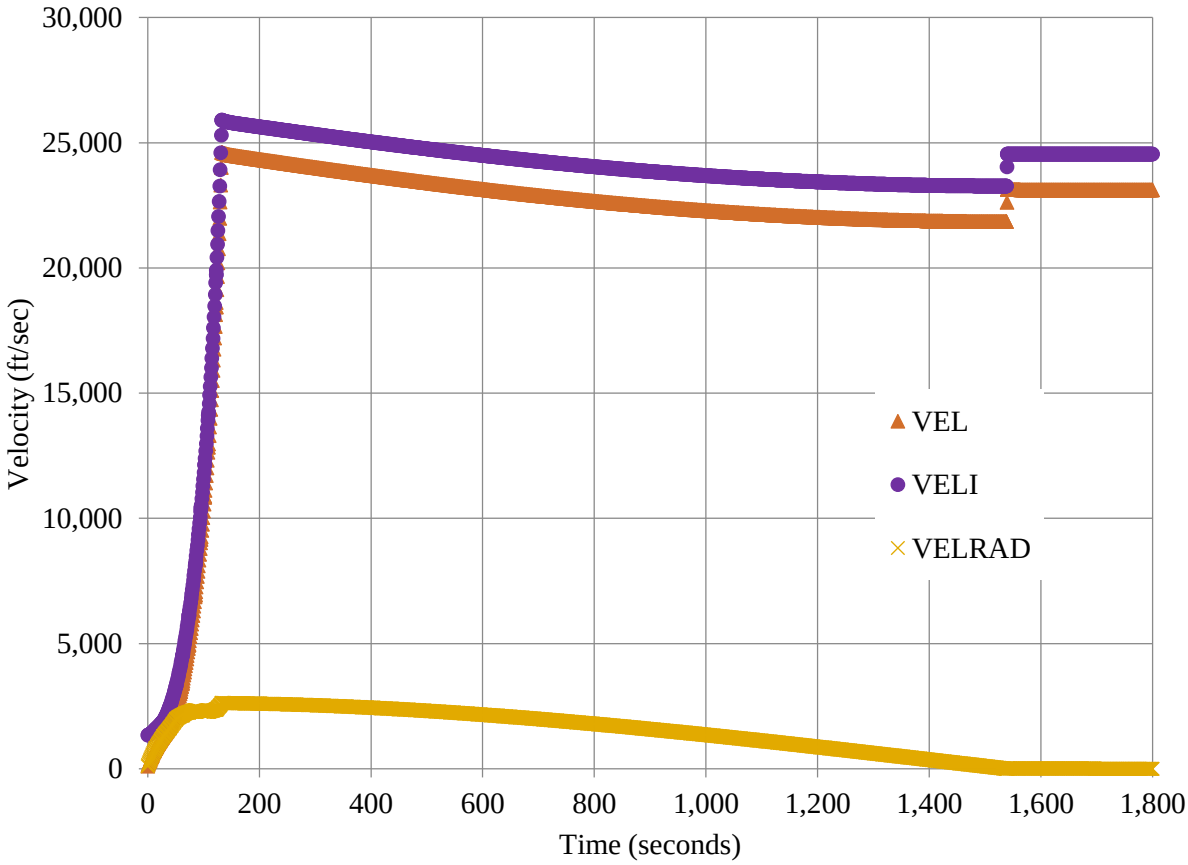



**Figure 46: Case 6 Velocity Profile**

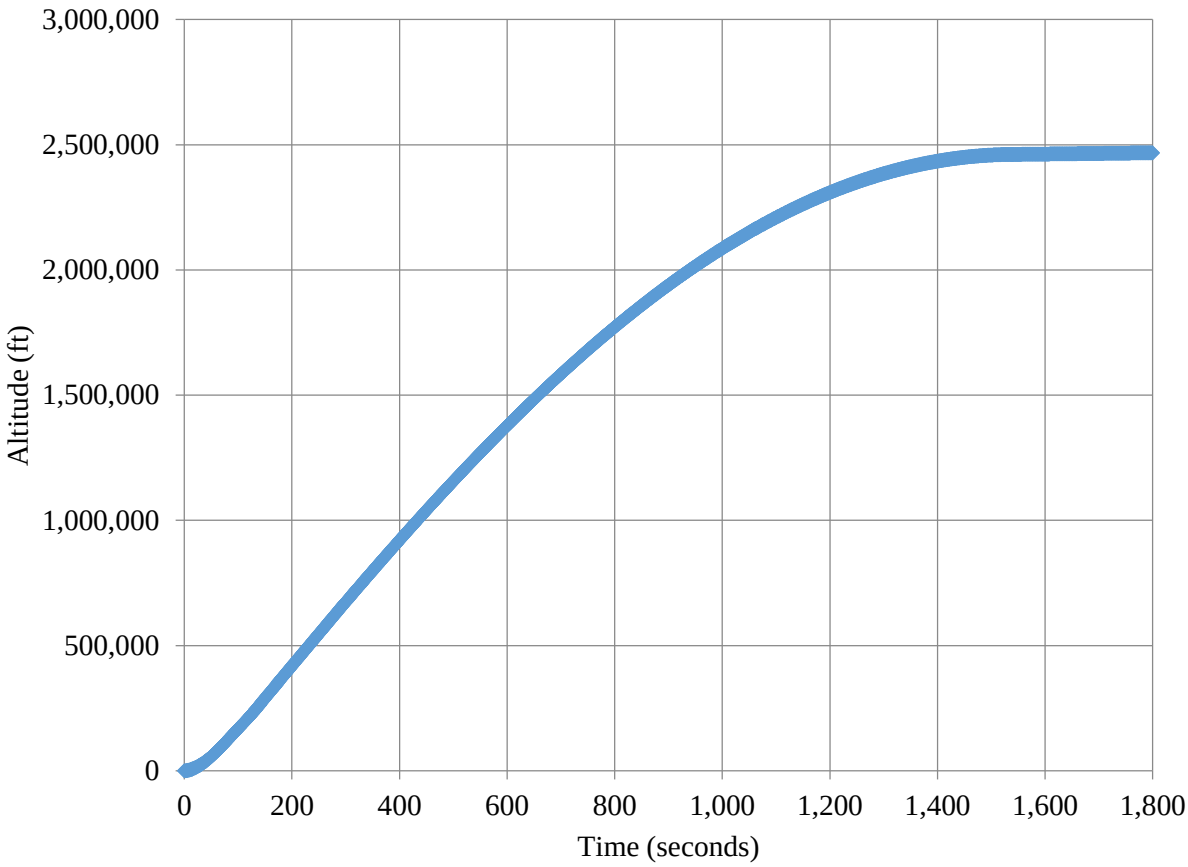



**Figure 47: Case 6 Altitude Profile**

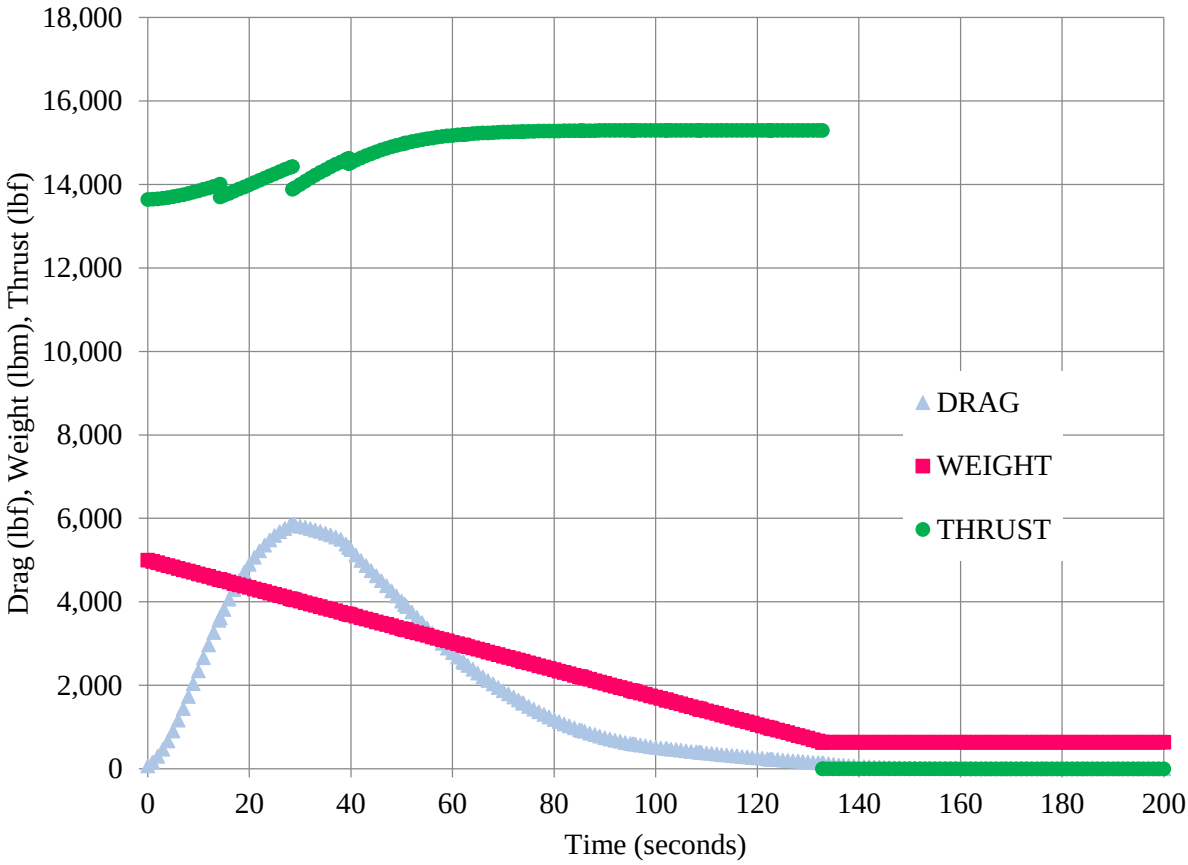



**Figure 48: Case 6 Drag, Weight, and Thrust Profile**

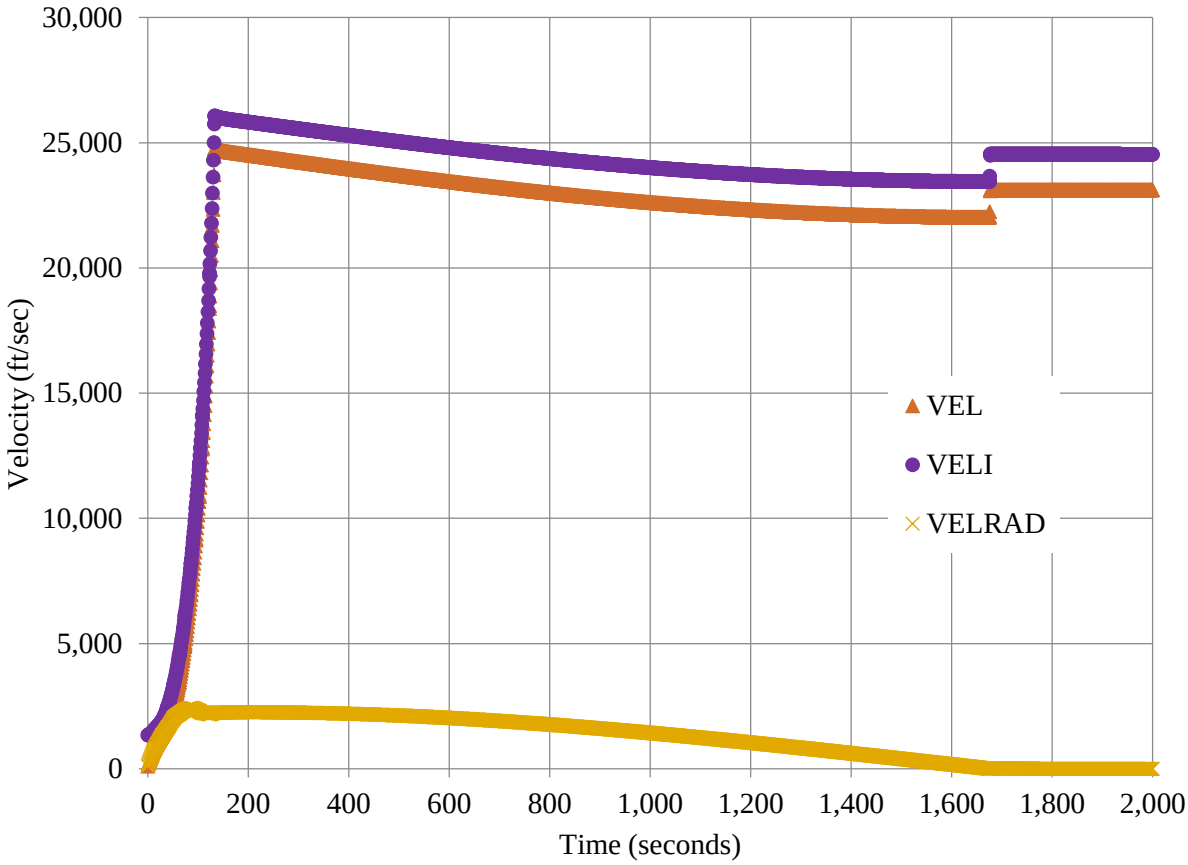



**Figure 49: Case 7 Velocity Profile**

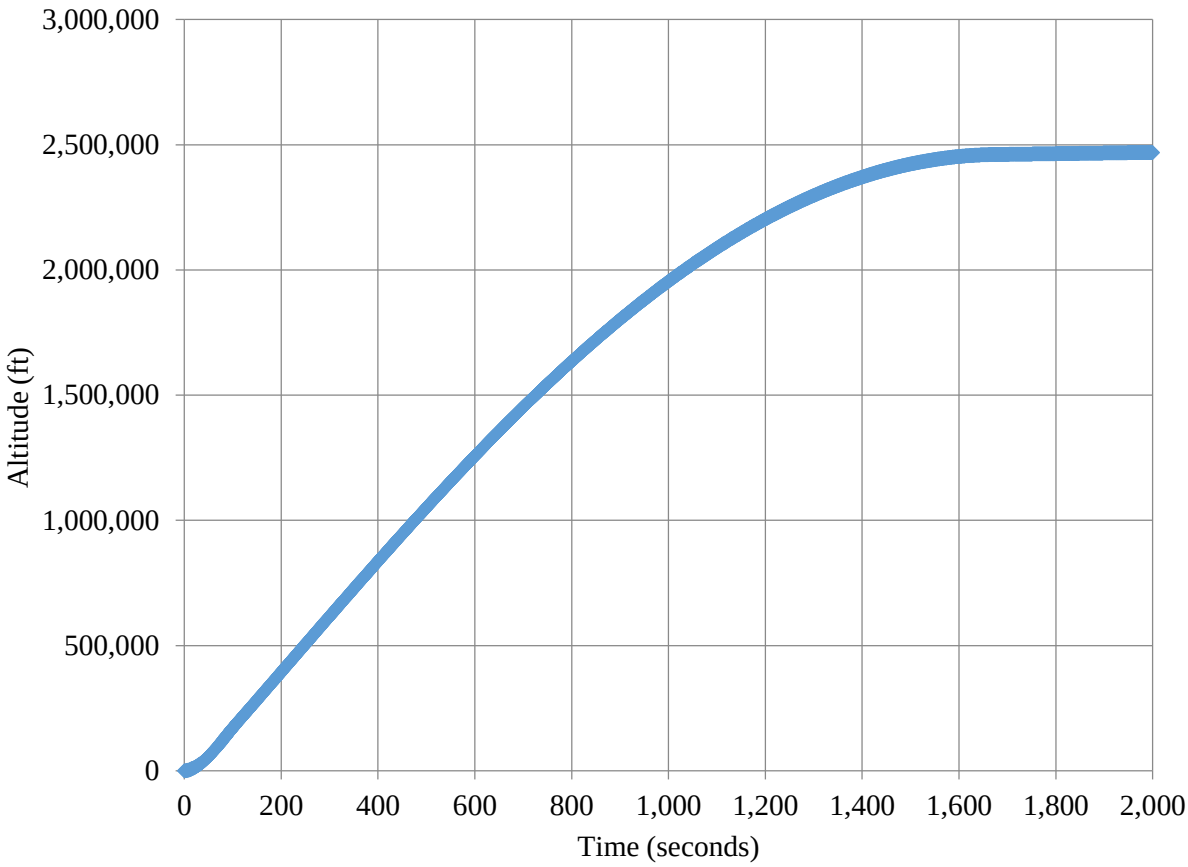



**Figure 50: Case 7 Altitude Profile**

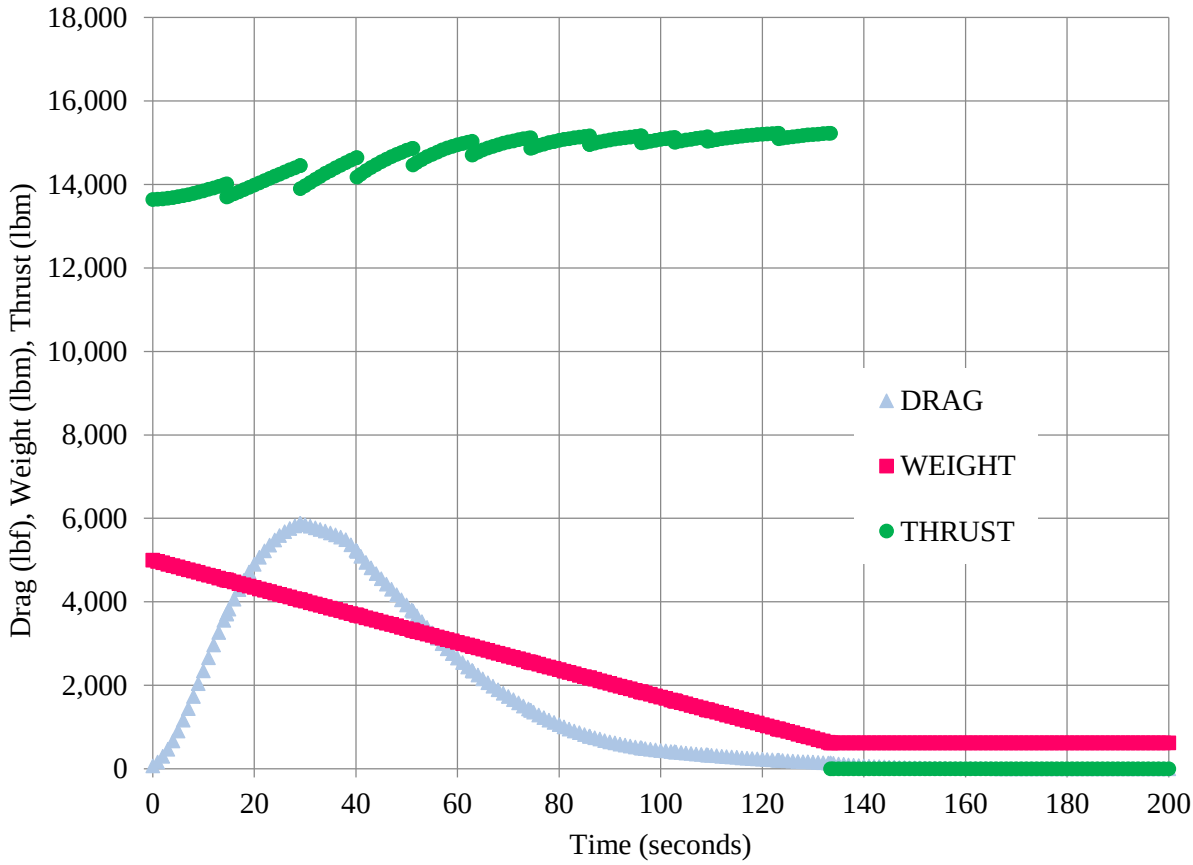



**Figure 51: Case 7 Drag, Weight, and Thrust Profile**

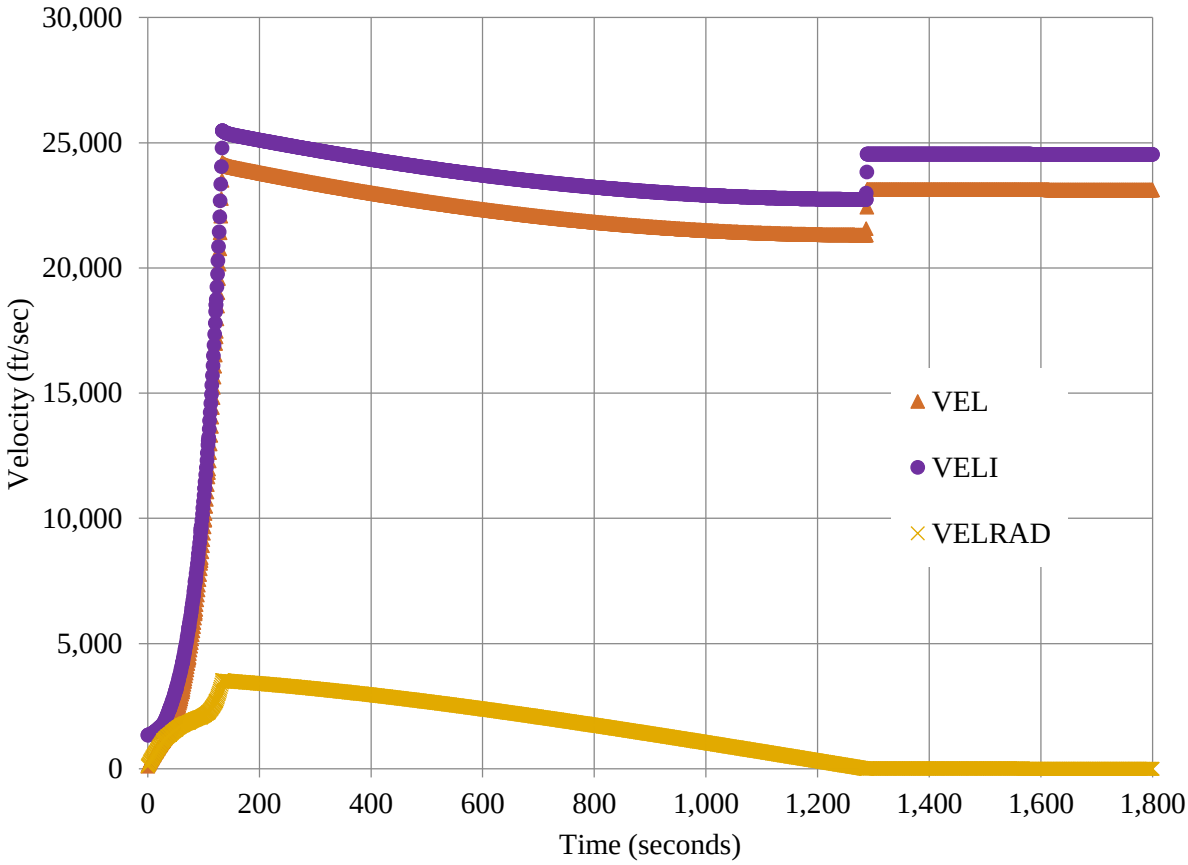



**Figure 52: Case 8 Velocity Profile**

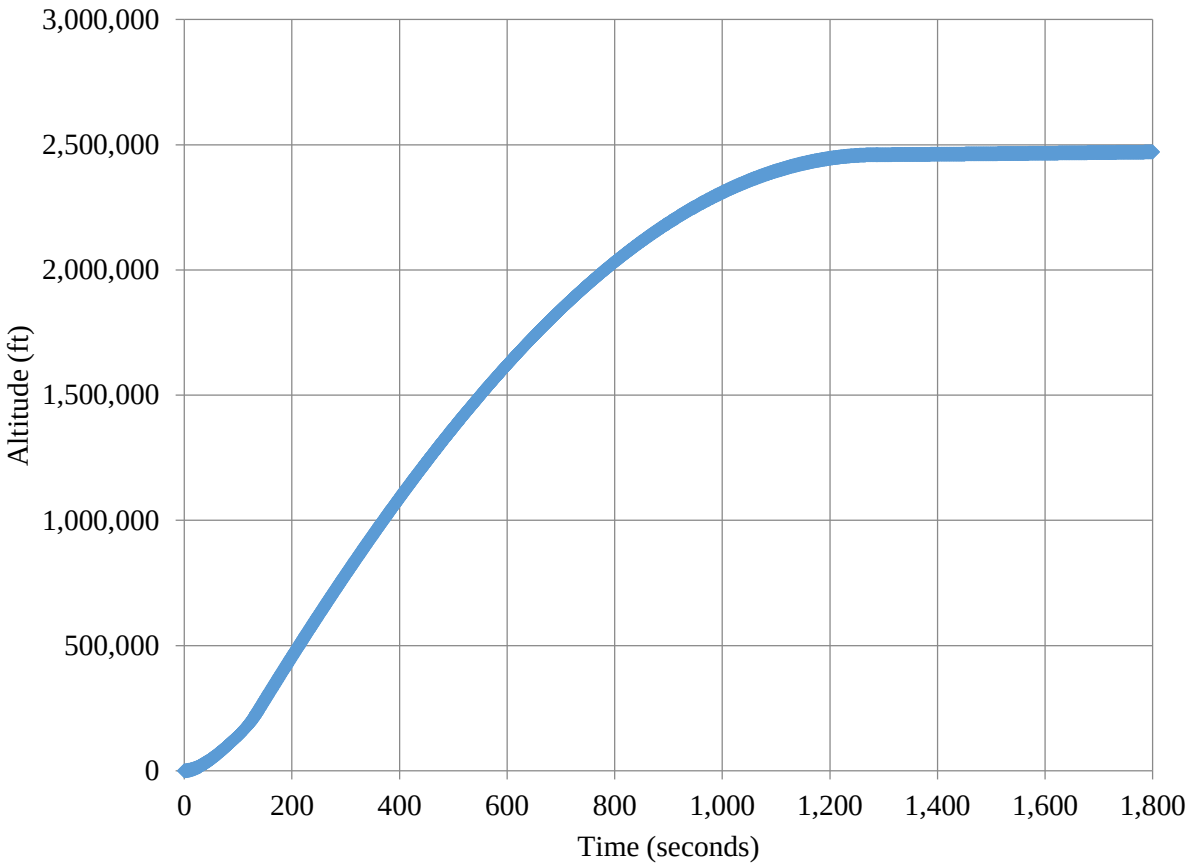



**Figure 53: Case 8 Altitude Profile**

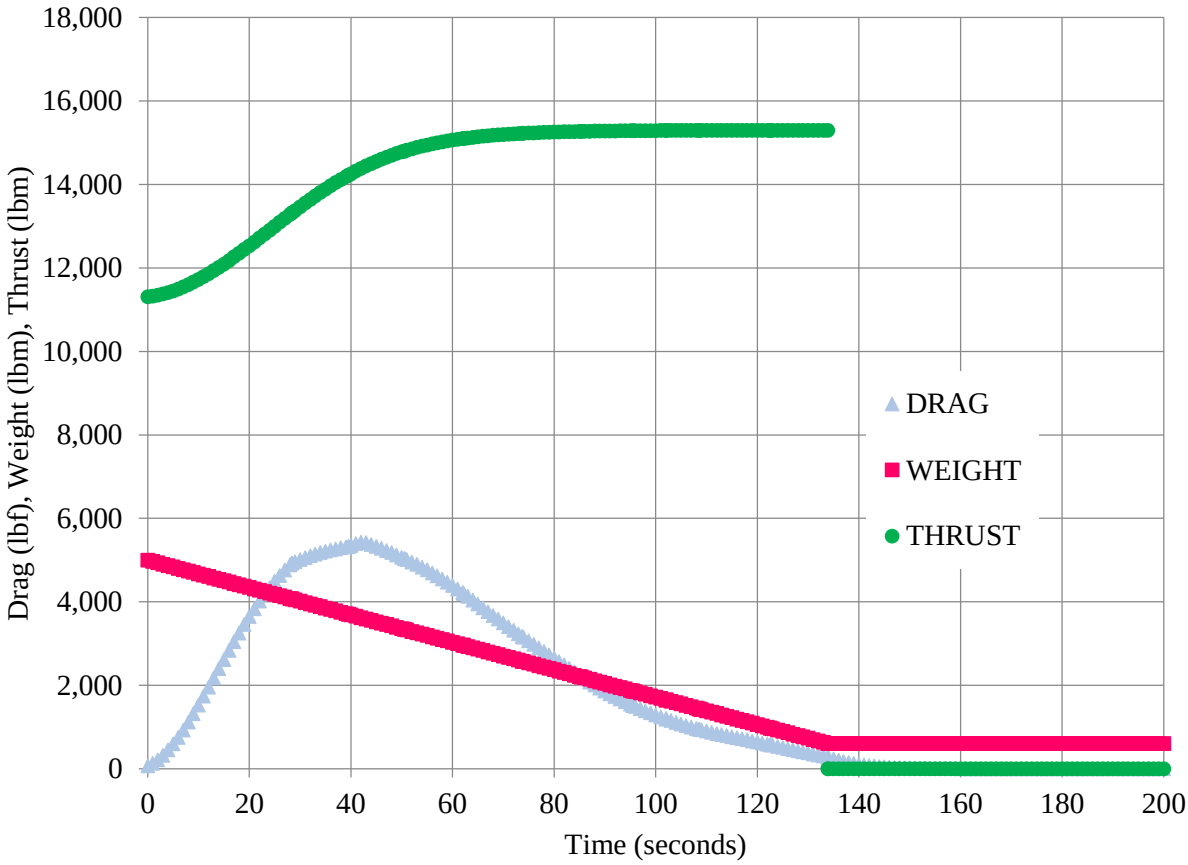



**Figure 54: Case 8 Drag, Weight, and Thrust Profile**

# VITA

E. Lara Lash was born in Springfield, IL, but grew up in Vienna, VA with her parents and older brother. She attended Westbriar Elementary, Joyce Kilmer Middle School, and continued on to George C. Marshall High School in Falls Church, VA. After graduation, she attended Lafayette College in Easton, PA to pursue her dream of obtaining an engineering degree in a liberal arts environment. During her tenure at Lafayette, Lara studied abroad at Jacobs University Bremen in Bremen, Germany for the spring 2011 semester, which broadened her horizons on science/engineering in the international community. She obtained her Bachelors of Science in Mechanical Engineering and a minor in History from Lafayette College in May 2013. She accepted a graduate research assistantship for a Master's program in Aerospace Engineering at The University of Tennessee Space Institute (UTSI), Tullahoma, under Dr. Trevor Moeller. She was then awarded the opportunity to work with OTIS and learn more about trajectory optimization and SSTO flight, which led to the results of this thesis. She hopes to continue her graduate work at UTSI and obtain her doctorate in Aerospace Engineering.